

1-29-2021 11:00 AM

## Experimental Study of Tornado-Induced Pressures

Aya Kassab, *The University of Western Ontario*

Supervisor: Hangan, Horia M., *The University of Western Ontario*

A thesis submitted in partial fulfillment of the requirements for the Doctor of Philosophy degree  
in Civil and Environmental Engineering

© Aya Kassab 2021

Follow this and additional works at: <https://ir.lib.uwo.ca/etd>



Part of the [Civil Engineering Commons](#), [Environmental Engineering Commons](#), and the [Other Civil and Environmental Engineering Commons](#)

---

### Recommended Citation

Kassab, Aya, "Experimental Study of Tornado-Induced Pressures" (2021). *Electronic Thesis and Dissertation Repository*. 7634.  
<https://ir.lib.uwo.ca/etd/7634>

This Dissertation/Thesis is brought to you for free and open access by Scholarship@Western. It has been accepted for inclusion in Electronic Thesis and Dissertation Repository by an authorized administrator of Scholarship@Western. For more information, please contact [wlsadmin@uwo.ca](mailto:wlsadmin@uwo.ca).

## Abstract

The increased devastation associated with tornadic flow-fields in terms of human lives or destruction of properties and their subsequent economic losses highlights the significance of understanding the tornado vortex structure, particularly near the ground where the majority of this destruction happens. While the body of research in this area is increasing there is a lack of resolution associated with physical near-surface measurements in tornado-like vortices (TLVs) and the effects of translation, surface roughness, and surface vortex dynamics are not yet well understood.

In order to address these gaps, high spatial and temporal surface pressure measurements were carried out at WindEEE Dome to explore the characteristics of stationary and translating tornado-like vortices (TLV) for a wide range of swirl ratios ( $S=0.21$  to  $1.03$ ). The translational speed of the TLV and the surface roughness were varied to examine their effects on tornado ground pressures, wandering, and vortex structure. It was found that wandering is more pronounced at low swirl ratios and has a substantial effect on the peak pressure magnitude for stationary TLV (error percentage  $\leq 35\%$ ). A new method for removing wandering was proposed which is applicable for a wide range of swirl ratios. For translating TLV, the near-surface part lagged behind the top of the vortex, resulting in a tilt of the tornado vertical axis at higher translating speeds. Also, a veering motion of the tornado base towards the left was observed. Wandering was less pronounced for higher translation speeds. Increasing the surface roughness caused an analogous effect as lowering the swirl ratio.

While surface pressure exploration of tornado-like vortices paved the way for understanding their complex structure near the ground, applying the acquired knowledge on buildings is intended to serve for the interpretation of tornado-induced pressures on buildings as a superposition of pressure deficit and aerodynamic effects. Thus, induced internal and external pressures on two generic low-rise buildings were quantified to assess the impacts of TLVs on low-rise buildings. The internal pressures were examined under different opening configurations, building orientations, building sizes, and offsets. It was found that a dominant opening on the roof induced the highest negative peak internal pressure. Increasing the building offset beyond the tornado core region caused a drastic reduction of the peak internal pressures

by two-thirds. The peak internal pressures were higher for the smaller of the two buildings investigated herein. On the other hand, external pressure measurements showed that the building's roof, leeward wall, and left side wall experienced the maximum uplift at the core radius location. The comparison with the recently modified ASCE 7-16 code showed that roof corner pressures are safely predicted for all the cases while the mid-roof zone and the middle of the walls experienced higher suctions exceeding the recommended wind loads in ASCE 7-16.

## Keywords

Tornado-like vortices, Surface pressure, WindEEE Dome, Swirl ratio, Roughness, Translation speed, Wandering, Tilting, Internal pressure, Opening, External pressure.

## Summary for Lay Audience

Tornadoes can cause enormous destruction to life and properties. The aftermath of these fierce storms has a great impact on the economy. Thus, it is crucial to understand their structure and their associated damage near the ground where most of the structures lie.

In this study, high-resolution pressure measurements on the ground were carried out to better characterize the tornado vortex effect on the ground surface. Multiple translational speeds of tornadoes and surface ground roughness were examined in a large-scale tornado simulator. While understanding the near-surface tornado vortex structure is essential, the study of their effect on buildings will provide a full insight into their probable damage. Hence, internal and external pressure measurements were performed on two low-rise building structures under translating tornado flow-field. The internal pressures associated with the natural leak in the buildings or due to sudden breakage of windows or doors play a significant role by either mitigating or intensifying the overall tornado wind loading on structures. Herein, the internal pressures were examined under different opening configurations, building orientations, building sizes, and offsets. Also, the study of the induced external pressures due to tornadic flow revealed that the building code needs more improvements regarding their recommended wind loadings on buildings.

## Co-Authorship Statement

This thesis has been prepared according to the regulations set by the School of Graduate and Postdoctoral Studies at Western University for an Integrated Article format thesis. The co-authorship statements of the thesis chapters are as follows:

Chapter 2 is a journal article submitted and currently under review in the Journal of Wind Engineering and Industrial Aerodynamics. It is co-authored by A. Kassab, C. Jubayer, A. Ashrafi, and H. Hangan.

A. Kassab designed and carried out the experiments and wrote the manuscript. C. Jubayer performed the experiments and revised the manuscript. A. Ashrafi assisted in the data analysis. H. Hangan supervised the whole research and revised the manuscript.

Chapter 3 is a journal article and will be submitted for publication to the Journal of Wind Engineering and Industrial Aerodynamics under the co-authorship of A. Kassab, P. Vickery, C. Jubayer, S. Banik, and H. Hangan.

A. Kassab wrote the manuscript, analyzed the data, and produced all figures. P. Vickery proposed and designed the experiments and revised the manuscript. C. Jubayer carried out the experiments and revised the manuscript. S. Banik assisted in the experimental design and the manuscript revision. H. Hangan supervised the whole research and revised the manuscript.

Chapter 4 is a journal article and will be submitted for publication to the ASCE Journal of Structural Engineering. It is co-authored by C. Jubayer, P. Vickery, A. Kassab, S. Banik, and H. Hangan.

C. Jubayer carried out the experiments and wrote parts of the manuscript. P. Vickery proposed and designed the experiments and revised the manuscript. A. Kassab wrote the majority of the manuscript, analyzed the data, and produced all figures. S. Banik assisted in the experimental design and the manuscript revision. H. Hangan supervised the whole research and revised the manuscript.

*This thesis is dedicated to **my late uncle, Shaker Elmoghazy**. You will always be in my heart.*

## Acknowledgments

Praise to Allah, the almighty, who has guided us to this; and we would never have been guided if Allah had not guided us.

I would like to express my sincere gratitude to my research supervisor, Dr. Horia Hangan for providing me with this great opportunity in the field of Wind Engineering. His endless support, valuable guidance, patience, and inspiration have guided my way throughout my research journey. It has been a great privilege to work under his supervision.

I am also very grateful to Dr. Jubayer Chowdhury for his continuous support and guidance from the first day of my doctoral journey. He assisted me in learning and understanding the experimental techniques. I also thank Dr. Djordje Romanic for his valuable comments and guidance.

I also offer my appreciation to Peter Vickery and Sudhan Banik from Applied Research Associates, Inc, for their collaboration.

I would like to extend my thanks and gratitude to the WindEEE staff, Gerald Dafoe, Dr. Jubayer Chowdhury, Adrian Costache, Priscilla De Luca, and Elisa Yaqiuan.

I also would like to thank my dear colleagues Marilena, Arash, Mohammad, and Junayed for their support and our shared thoughts throughout my Ph.D. journey.

I would like to acknowledge the financial support from the Department of Civil and Environmental Engineering at Western University and Natural Sciences and Engineering Research Council of Canada (NSERC) Discovery grants.

Above all, I would like to thank my dad Sadek, my mom Hanaa, my sisters Asma and Heba for their love, care, support, and prayers, I would not have done anything without you. Many thanks to my father-in-law Alaaeldeen, my mother-in-law Safaa, my brothers-in-law Ahmed and Sami, my sisters-in-law Dina and Esraa for their endless support and care. Thanks to the great support I received from my life-time friends, Heba, Aya, and Omneya.

Lastly and most importantly, I would like to thank my beloved husband, Ahmed for his love, continuous support, all the sacrifices that he made to support me in completing my Ph.D..

Thank you from the bottom of my heart, I owe you everything. I am so thankful to my lovely twins, Omar and Judy, who were only five months when I started my Ph.D. Thank you for the joy and love you bring to my life.



# Table of Contents

Abstract .....	ii
Summary for Lay Audience .....	iv
Co-Authorship Statement.....	v
Acknowledgments.....	vii
Table of Contents .....	ix
List of Tables .....	xii
List of Figures .....	xiii
List of Appendices .....	xvii
Nomenclature .....	xviii
Chapter 1 .....	1
1 Introduction and background .....	1
1.1 General Introduction .....	1
1.2 Motivation and objectives.....	2
1.3 Scope of the Thesis .....	6
References .....	7
Chapter 2 .....	13
2 Surface Pressure Measurements in Translating Tornado-Like Vortices.....	13
2.1 Introduction and background .....	13
2.2 Experimental setup.....	19
2.2.1 Tornado simulator description .....	19
2.2.2 Experimental setup and data processing .....	20
2.3 Results and discussion .....	23
2.3.1 Stationary tornado .....	24

2.3.2 Translating tornado .....	29
2.4 Conclusions .....	39
Acknowledgement .....	41
References .....	41
Chapter 3 .....	50
3 Tornado-Induced Internal Pressures on Low-Rise Buildings with Multiple Openings	50
3.1 Introduction and background .....	50
3.2 Tornado simulator description .....	53
3.3 Experimental setup.....	55
Building models and Pressure system: .....	55
Reference velocity measurements: .....	57
Opening arrangements: .....	58
Internal volume scaling:.....	59
Test cases: .....	61
3.4 Results and discussion .....	62
Internal pressure correlation .....	63
The effect of offset.....	66
The effect of building size .....	67
The effect of orientation.....	68
The effect of openings .....	69
Conclusions .....	73
Acknowledgment .....	74
References .....	74
Chapter 4 .....	80
4 Estimation of tornadic wind loads on building components and cladding as outlined in ASCE7 for straight line winds .....	80

4.1	Introduction.....	80
4.2	Component and cladding (C&C) wind load in ASCE 7-16.....	82
4.3	Reference static and dynamic pressures in calculating pressure coefficients .....	84
4.4	Methodology .....	86
4.4.1	Building Model .....	87
4.4.2	Test Cases .....	89
4.4.3	Measurement Details .....	90
4.5	Results and discussion .....	91
4.5.1	Distribution of external pressure coefficients .....	92
4.5.2	Comparison with ASCE 7-16 .....	97
4.6	Conclusions.....	103
	Acknowledgment .....	104
	References .....	104
	Chapter 5 .....	107
5	Conclusion .....	107
5.1	Summary of findings.....	108
5.2	Recommendations for future work .....	110
	Appendix A: Damage Indicators and Degree of Damage .....	111
	Curriculum Vitae .....	113

## List of Tables

Table 1.1 The Fujita scale categories (FEMA 2011).....	2
Table 2.1 Effect of removing wandering on minimum mean surface pressure values of stationary tornado.....	26
Table 3.1 Geometry and porosity ratios of leakage and dominant openings.....	59
Table 3.2 Internal volume scaling parameters .....	61
Table 3.3 Test cases .....	61
Table 3.4 Internal pressure correlation .....	65
Table 4.1 Test cases .....	89

## List of Figures

Figure 2.1 Schematic of tornado creation at WindEEE Dome .....	20
Figure 2.2 Baseplate tap distribution .....	22
Figure 2.3 Ground floor with added roughness elements at WindEEE dome .....	23
Figure 2.4 mean surface pressure deficits for all swirl ratios. The pressure deficits are normalized based on $(0.5\rho v_{ax}^2)$ .....	24
Figure 2.5 Non-dimensional mean pressure deficit contour plot for $S=0.21$ and $S=1.03$ (a) with wandering( $S=0.21$ ), (b) after removing wandering ( $S=0.21$ ), (c) with wandering( $S=1.03$ ), and (d) after removing wandering ( $S=1.03$ ). .....	27
Figure 2.6 Stationary TLV vortex structure.....	29
Figure 2.7 Effect of increasing swirl ratio on the surface pressure deficit for translating tornado-like vortices. ....	30
Figure 2.8 Effect of multiple runs on pressure deficit profile for (a) $S=0.48$ and (b) $S=0.76$ .....	31
Figure 2.9 Surface pressure deficit for Stationary ( <b>T0</b> ) and Translating ( <b>T1.5</b> ) tornado-like vortices for (a) $S=0.48$ , and (b) $S=0.76$ .....	32
Figure 2.10 Maximum central pressure deficit vs swirl ratio for stationary ( <b>T0</b> ) and translating tornado ( <b>T1.5</b> ) .....	33
Figure 2.11 Effect of tornado translation speed on ground pressure (a) $S=0.76$ , and (b) $S=0.48$ .....	34
Figure 2.12 Tornado axis inclination angle (a) Stationary tornado, (b) Translating tornado .	35
Figure 2.13 Tornado paths (a) Damage path of the Greensburg, KS tornado. Adapted from “The Greensburg, KS tornadic storm: a storm of extremes.” by L. R. Lemon, & M. Umscheid, 2008, 24th Conf. on Severe Local Storms, 2.4. and (b) at WindEEE Dome.....	37

Figure 2.14 Effect of adding roughness to the ground on translating tornado surface loading (a) $S=0.48$ , and (b) $S=0.76$ .....	39
Figure 2.15 Tornado trajectory for $S=0.48$ and $S=0.76$ for smooth and rough surfaces .....	39
Figure 3.1 Schematic sketch of tornado at WindEEE dome.....	54
Figure 3.2 Building models (a) Large building, and (b) Small building .....	55
Figure 3.3 an exploded view of the internal and external pressure taps layout and dominant openings for (a) the large building model, (b) the small building model. ....	57
Figure 3.4 Large building model with openings: (a) uniform leakage, uniform leakage with dominant opening on (b) the large wall, (c) the roof and (d) both the wall and roof .....	58
Figure 3.5 Internal volume attached to the building model underneath the turntable .....	60
Figure 3.6 Schematic of the tornado translation in the WindEEE Dome .....	63
Figure 3.7 Comparison between internal pressure and the spatial average of external pressure for uniform leakage (Small building) at (a) +RMW (as per case 4), (b) +2RMW (as per case 5), and (c) >+2RMW (as per case 6), .....	65
Figure 3.8 Effect of offset on internal pressure (Small building) for (a) $S=0.76$ (EF-2) (as per cases 1,2, and 3), (b) $S=0.48$ (EF-1) (as per cases 4,5, and 6).....	66
Figure 3.9 Effect of building size on internal pressure (uniform leakage) for (a) $S=0.76$ (EF- 2) at +RMW (as per cases 1 and 7), (b) $S=0.76$ (EF-2) at +2RMW (as per cases 2 and 8). ..	68
Figure 3.10 Effect of building orientation on internal pressure for (a) $S=0.48$ (EF-1) for the small building (as per cases 4 and 21), (b) $S=0.48$ (EF-1) for the large building (as per cases 22 and 23). ....	69
Figure 3.11 Effect of opening configuration on internal pressure for (a) $S=0.76$ (EF-2) for the large building (as per cases 9, 10 and 11), (b) $S=0.48$ (EF-1) for the large building (as per cases 12, 13 and 14), (c) $S=0.76$ (EF-2) for the large building (as per cases 15, 16 and 17), (d) $S=0.76$ (EF-2) for the small building (as per cases 18, 19 and 20).....	70

Figure 3.12 Comparison between internal pressure coefficients and APD for (a) ) $S=0.76$ (EF-2) for the large building at +2RMW (as per cases 9, 10 and 11), and (b) $S=0.76$ (EF-2) for the large building at +RMW (as per cases 15, 16 and 17). .....	72
Figure 4.1 Different zones as defined by ASCE7-16 on (a) walls and (b) roof .....	83
Figure 4.2 Components and cladding external pressure coefficients for (a) wall and (b) roof (ASCE/SEI 7-16, 2017, Figure 30.3-1 and 30.3-2A). <b>GCP</b> values for walls have been reduced by 10% for $\theta \leq 10^\circ$ .....	84
Figure 4.3: Schematic of tornado flow at WindEEE Dome (a) side view and (b) top view...	87
Figure 4.4 Building models (a) Large building, and (b) small building .....	88
Figure 4.5 Exploded views of the external pressure taps layout and for (a) the large building model, (b) the small building model. ....	88
Figure 4.6 Set of cobra probes to measure reference velocity .....	91
Figure 4.7 Contour plots of ensemble-averaged peak pressure coefficients ( <b>GCP</b> ) for the small building for $S=0.76$ at (a) +RMW (case 1), (b) +2RMW (case 2),, (c) >+2RMW (case 3), and for $S=0.48$ at (d) +RMW (case 4), (e) +2RMW (case 5), (f) >+2RMW (case 6).....	94
Figure 4.8 Surface pressure deficit of stationary tornado for (a) $S=0.76$ (EF-2 rated), and (b) $S=0.48$ (EF-1 rated) .....	94
Figure 4.9 Effect of building size on <b>GCP</b> distribution for $S=0.76$ at (a) +RMW (cases 1 and 7), (b) +2RMW (cases 2 and 8) .....	96
Figure 4.10 Effect of building orientation on <b>GCP</b> distribution at +RMW for (a) $S=0.48$ (cases 4 and 9), small building, (b) $S=0.48$ , large building (cases 10 and 11) .....	97
Figure 4.11 Building zones according to ASCE 7-16 for (a) Large building, and (b) small building .....	99
Figure 4.12 Comparison between ASCE-17 and measured external pressure coefficient ( <b>GCP</b> ) for low-rise buildings for zone 1' .....	100

Figure 4.13 Comparison between ASCE-17 and measured external pressure coefficient ( <b>GCP</b> ) for low-rise buildings for zone 1 .....	100
Figure 4.14 Comparison between ASCE-17 and measured external pressure coefficient ( <b>GCP</b> ) for low-rise buildings for zone 2 .....	101
Figure 4.15 Comparison between ASCE-17 and measured external pressure coefficient ( <b>GCP</b> ) for low-rise buildings for zone 3 .....	101
Figure 4.16 Comparison between ASCE-17 and measured external pressure coefficient ( <b>GCP</b> ) for low-rise buildings for zone 4 .....	102
Figure 4.17 Comparison between ASCE-17 and measured external pressure coefficient ( <b>GCP</b> ) for low-rise buildings for zone 5 .....	102



## List of Appendices

Appendix A: Damage Indicators and Degree of Damage

# Nomenclature

## Abbreviations

ABL	Atmospheric Boundary Layer
WindEEE	Wind Engineering Energy and Environment
TLV	Tornado-Like Vortex
DI	Damage Indicators
DOD	Degree of Damage
EF	Enhanced Fujita
TTU	Texas Tech University
ISU	Iowa State University
DOW	Doppler On Wheels
TVC	Tornado Vortex Chamber
MWD	Model WindEEE Dome
HITPR	Hardened In-Situ Tornado Pressure Recorder
PIV	Particle Image Velocimetry
GBVTD	Ground-Based Velocity Track Display
DTC	Digital Temperature Compensation
ESP	Electronically Scanned Pressure
VBD	Vortex Break Down
APD	Atmospheric Pressure Deficit

RMW	Radius of Maximum Wind
NOAA	National Oceanic and Atmospheric Administration
NIST	National Institute of Standards and Technology

### Symbols

$S$	Swirl Ratio
Re	Reynolds Number
$v_T$	Translating Velocity
$v_{tang,max}$	Maximum Tangential Velocity
$Re_r$	Radial Reynolds Number
$a$	Aspect Ratio
$h$	Inflow Depth
$r_o$	Updraft Radius
$\Gamma_{max}$	Maximum Flow Circulation
$Q$	Volumetric Flow Rate Per Unit Axial Length
$\Delta P$	Pressure Differential
$p_i$	The $i$ th Tap Static Pressure
$p_o$	The Testing Chamber' Static Pressure
$\Delta P^*$	Normalized Mean Ground Pressure Deficit
$v_{ax}$	Mean Axial Velocity

$\theta$	Inclination Angle
$C_{pi}$	Internal Pressure Coefficient
$P_{ref}$	The Ambient Pressure Outside The Test Chamber
$V_{ref}$	The Reference Velocity
$Z$	Height
$L$	Characteristic Length
$U_H$	Mean Wind Speed at Roof Height
$V_o$	Internal Volume
$\lambda_v$	Volumetric Scale
$\lambda_L$	Length Scale
$\lambda_U$	Velocity Scale
$R_{xy}$	Cross-Correlation Coefficient
$\tau$	Time Lag
$h$	Roof Height
$GC_p$	Peak External Pressure Coefficients
$G$	Gust-Effect Factor
$q_{ref}$	Reference Dynamic Pressure

## Chapter 1

### 1 Introduction and background

#### 1.1 General Introduction

For many decades, extreme wind events both synoptic and non-synoptic have been an urging subject for many researchers due to their hazardous and devastating outcomes. However, tornadoes are considered one of the most powerful storms of nature. Tornadoes are fiercely spinning columns of rising air that extend from the base of thunderstorm clouds to the ground causing a low-pressure area close to the surface layer. More than 1,000 tornadoes are reported in the United States per annum resulting in over one billion dollars of damage (NOAA, 2012). Generally, tornadoes, on average, are 150 m wide and can travel on the ground for 8.0 km (Lyons, 1997) with a translational speed of 9 m/s to 18 m/s (Ying and Chang, 1990).

In 1971, Tetsuya Fujita, a University of Chicago meteorologist, introduced the “Fujita scale (F-scale)”. The Fujita scale (F-Scale) is a scale that is used to rate tornado intensity by investigating the tornado-affected areas and measuring the extent of the destruction. Although the F-scale was considered a tremendous shift in classifying tornadoes, it has some limitations. Some of the main limitations are the absence of incontrovertibly defined Damage Indicators (DI) and the lack of a direct correlation between the resulted damage of tornado and the wind speed. For more information about the Damage Indicators (DI) and the Degree of Damage (DOD) associated with the EF-scale, (See Appendix A). These limitations resulted in an overestimation of the wind speeds associated with each F-category and inconsistency of tornado rating. Thus, a new scale, the Enhanced Fujita scale (EF-scale), was proposed by McDonald and Mehta in 2006 (McDonald and Mehta 2006). The EF-scale was used in the United States in 2007 while Environment Canada started using it in 2013. Table (1.1) shows a comparison between F-scale and EF-scale in terms of velocity range (FEMA 2011).

**Table 1.1 The Fujita scale categories (FEMA 2011)**

Fujita Scale	Fujita Scale: 3-Second Gust (mph)	EF Scale	EF Scale: 3-Second Gust (mph)
F0	45–78	EF0	65–85
F1	79–117	EF1	86–110
F2	118–161	EF2	111–135
F3	162–209	EF3	136–165
F4	210–261	EF4	166–200
F5	262–317	EF5	Over 200

mph = miles per hour; EF = Enhanced Fujita

## 1.2 Motivation and objectives

Tornadoes are considered one of the most devastating and destructive storms ever known to date. They produce the highest wind speeds that can reach up to 1000 km/hr (Solari et al. 2015). 2011 had witnessed the highest death toll in the current century with 553 fatalities, where about 30% of this percentage (161 deaths) was reported after the EF-5 rated tornado hit Joplin, Missouri, United States on May 22, 2011, that marked this year as the deadliest year of tornadoes since 1936 (Kuligowski et al. 2014). This tragic loss of life and properties led to increased attention and detailed post-damage surveys about these fierce storms and their associated damage. A worldwide call for a change in the design of the buildings to withstand such storms had risen. The reason behind the destruction of the structures is due to exceeding the allowable design wind loads stated in the building codes, e.g., ASCE 7-16 (ASCE/SEI, 2016) or NBCC 2015 (NRCC, 2015) that only depend on Atmospheric Boundary Layer flows (ABL) in deducing the pressure coefficients. Thus, a need for a better characterization of the tornado surface loading, where most of the buildings lie, as well as the tornado-structure interaction in terms of internal and external pressure loading is pivotal. This will eventually help in re-evaluating the recommended wind loads in the building codes that will lead to tornado-resilient communities.

Tornado flow-field studies had started as early as the late nineteenth century. Since then, numerical, experimental, and full-scale studies have been emerging sequentially as the need to understand the tornadic flow and their associated damage necessitate such research.

Field tornado measurements started in the mid-fifties when barometers and weather stations were used as a first attempt to record tornadoes by realizing the change in temperature, pressure, and relative humidity (Tepper and Eggert 1956). More advancements took place in full-scale measurement instrumentations where the Doppler radars and Doppler on wheels (DOW) were exploited to better characterize tornadoes (e.g. Wurman et al. 1996; Wurman et al. 1997; Bluestein et al. 2004; Lee and Wurman 2005; Wakimoto et al. 2012). While the majority of field measurements were focused on wind velocity, very few studies employed ground pressure instrumentations where mobile mesonets and Hardened In-Situ Tornado Pressure Recorder (HITPR) probes were utilized to record velocity and pressure data (Lee and Samaras 2004; Wurman and Samaras 2004; Karstens et al. 2010). Although field measurements are reliable, they have limitations in lower heights as the radar is placed away from obstacles in the low ground levels. These limitations as well as the complex preparations and the unpredictable tornado trajectories made the field measurements challenging.

On a parallel path, Numerical simulations were considered a reasonable method in understanding tornadic flow-field if validated with available full-scale or experimental results (e.g. Lewellen et al. 1997; Nolan 2005; Natarajan and Hangan 2012; Liu and Ishihara 2015; Nasir and Bitsuamlak 2018; Nolan et al. 2017; Gairola and Bitsuamlak 2019). The effect of translation and roughness were studied where the translation was found to develop some secondary vortices (Diamond and Wilkins 1984) while roughness resulted in decreasing the tornado vortex diameter in some studies (Diamond and Wilkins 1984; Zhang and Sarkar 2008) or increasing the vortex diameter (Dessens 1972; and Natarajan and Hangan 2012). These opposing results highlight the role of validation with field measurements or experimental results.

Ward (1972) started a new era of tornadic flow by introducing the famous Ward-type Tornado Vortex Chamber (TVC) at the National Severe Storm Laboratory in Oklahoma. Ward (1972) examined the structure of tornado-like vortices and compared his results with full-scale measurements where he observed the sensitivity of the tornado vortex to the tornado simulator's boundaries. Thereafter, multifold tornado vortex chambers (TVC's) were built to aid in understanding the tornado flow-field structure and interaction with

buildings (Church et al. 1979; Mishra et al. 2005; Haan et al. 2008; Hangan 2014). Albeit the pioneering efforts exerted in understanding the tornado vortex structure inside laboratories, they have some limitations. Most of the simulators do not have the capability to produce translating tornado vortex (Ward 1972; Church et al. 1979; Mishra et al. 2005; Hashemi Tari et al., 2010). In addition, the available space resolution is not sufficient in some TVCs to provide acceptable tornado loading on structures (Ward, 1972; Church et al., 1979; Snow, 1982).

Near-surface examination of tornado-like vortices had been reported in the literature (Tari et al. 2010; Zhang and Sarkar 2012; Refan et al. 2014; Tang et al 2018; Refan and Hangan 2018). Despite all the efforts in characterizing the tornadic flow field in these studies, all the studies were confined to stationary tornadoes without accounting for the translation motion of tornadoes that resemble the real tornadoes.

Wandering behavior of the tornado vortex is observed inside tornado simulators (e.g. Baker 1981; Zhang and Sarkar 2012; Ashton et al 2019; Refan and Hangan 2018; Karami et al. 2019). Ashton et al. (2019) studied the effect of tornado wandering on the TLV structure utilizing the data obtained from the Model WindEEE Dome (MWD). An error percentage reaching 17% was quantified in the velocity flow-field. They proposed two methods to eliminate the wandering effect from the resulted velocity flow-field where the first technique relied on re-centering the vortex based on minimum pressure, while the other method utilized a deconvolution approach.

Tornado-structure interaction was investigated experimentally in the literature ranging between external pressure loadings (e.g. Ho et al. 2005; Mishra et al. 2008b; Sengupta et al. 2008; Haan et al. 2010; Hu et al. 2011; Razavi and Sarkar 2018) and internal pressure studies (e.g. Sarkar and Kikitsu 2009; Letchford et al. 2015; Wang et al. 2018; Roueche et al. 2020). Sarkar et al. (2006) investigated the tornadic loading on a high-rise building and deduced that tornado intensity of F2 or higher would surpass the permissible design loads stated in ASCE 7-02 by a factor of 1.8. Haan et al. (2010) utilized a low-rise gable-roofed building in their study where he found that the peak uplift forces exceeded the building code ASCE 7-05 by factors of (1.8-3.2). These studies concentrated on evaluating the



maximum uplift forces without delving into the various building zones that are the base in the components and claddings design as stated in ASCE 7-16 (ASCE/SEI 7-16, 2017). On the other hand, very few internal pressure studies exist in the literature, unlike external pressure loadings. Sarkar and Kikitsu (2009) started one of the first attempts to quantify the internal pressures in tornado flow-field in the ISU tornado simulator at Iowa State University utilizing a dominant opening. They deduced that the internal pressure is a function of porosity and opening configuration. Letchford et al. (2015) studied the effect of porosity and dominant openings on the induced internal pressure loadings for a low-rise building model utilizing a stationary tornado simulator, the VorTECH simulator at Texas Tech University. Their study revealed that a dominant opening in the windward wall produced the largest peak internal pressures irrespective of the porosity. Most recently, Roueche et al. (2020) proposed a numerical model that predicts the internal pressure based on external pressures. Comparing stationary tornado and ABL induced loads they found that building corners experience 13% higher wind loads than ABL flow.

After reviewing the previous studies regarding the tornado-like vortices characteristics and their impact on low-rise buildings, some gaps in the literature initiated the present study. Some uncertainties in the parametric scaling of most of the simulators may lead to some questionable wind loads (Baker and Sterling, 2019). In addition, most near-surface studies adopted stationary tornado concepts, due to limited capabilities of the utilized tornado simulators, without giving attention to translating tornadoes that are more representable of field tornadoes. Very few studies examined the surface roughness effect on tornadic flow field due to the inexistence of a standardized representation of roughness in tornadic flows. The limited size of most of the tornado simulators does not provide the appropriate spatial resolution for the aerodynamic loading. Very few tornadic wind loading studies adopted translating TLV (Sarkar and Kikitsu 2009; Rajasekharan et al. 2019) where the translation speed was in the lower range ( $\leq 0.61$  m/s). Also, most of the studies that implemented comparisons with the standard building codes did not delve into the associated peak wind loads for each building zone which is a key point in the design of components and claddings as outlined in the ASCE 7-16 (ASCE/SEI 7-16, 2017) building code.

The main objectives of the thesis are:

1. Characterizing the tornado-like vortices, stationary and translating, structure utilizing high-resolution ground pressure measurements.
2. Addressing wandering, tilting, and veering motions in simulated tornado-like vortices (TLVs) for a wide range of swirl ratios and two surface roughness.
3. Investigating the induced internal and external pressures in generic low-rise buildings under translating tornado-like vortices (TLVs).
4. Comparison with ASCE 7-16 code to assess its applicability for tornadic flow.

### 1.3 Scope of the Thesis

The present thesis is written in the "integrated-article" format as per Western University's thesis regulations. The thesis has five chapters out of which three are journal articles.

Chapter 1 outlines a general introduction and background about tornado flow-field and the motivation behind the current study. Chapter 2 provides a comprehensive study about stationary and translating tornado-like vortices (TLV) based on ground pressures.

Tornado vortex wandering, tilting, and veering motions are analyzed. Chapter 3 focuses on the induced internal pressures under translating tornado-like vortices (TLV) on two low-rise building models. This study expands the knowledge about internal pressures, their variability with different opening configurations, and their impact on the properties. Chapter 4 investigates the external pressure loadings on two low-rise building models as well as a comparison between the peak pressures and the latest ASCE code. Chapter 5 portrays the conclusions derived from the present study and recommendations for future work.

## References

- Ashton, R., Refan, M., Iungo, G. V., & Hangan, H. (2019). Wandering corrections from PIV measurements of tornado-like vortices. *Journal of Wind Engineering and Industrial Aerodynamics*, 189(February), 163–172. <https://doi.org/10.1016/j.jweia.2019.02.010>
- Baker, C., & Sterling, M. (2019). Are Tornado Vortex Generators fit for purpose?. *Journal of Wind Engineering and Industrial Aerodynamics*, 190, 287-292. <https://doi.org/10.1016/j.jweia.2019.05.011>
- Bluestein, H. B., Weiss, C. C., & Pazmany, A. L. (2004). The vertical structure of a tornado near Happy, Texas, on 5 May 2002: High-resolution, mobile, W-band, doppler radar observations. *Monthly Weather Review*, 132(10), 2325–2337. [https://doi.org/10.1175/1520-0493\(2004\)132<2325:TVSOAT>2.0.CO;2](https://doi.org/10.1175/1520-0493(2004)132<2325:TVSOAT>2.0.CO;2)
- Church, C. & Snow, John & Baker, G. & Agee, Ernest. (1979). Characteristics of Tornado-Like Vortices as a Function of Swirl Ratio: A Laboratory Investigation. *Journal of Atmospheric Sciences*. 36. 1755-1776. [https://doi.org/10.1175/1520-0469\(1979\)036<1755:COTLVA>2.0.CO;2](https://doi.org/10.1175/1520-0469(1979)036<1755:COTLVA>2.0.CO;2)
- Dessens J. Jr. (1972) Influence of ground roughness on tornadoes: a laboratory simulation. (1972). *Journal of Applied Meteorology* 11(1):72–75. [https://doi.org/10.1175/1520-0450\(1972\)0112.0.CO;2](https://doi.org/10.1175/1520-0450(1972)0112.0.CO;2)
- Diamond, C. J., & Wilkins, E. M. (1984). Translation effects on simulated tornadoes. *Journal of the atmospheric sciences*, 41(17), 2574-2580. [https://doi.org/10.1175/1520-0469\(1984\)041<2574:TEOST>2.0.CO;2](https://doi.org/10.1175/1520-0469(1984)041<2574:TEOST>2.0.CO;2)
- Gairola, A., & Bitsuamlak, G. (2019). Numerical tornado modeling for common interpretation of experimental simulators. *Journal of Wind Engineering and Industrial Aerodynamics*, 186, 32-48. <https://doi.org/10.1016/j.jweia.2018.12.013>
- Haan Jr, F. L., Sarkar, P. P., & Gallus, W. A. (2008). Design, construction and performance of a large tornado simulator for wind engineering applications. *Engineering Structures*, 30(4), 1146-1159. <https://doi.org/10.1016/j.engstruct.2007.07.010>

- Hangan, H. (2014). The wind engineering energy and environment (WindEEE) dome at western university, Canada. *Wind Engineers, JAWE*, 39(4), 350-351.  
<https://doi.org/10.5359/jawe.39.350>
- Hangan, H., Refan, M., Jubayer, C., Parvu, D., & Kilpatrick, R. (2017). Big data from big experiments. The WindEEE dome. In *Whither Turbulence and Big Data in the 21st Century?* (pp. 215-230). Springer, Cham. [https://doi.org/10.1007/978-3-319-41217-7\\_12](https://doi.org/10.1007/978-3-319-41217-7_12)
- Ho, T. C. E., Surry, D., Morrish, D., & Kopp, G. A. (2005). The UWO contribution to the NIST aerodynamic database for wind loads on low buildings: Part 1. Archiving format and basic aerodynamic data. *Journal of Wind Engineering and Industrial Aerodynamics*, 93(1), 1-30. <https://doi.org/10.1016/j.jweia.2004.07.006>
- Hu, H., Yang, Z., Sarkar, P., & Haan, F. (2011). Characterization of the wind loads and flow fields around a gable-roof building model in tornado-like winds. *Experiments in Fluids*, 51(3), 835–851. <https://doi.org/10.1007/s00348-011-1102-6>
- Karami, M., Hangan, H., Carassale, L., & Peerhossaini, H. (2019). Coherent structures in tornado-like vortices. *Physics of Fluids*, 31(8), 085118.  
<https://doi.org/10.1063/1.5111530>
- Karstens, C. D., Samaras, T. M., Lee, B. D., Gallus Jr, W. A., & Finley, C. A. (2010). Near-ground pressure and wind measurements in tornadoes. *Monthly Weather Review*, 138(7), 2570-2588. <https://doi.org/10.1175/2010MWR3201.1>
- Kuligowski, E. D., Lombardo, F. T., Phan, L. T., Levitan, M. L., & Jorgensen, D. P. Progress Report, National Institute of Standards and Technology (NIST) Technical Investigation of the May 22, 2011, Tornado in Joplin, Missouri.
- Lee, J. J., Samaras, T., & Young, C. R. (2004, October). Pressure measurements at the ground in an F-4 tornado. In *Preprints, 22d Conf. on Severe Local Storms*, Hyannis, MA, Amer. Meteor. Soc., 15.3.

Lee, W. C., & Wurman, J. (2005). Diagnosed three-dimensional axisymmetric structure of the Mulhall tornado on 3 May 1999. *Journal of the atmospheric sciences*, 62(7), 2373-2393. <https://doi.org/10.1175/JAS3489.1>

Letchford, C., Levitz, B., & James, D. (2015). Internal pressure dynamics in simulated tornadoes. In *Structures Congress 2015* (pp. 2689-2701).

Lewellen, W. S., Lewellen, D. C., & Sykes, R. I. (1997). Large-eddy simulation of a tornado's interaction with the surface. *Journal of the atmospheric sciences*, 54(5), 581-605. [https://doi.org/10.1175/1520-0469\(1997\)054<0581:LESOAT>2.0.CO;2](https://doi.org/10.1175/1520-0469(1997)054<0581:LESOAT>2.0.CO;2)

Liu, Z., & Ishihara, T. (2015). Numerical study of turbulent flow fields and the similarity of tornado vortices using large-eddy simulations. *Journal of Wind Engineering and Industrial Aerodynamics*, 145, 42-60. <https://doi.org/10.1016/j.jweia.2015.05.008>

Lyons, W. A. (1997). *The handy weather answer book* (pp. 175-200). Visible Ink Press.

McDonald, J., Mehta, K. C., & Mani, S. (2006). A recommendation for an enhanced Fujita scale (EF-scale), revision 2. *Texas Tech University Wind Science and Engineering Research Center Rep.*

Mishra, A. R., James, D. L., & Letchford, C. W. (2008). Physical simulation of a single-celled tornado-like vortex, part A: flow field characterization. *Journal of Wind Engineering and Industrial Aerodynamics*, 96(8-9), 1243-1257. <https://doi.org/10.1016/j.jweia.2008.02.063>

Mishra, A. R., James, D. L., & Letchford, C. W. (2008). Physical simulation of a single-celled tornado-like vortex, Part B: Wind loading on a cubical model. *Journal of Wind Engineering and Industrial Aerodynamics*, 96(8-9), 1258-1273. <https://doi.org/10.1016/j.jweia.2008.02.027>

Nasir, Z., & Bitsuamlak, G. T. (2018). Topographic effects on tornado-like vortex. *Wind and Structures*, 27(2), 123-136. <https://doi.org/10.12989/was.2018.27.2.123>

Natarajan, D., & Hangan, H. (2012). Large eddy simulations of translation and surface roughness effects on tornado-like vortices. *Journal of Wind Engineering and Industrial Aerodynamics*, 104, 577-584. <https://doi.org/10.1016/j.jweia.2012.05.004>

NBCC (National Building Code of Canada). (2015). National building code of Canada.

NOAA National Centers for Environmental Information, State of the Climate: Tornadoes for Annual 2011, published online January 2012, retrieved on March 14, 2018 from <https://www.ncdc.noaa.gov/sotc/tornadoes/201113>.

Nolan, D. S. (2005). A new scaling for tornado-like vortices. *Journal of the atmospheric sciences*, 62(7), 2639-2645. <https://doi.org/10.1175/JAS3461.1>

Nolan, D. S., Dahl, N. A., Bryan, G. H., & Rotunno, R. (2017). Tornado vortex structure, intensity, and surface wind gusts in large-eddy simulations with fully developed turbulence. *Journal of the Atmospheric Sciences*, 74(5), 1573-1597. <https://doi.org/10.1175/JAS-D-16-0258.1>

Rajasekharan, S. G., Masahiro, M., & Tamura, Y. (2019). Vulnerability of roof and building walls under a translating tornado like vortex. *Frontiers in built environment*, 5, 53. <https://doi.org/10.3389/fbuil.2019.00053>

Razavi, A., & Sarkar, P. P. (2018). Tornado-induced wind loads on a low-rise building: Influence of swirl ratio, translation speed and building parameters. *Engineering Structures*, 167, 1-12. <https://doi.org/10.1016/j.engstruct.2018.03.020>

Refan, M., & Hangan, H. (2018). Near surface experimental exploration of tornado vortices. *Journal of Wind Engineering and Industrial Aerodynamics*, 175, 120-135. <https://doi.org/10.1016/j.jweia.2018.01.042>

Roueche, D. B., Prevatt, D. O., & Haan, F. L. (2020). Tornado-induced and straight-line wind loads on a low-rise building with consideration of internal pressure. *Frontiers in built environment*, 6, 18. <https://doi.org/10.3389/fbuil.2020.00018>

Sarkar, P. P., & Kikitsu, H. (2009). Experimental studies on internal pressure and debris strike for improved tornado induced loads of low-rise buildings. Proceedings of the 41st US-Japan Panel on Wind and Seismic Effects, Tsukuba, Japan.

Sarkar, P. P., Haan, Jr, F. L., Balaramudu, V., & Sengupta, A. (2006). Laboratory simulation of tornado and microburst to assess wind loads on buildings. In *Structures Congress 2006: Structural Engineering and Public Safety* (pp. 1-10).

Sengupta, A., Haan, F. L., Sarkar, P. P., & Balaramudu, V. (2008). Transient loads on buildings in microburst and tornado winds. *Journal of Wind Engineering and Industrial Aerodynamics*, 96(10-11), 2173-2187. <https://doi.org/10.1016/j.jweia.2008.02.050>

Solari, G., Burlando, M., De Gaetano, P., & Repetto, M. P. (2015). Characteristics of thunderstorms relevant to the wind loading of structures. *Wind Struct*, 20(6), 763-791.

Tari, P. H., Gurka, R., & Hangan, H. (2010). Experimental investigation of tornado-like vortex dynamics with swirl ratio: The mean and turbulent flow fields. *Journal of Wind Engineering and Industrial Aerodynamics*, 98(12), 936-944.  
<https://doi.org/10.1016/j.jweia.2010.10.001>

Tepper, M., & Eggert, W. E. (1956). Tornado proximity traces. *Bulletin of the American Meteorological Society*, 37(4), 152-159. <https://doi.org/10.1175/1520-0477-37.4.152>

The Federal Emergency Management Agency (FEMA), TORNADO OUTBREAK OF 2011, MITIGATION ASSESSMENT TEAM REPORT, retrieved on December 01, 2020 from [https://www.fema.gov/media-library-data/20130726-1827-25045-5594/tornado\\_mat\\_chapter2\\_508.pdf](https://www.fema.gov/media-library-data/20130726-1827-25045-5594/tornado_mat_chapter2_508.pdf)

Wakimoto, R. M., Stauffer, P., Lee, W. C., Atkins, N. T., & Wurman, J. (2012). Finescale structure of the LaGrange, Wyoming, tornado during VORTEX2: GBVTD and photogrammetric analyses. *Monthly weather review*, 140(11), 3397-3418.  
<https://doi.org/10.1175/MWR-D-12-00036.1>

Wang, J., Cao, S., Pang, W., & Cao, J. (2018). Experimental study on tornado-induced wind pressures on a cubic building with openings. *Journal of Structural Engineering*, 144(2), 04017206. [https://doi.org/10.1061/\(ASCE\)ST.1943-541X.0001952](https://doi.org/10.1061/(ASCE)ST.1943-541X.0001952)

Ward, N. B. (1972). The exploration of certain features of tornado dynamics using a laboratory model. *Journal of the Atmospheric Sciences*, 29(6), 1194-1204. [https://doi.org/10.1175/1520-0469\(1972\)029<1194:TEOCFO>2.0.CO;2](https://doi.org/10.1175/1520-0469(1972)029<1194:TEOCFO>2.0.CO;2)

Wurman, J., & Samaras, T. (2004). Comparison of in-situ pressure and DOW Doppler winds in a tornado and RHI vertical slices through 4 tornadoes during 1996–2004. Preprints, 22nd Conf. on Severe Local Storms, Hyannis, MA, Amer. Meteor. Soc., 15.4. [Available online at <http://ams.confex.com/ams/pdfpapers/82352.pdf>.]

Wurman, J., Straka, J. M., & Rasmussen, E. N. (1996). Fine-scale Doppler radar observations of tornadoes. *Science*, 272(5269), 1774-1777. <https://doi.org/10.1126/science.272.5269.1774>

Wurman, J., Straka, J., Rasmussen, E., Randall, M., & Zahrai, A. (1997). Design and deployment of a portable, pencil-beam, pulsed, 3-cm Doppler radar. *Journal of Atmospheric and Oceanic Technology*, 14(6), 1502-1512. [https://doi.org/10.1175/1520-0426\(1997\)014<1502:DADOAP>2.0.CO;2](https://doi.org/10.1175/1520-0426(1997)014<1502:DADOAP>2.0.CO;2)

Ying, S. J., & Chang, C. C. (1970). Exploratory model study of tornado-like vortex dynamics. *Journal of the Atmospheric Sciences*, 27(1), 3-14.

Zhang, W., & Sarkar, P. P. (2008). Effects of ground roughness on tornado like vortex using PIV. In *Proceedings of the AAWE workshop*, Vail, CO.

Zhang, W., & Sarkar, P. P. (2012). Near-ground tornado-like vortex structure resolved by particle image velocimetry (PIV). *Experiments in fluids*, 52(2), 479-493. <https://doi.org/10.1007/s00348-011-1229-5>



## Chapter 2

### 2 Surface Pressure Measurements in Translating Tornado-Like Vortices

#### 2.1 Introduction and background

Tornadoes are considered one of the most violent and destructive storms. Nearly over 1,000 tornadoes are reported annually in the United States and their damages can exceed over one billion dollars (NOAA, 2012). One of the deadliest tornadoes on record was the Joplin tornado on May 22, 2011, an EF-5 rated tornado that caused 158 fatalities, more than 1,000 injuries, and left nearly 7,500 residential structures partially or totally collapsed (NWS, 2011). This demonstrates the severity of tornadoes and the vulnerability of buildings under these fierce storms. The destruction of structures due to tornadic hits is associated with exceeding the permissible design wind loads in building codes, e.g., ASCE 7-16 (ASCE/SEI, 2016) or NBCC 2015 (NRCC, 2015) which rely solely on the atmospheric boundary layer (ABL) flow-fields in calculating pressure coefficients. This destruction can be minimized substantially by designing the buildings to withstand tornadoes up to EF-2 rated tornadoes which occupy 95% of tornado hits in the United States according to NOAA. In order to achieve this, a rigorous analysis of the induced pressures and the resulting loading on structures is needed. A key component in this analysis is the characterization of tornadic ground pressures for various tornado intensities, translational speeds, and surface roughness. While full scale, numerical and experimental studies of tornado induced pressures have been performed (e.g. Lee and Wurman 2005; Natarajan and Hangan 2012; Mishra et al. 2005), there are gaps in understanding the effects of translation and roughness of TLV as well as their relation to tornado surface trajectories and wandering.

Owing to the difficulty to predict tornado onset, their probable trajectory, and the adversity of implementing measuring instruments of tornado flow-field near the ground, very few field tornado measurements have been reported in the literature. Field tornado measurements have seen developments since their earliest attempts utilizing weather stations and barometers (Tepper and Eggert 1956; Fujita 1958). Doppler radars were later employed to explore tornado characteristics (Wurman et al. 1996; Wurman and Gill 2000;

Wurman 2002; Bluestein et al. 2004; Lee and Wurman 2005; Alexander and Wurman 2005a, 2005b; Wakimoto et al. 2011; Wakimoto et al. 2012). By 1995, the Doppler On Wheels (DOW) was introduced which permitted a safer environment for scientists to record data (Wurman et al. 1997). Moreover, very few studies about ground pressure measurements were accomplished due to the difficulty and challenges in setting up the instruments in the unpredictable path of the tornado (Lee and Samaras 2004; Wurman and Samaras 2004; Karstens et al. 2010). Hardened In-Situ Tornado Pressure Recorder (HITPR) probes and mobile mesonet were utilized in those studies to obtain pressure and velocity measurements. Furthermore, the signature of the tornado on the ground was reported in most of the field studies utilizing satellite images and tornado damage on the ground, where the tornado path in most of the cases veers in a curved path rather than a straight-line path (Wakimoto et al. 2003; Lemon and Umscheid 2008; Karstens et al. 2010; Wurman and Gill 2010). Lee et al. (2004) deployed three conical-shaped HITPR probes in the path of an F-4 tornado in Manchester, SD to measure the tornado loading on the ground, temperature, wind speed, and humidity. They deduced that the tornado path is curved rather than a straight line and that the pressure deficit is not perfectly symmetrical. Moreover, they compared the pressure deficit profile with two analytical models, Rankine and Burgers-Rott models, where the latter proved to provide better agreement. Karstens et al. (2010) utilized HITPR, mobile mesonets, and video probes in nine tornado events since 2002 to reveal the near-ground characteristics of tornadoes in terms of pressure deficits, and in some cases velocity profiles as well. They revealed the structure of the nine tornado volumes and found that they are ranging between single-celled, double-celled, and multiple-celled tornadoes. They also calculated the translation speed of all nine events and analyzed the tornado path using visualization, video probes, and radar images. Albeit the reliability and robustness of field tornado measurements in characterizing tornado flow-field, the measurements are confined to higher heights above most of the vital structures, particularly low-rise buildings. This is because the radar should be positioned distantly above all the obstacles to provide reliable data. These challenges associated with the field measurements lead to the rising of experimental work using tornado vortex chambers and numerical simulations in parallel with the hard-to-accomplish field studies.

Numerical simulations have been broadly used by many researchers due to their adjustability and lower cost compared to experimental and field studies and have been improved through the years (e.g. Lewellen et al. 1997; Nolan and Farrell 1999; Nolan 2005; Ishihara et al. 2011; Natarajan and Hangan 2012; Liu and Ishihara 2015, 2016; Nasir and Bitsuamlak 2018; Nolan et al. 2017; Gairola and Bitsuamlak 2019). Numerical studies covered different topics exploring the stationary and translating tornadic flow field, examining tornado-structure interaction, and tornadic post-damage studies. Tornado translation was found to create secondary vortices (e.g. Diamond and Wilkins 1984). Also, the effect of roughness was investigated in some studies that provided contradicting results regarding the vortex diameter either decreasing with increasing roughness (Diamond and Wilkins 1984; Zhang and Sarkar 2008) or increasing with increasing roughness (Dessens 1972; Leslie 1977; and Natarajan and Hangan 2012). These contradicting results are indicative of the need to validate numerical simulations against laboratory or where possible field measurements.

Laboratory simulations of tornado-like vortices have been started since the early seventies when Ward (1972) built the first tornado simulator. Ward (1972) explored tornado features by comparing laboratory results with field tornadoes and found that the radial momentum flux is a vital factor in producing tornadoes and that the vortex is very sensitive to the geometrical parameters of the simulator. The simulator's main drawbacks were its limited access to the vortex chamber due to its small size which did not allow adding appropriate-sized building models for studying tornado-structure interaction and that it did not support tornado translation. Subsequently, several Tornado Vortex Chambers (TVC's) have been constructed to identify and examine the aerodynamic behavior of tornado-like flows (Church et al. 1979; Mishra et al. 2005; Haan et al. 2008; Hangan 2014). Although laboratory simulation was adopted by many researchers who performed vast advancements for better characterization of tornado flow-field, it has some restrains. Most of the tornado simulators lack the ability to create the translational motion of simulated tornadoes (Ward 1972; Church et al. 1979; Mishra et al. 2005; Tari et al., 2010). Moreover, the limited size of most of the tornado simulators confines the ongoing research as it does not provide an adequate resolution for measuring the tornadic loads on buildings (Ward, 1972; Church et al., 1979; Snow, 1982). Posterior efforts were exerted to investigate the pressure loadings

on different structures (e.g. Mishra et al. 2008b; Haan et al. 2010; Kikitsu and Sarkar 2011; Hu et al. 2011; Thampi et al. 2011; Rajasekharan et al. 2013; Case et al. 2014). However, there are some uncertainties about the geometric and the velocity scaling of most simulators which have a direct effect on the aerodynamic loading (Baker and Sterling, 2019).

Tari et al. (2010) conducted experiments in a small tornado vortex simulator (TVS) at Western University, Canada to investigate the swirl ratio effects on tornadic flow characteristics. They concluded that the core radius, the tangential, and radial velocities rise with increasing swirl ratio. In addition, the vortex touchdown stage recorded the highest turbulent kinetic energy. Zhang and Sarkar (2012) investigated the near-ground flow-field of stationary tornado-like vortices using PIV system. They found that wandering affected the results, particularly for lower swirl ratios and that the intensified mean flow in collaboration with high turbulence near the ground and large pressure deficit would have a prominent role in buildings' destruction. Nevertheless, this investigation was circumscribed to lower swirl ratios ( $S < 0.3$ ), and the radial Reynolds number range was debatable. Refan et al. (2014) utilized Particle Image Velocimetry (PIV) in the Model WindEEE Dome (MWD) to investigate the TLV structure and compared the results with full-scale data utilizing the Ground-Based Velocity Track Display (GBVTD) method. They deduced the geometric scale and the equivalent swirl ratio of tornadoes in MWD and found that the MWD is capable of reproducing tornadoes equivalent to EF0 to EF3 tornadoes in field tornadoes. Tang et al. (2018) carried out experiments in the VorTECH tornado simulator at Texas Tech University. They studied the mean and turbulent characteristics of stationary tornado-like vortices using cobra probes and omniprobes for velocity measurements and static pressure taps on the ground for surface loading calculations. It was revealed that the fluctuating pressure widely contributes to the tornado loading and that the pressure deficit has a good agreement with field tornadoes. Refan and Hangan (2018) explored the characteristics of stationary tornado-like vortices close to the ground over a broad range of swirl ratios using Particle Image Velocimetry (PIV) and surface pressure measurements. They deduced that wandering behavior is more pronounced at low swirl ratios and that the tornadic near-surface pressures become independent of the radial Reynolds number for  $Re > 4.5 \times 10^4$ .

All the efforts in examining the near-surface of tornado-like vortices have been concentrated on stationary tornadoes (Tari et al. 2010; Zhang and Sarkar 2012; Refan et al. 2014; Tang et al. 2018; Refan and Hangan 2018). Hence, studying the structure of translating tornado-like vortices close to the ground, where the majority of structures lie, is crucial as this represents the actual behavior of real tornadoes.

In real tornadoes, the ratio between the translation velocity and the maximum tangential velocity varies in the range of 0.03 to 5 (Lombardo et al. 2015; Refan et al. 2017; Rhee and Lombardo 2018). The lack of the ability to produce a translation in most of the tornado simulators resulted in few experimental studies about translating tornadoes at relatively reduced translational speeds (e.g., Haan et al. 2010; Sengupta et al. 2006, 2008; Wang et al. 2016). Haan et al. (2010) studied experimentally the effect of translating tornadic flow ( $v_{translating} \leq 0.61$ ) on a one-story, gable-roofed building and compared it with ABL flow. They reported that translation resulted in an inclination of the vortex axis towards translation direction. However, they did not explain this phenomenon in detail. Sengupta et al. (2008) explored the difference between simulating stationary and translating tornado-like-vortices utilizing LES on a cubic building and compared it to experimental results. They deduced that tornadic loading of F2 intensity or higher exceeded the ASCE 7-05. Most of the translating tornado studies were focused on the loading on the buildings without delving into the characteristics of the translating tornado structure near the ground. Hence, more detailed research needs to be performed to understand the characteristics of the translating tornadoes near the surface. This will provide a better understanding of the tornadic hit's outcomes in this critical region where most of the structures exist and will lead to building more tornado-resilient communities.

Although reproducing tornadoes in tornado simulators proved to be a robust method, the resulting tornadic swirl is affected by the wandering behavior of the vortex (Baker 1981; Snow and Lund 1997; Zhang and Sarkar 2012; Ashton et al. 2019; Refan and Hangan 2018; Karami et al. 2019). Ashton et al. (2019) explored the wandering behavior of tornado-like vortices in tornado simulators using the data obtained from the Model WindEEE Dome (MWD). It was concluded that the extent of wandering could produce an error as high as 17%. The necessity of removing the wandering effect from the time-averaged velocity field

was emphasized and two techniques were proposed to remove the wandering effect; one, re-centering the vortex by detecting the vortex center, and two, using the deconvolution method. The first method was reported to provide more rigorous results.

Most of the previous experimental studies were performed over smooth ground. Few studies adopted rough surfaces that may represent different exposures (e.g. Dessens 1972; Zhang and Sarkar 2008; Matsui and Tamura 2009; Fleming et al. 2013; Wang et al. 2017). Moreover, numerical simulations of the effect of ground roughness on tornado structure were performed (Natarajan and Hangan 2012; Liu and Ishihara 2016). Wang et al. (2017) found that the radial and vertical velocity fluctuations in tornadic flow are influenced by surface roughness and that introducing roughness resulted in transitioning to a lower swirl ratio. Generally, previous studies revealed that increasing roughness has a similar effect to decreasing the swirl ratio on the mean flow-field, unlike few studies that showed the reverse effect (e.g. Fleming et al. 2013). Despite all the efforts in the literature, a lack of a rigorous standardization of roughness in tornadic flow and pressure deficit dominated TLV flows led to high uncertainty in the results. More research needs to be accomplished for better characterization of surface roughness in tornado simulators.

The state-of-the-art tornado simulator, the WindEEE dome, is capable of producing a wide range of swirl ratios of tornado-like vortices utilizing their 4.5 m updraft diameter and around 4 m height (Hangan 2014; Hangan et al. 2017a, 2017b). This large-scale simulator can provide high spatial resolution for near-ground measurements. It is considered one of the best performing simulators as it accounts for geometric similarity based on multiple length scales as well as dynamic similarity represented by the high Reynolds number (Baker and Sterling, 2019). Therefore, ground surface and structural loadings can be explored adequately.

In this study, ground pressures analysis for stationary as well as translating tornado-like vortices was carried out over a wide range of swirl ratios ( $S=0.21$  to  $S=1.03$ ). The effect of variation of tornado translational speed reaching up to 1.5 m/s, (or  $v_T/v_{tang,max} \leq 0.2$ ) for the first time in tornado simulators, was investigated in terms of ground pressure distributions, and TLV trajectories. Moreover, a preliminary study of surface roughness

sequel on translating tornado-like vortices structure was performed. Finally, the effects of both translation speed and roughness on tornado tilting, veering, and wandering have been examined for the first time.

## 2.2 Experimental setup

### 2.2.1 Tornado simulator description

The WindEEE dome is a novel three-dimensional wind testing chamber that can simulate a wide variety of atmospheric flows such as atmospheric boundary layer (ABL), gust fronts, separated flows, thunderstorm downbursts, and tornadoes in a large-scale (4.5 m max. updraft diameter and 4 m height) and high Reynolds numbers (up to  $2 \times 10^6$ ) (Hangan 2014; Hangan et al. 2017a; 2017b). The test chamber has a hexagonal footprint with a diameter of 25 m. It is composed of 106 fans in total, 100 fans distributed along the circumference of the testing chamber, and the rest of the fans are positioned in the upper plenum above the test chamber (Fig. 2.1). The integration between the upper fans and the periphery fans doubled by an advanced control system sets the basis to produce a variety of flow-fields. Active control of the floor allows 1600 floor roughness elements to vary their heights between 0 and 30 cm to mimic different terrain exposures. Tornadoes can be simulated at WindEEE dome for a broad range of intensities out of which swirl ratios  $S=0.21$  to 1.03 have been already explored. For the present experiments, mode A tornado was employed in which 6 fans in the upper plenum can produce the desired updraft in conjunction with a set of vanes situated at the base of the peripheral walls which when set at different angles can create the desired tornado swirl (see Fig. 2.1). The upper plenum is connected to the test chamber by a bell-mouth with mechanical louvers.

An important feature of the simulator is its capability to generate translating tornadoes by utilizing a guillotine system that translates the bell-mouth for up to 1.5 m/s over a 5 m distance. This is, to the authors knowledge, the largest achievable translating speed in tornado simulators which can closely mimic the significant aerodynamic properties of tornadic flows (Baker and Sterling 2019). Moreover, the simulator's large size assures measurement resolution both in plane and in height which is very important for the

characterization of tornado near-surface layer where most of the buildings and structures lie.

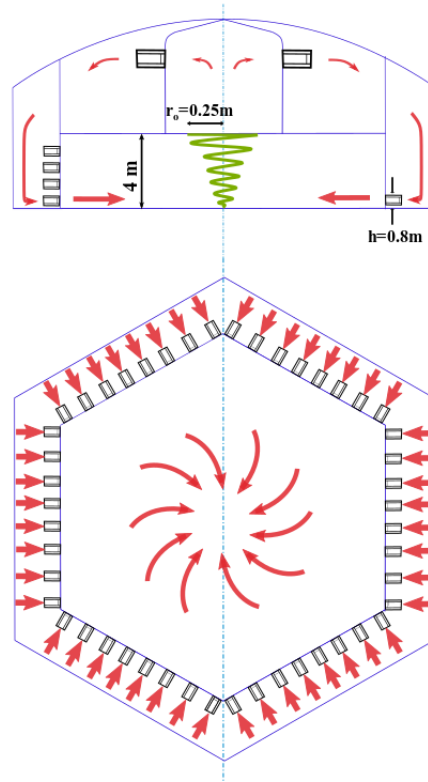


**Figure 2.1 Schematic of tornado creation at WinDEEE Dome**

### 2.2.2 Experimental setup and data processing

Tests were conducted at the WinDEEE Dome. Detailed surface pressure measurements were carried out over a large area of the chamber floor ( $460 \text{ cm} \times 240 \text{ cm}$ ) to give a thorough insight into the tornado vortex dynamics near the ground where velocity measurements are difficult. Tornado-like vortices were tested for swirl ratios between ( $S=0.21$  to  $1.03$ ) and ( $S=0.48$  and  $S=0.76$ ) for stationary and translating TLV respectively. Surface roughness was added utilizing the active control roughness blocks on the floor of a 3 cm mean height to examine the tornado flow-field characteristics.

*Vortex flow-field:*



The main parameters that control the tornado flow are: the geometric aspect ratio “ $a$ ”, the kinematic swirl ratio “ $S$ ”, and the dynamic radial Reynolds number “ $Re_r$ ”. The aspect ratio ( $a = h/r_o$ ) is defined as the ratio between the inflow depth ( $h$ ) and the updraft radius ( $r_o$ ). The swirl ratio is defined as the ratio between the angular momentum and the radial momentum which can be calculated using this expression:  $S = r_o \Gamma_{max} / 2Qh$ , where  $\Gamma_{max}$  is the maximum flow circulation and ( $Q$ ) is the volumetric flow rate per unit axial length. The radial Reynolds number is expressed as:  $Re_r = Q / 2\pi\nu$ , where  $\nu$  is the kinematic viscosity of the fluid.

The swirl ratio at the test chamber can be controlled by means of altering the vanes’ angles on the periphery walls and the flowrate is adjusted by regulating the top fans’ rpm. For this set of experiments, the inflow depth was set at 0.8 m, the updraft radius was 2.25 m which resulted in an aspect ratio of 0.35 and the swirl ratios were 0.21, 0.48, 0.59, 0.76, 1.03. For more details on the flowrate measurement and swirl ratio calculations, see Refan and Hangan (2018).

#### *Static pressure instrumentation:*

A large rectangular base plate (460 mm × 240 mm) instrumented with 489 pressure taps were employed in the present study, (see Fig. 2.2). The tap layout of the pressure plate was designed to ensure the full coverage of the whole travel distance of the translating tornado, with an adequate spatial resolution, particularly around the center of the tornado simulator, and to enclose larger width to account for translating tornado veering motion which was observed from flow visualization as discussed later in the results section. This tap layout was determined to guarantee the accuracy of detecting the tornado trajectory path, specifically near the plate center, which is the region of interest, for future investigations of tornado loading on buildings. The pressure system consists of sixteen electronically scanned pressure (ESP) scanners (pressure range  $\pm 1$  kPa) and two digital temperature compensation (DTC) Initiiums (Pressure Systems, Inc.), which were employed to accommodate the large number of pressure taps. The ESP scanners are minute electronic differential pressure units that incorporate a band of silicon piezoresistive pressure sensors, one for each pressure slot. Each ESP scanner can encompass up to 32 pressure ports and each port can accommodate PVC tubing with an outer diameter of 1 mm. The accuracy of

the pressure scanners is  $\pm 0.03\%$ . The DTC initium system delivers a vigorous data acquisition system for the ESP scanners. Each Ethernet-based DTC initium can be hooked up to up-to 8 pressure scanners. The initiums' uncertainty is  $\pm 0.05\%$  over the whole 0 - 70 °C temperature range. For more information about the pressure system, see Refan and Hangan (2018).

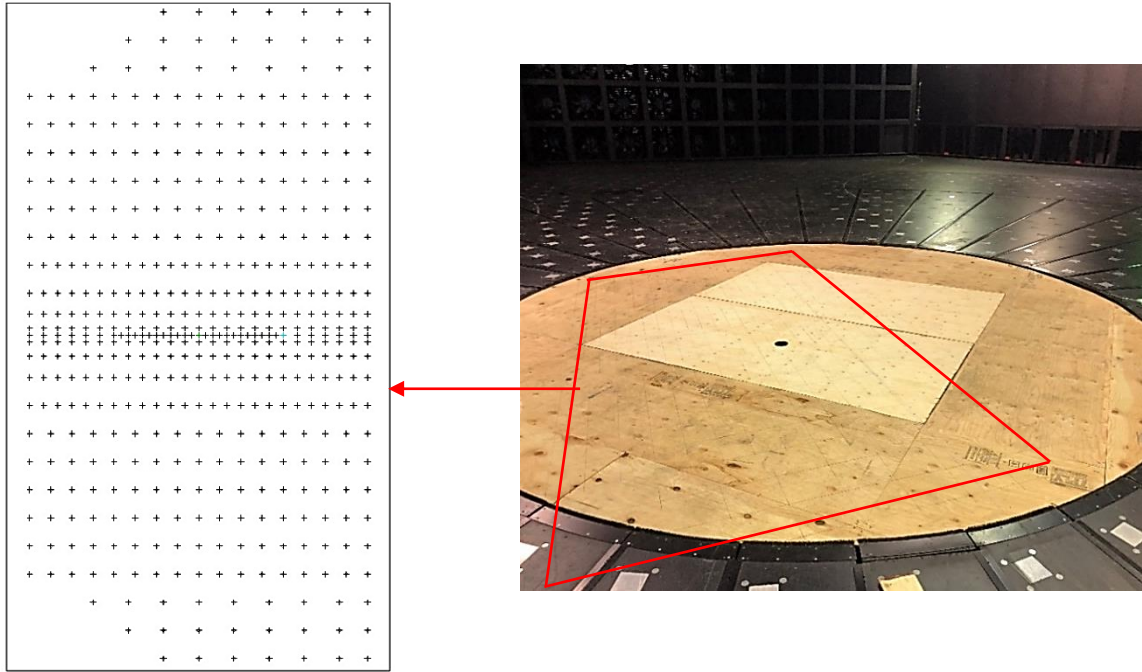


**Figure 2.2 Baseplate tap distribution**

To measure the pressure differential ( $\Delta P = p_i - p_o$ ), where  $P_i$  is the  $i$ th tap static pressure, sensed by each pressure tap, the testing chamber' static pressure ( $p_o$ ) was measured, outside the test chamber. Pressure measurements were acquired for five swirl ratios for stationary TLV,  $S = 0.21$ ,  $S = 0.48$ ,  $S = 0.59$ ,  $S = 0.76$ , and  $S = 1.03$ , and for  $S = 0.48$  and  $S = 0.76$  for translating TLV at  $Re_r = 10^6$ . The selection of these two swirl ratios for translating TLV was attributed to simulating two important stages of TLV, the before and after touchdown of the tornado vortex (Refan and Hangan 2018). The sampling frequency and sampling time for the pressure measurements were 500 Hz and 40 s, respectively for translating tornado and 500 Hz and 16 s for stationary tornado. This high frequency was chosen to keep a good temporal resolution and the sampling time was long enough to cover the whole translating tornado movement.

### *Ground roughness:*

Active control of 1600 roughness elements is one of the main features of WindEEE dome. The automated roughness blocks are made from metal and are designed to accommodate a variety of exposure conditions for atmospheric boundary layer flows (ABL) and tornadic flow (Fig. 2.3). In this study, the employed roughness blocks have a mean height of 3 cm. This is used to perform a preliminary investigation of the roughness effect on translating tornado-like vortices structure.

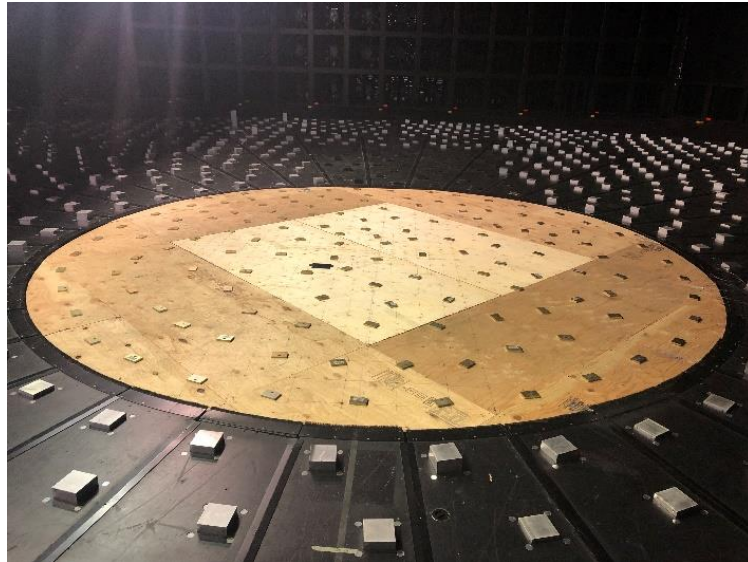


**Figure 2.3 Ground floor with added roughness elements at WindEEE dome**

## 2.3 Results and discussion

In this section, the tornado vortex structure near the ground is analyzed utilizing surface pressure measurements for a wide range of swirl ratios ( $S = 0.21, 0.48, 0.59, 0.76$ , and  $1.03$ ) for stationary tornado and two swirl ratios ( $S = 0.48$  and  $0.76$ ) for translating tornado at two translation speeds ( $0.11$  m/s and  $1.5$  m/s) and for two surface roughnesses of  $0$  cm (smooth) and  $3$  cm (rough), respectively.

### 2.3.1 Stationary tornado

Fig. 2.4 shows the radial profiles of the normalized mean ground pressure deficits ( $\Delta P^*$ ) for several swirl ratios of stationary (non-translating) TLVs, where  $\Delta P^* = \Delta P / 0.5 \rho v_{ax}^2$ . The pressure was normalized employing the mean axial velocity “ $v_{ax}$ ” measured at the bell-mouth location (Refan and Hangan, 2018). The mean axial velocity was chosen for normalization as it is uniform irrespective of the swirl ratio rather than the maximum tangential velocity which changes with swirl ratio. Using the maximum tangential velocity can be misleading as the effect of the increase in the tangential velocity with swirl will dominate the increase in the pressure deficit with increasing the swirl ratio (Refan and Hangan 2018). For the current study, the pressure data for each tap was averaged only over the whole sampling time of 16 s (8000 samples) without considering azimuthal averaging. This is because azimuthal averaging will provide misleading results as it causes smoothing up of the pressure deficit profile into only a one-vortex structure regardless of the real vortex structure, one, two, or three-vortex.

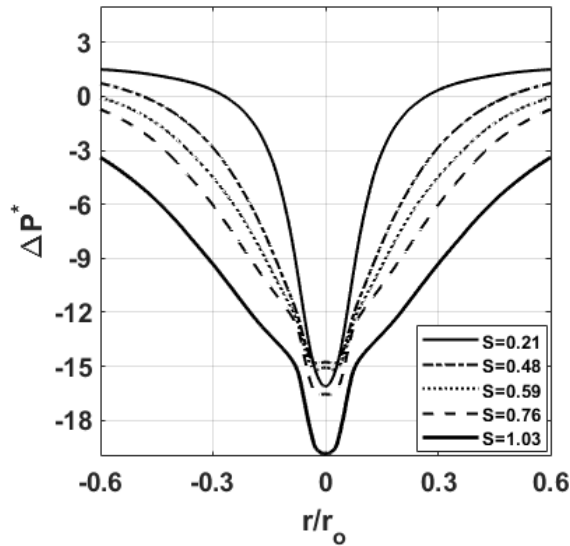


**Figure 2.4 mean surface pressure deficits for all swirl**

#### 2.3.1.1 Wandering effects:

The pressure data shown in Fig. 2.4 represents the data after removing the effects of wandering. Wandering is a random oscillation of the vortex core departed from its real

spatial position that would affect the resultant time-averaged data. The wandering behavior of tornado-like vortices influences the ground pressure profiles, particularly for low swirl ratios (e.g. Ashton et al. 2019; Refan and Hangan 2018).

In order to understand the extent of the tornado wandering behavior, the root mean square “rms” of the distance between the tornado instantaneous vortex center and the overall vortex center (i.e. the average vortex center over the whole sampling time) is quantified. Herein, the vortex center is determined by the detection of the minimum pressure at each instance. For the lowest swirl ratio,  $S=0.21$ , the high value of the rms 0.21 reflects the instability of the vortex at this supercritical stage before the touchdown of the vortex. Increasing the swirl ratio to  $S=0.48$  resulted in a slight decrease of the rms value to 0.2 which was expected as increasing the swirl ratio should reduce the extent of vortex instability. Further increasing the swirl ratio resulted in a counterintuitive gradual increase (0.2- 0.3) in the rms value. This is attributed to the multiple sub-vortices intermittently present with increasing swirl ratio that makes detecting the vortex center challenging and adds error in the rms value. As a result, there is a need for a new method that can detect the vortex center rather than the minimum pressure which can be applicable for higher swirl ratios.

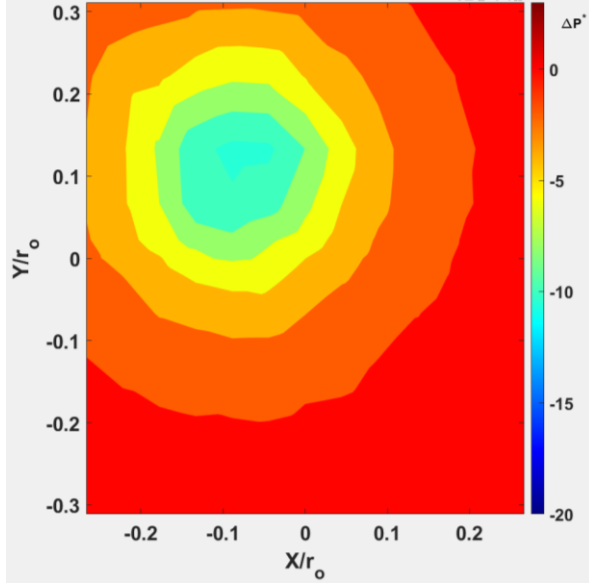
In order to obtain more precise results, the data should be corrected by removing wandering. Different approaches for eliminating wandering were implemented in previous studies: one approach is based on re-centering the vortex while another method uses a deconvolution procedure, but the foremost showed more accurate results as the second method resulted in an overestimation of the maximum tangential velocity in some cases (Ashton et al. 2019). Therefore, in this study, the first method of re-centering the vortex at each instance was initially adopted. Albeit the simplicity and efficiency of this approach in removing wandering for low swirl ratios, it did not provide meaningful results for high swirls. This happened because the algorithm depends on determining the center of the tornado vortex based on the global minimum pressure recorded by the pressure taps. This approach works for only a one-vortex structure while it fails for two or three-vortex structures that appear mostly at higher swirl ratios ( $S > 0.21$ ). Hence, a new approach is proposed which proved to be more robust for this wide range of swirl ratios, particularly

higher swirls. The adopted strategy was based on a moving average approach with proper window size. The pressure deficit profile was re-aligned at each instant utilizing the minimum of the moving average pressure deficit. This method maintained the real shape of the pressure deficit, particularly for high swirl ratios, by accounting not only for the global minimum but also for the local minimums of the surface pressure profile which preserved the real shape of the vortex, either one-vortex or two-vortex. Wandering elimination resulted in a substantial difference in the minimum mean surface pressure magnitude, particularly for low swirl ratios as summarized in Table (2.1). The results in Table (2.1) clearly show that not accounting for wandering will lead to a drastic underestimation of the pressure deficit.

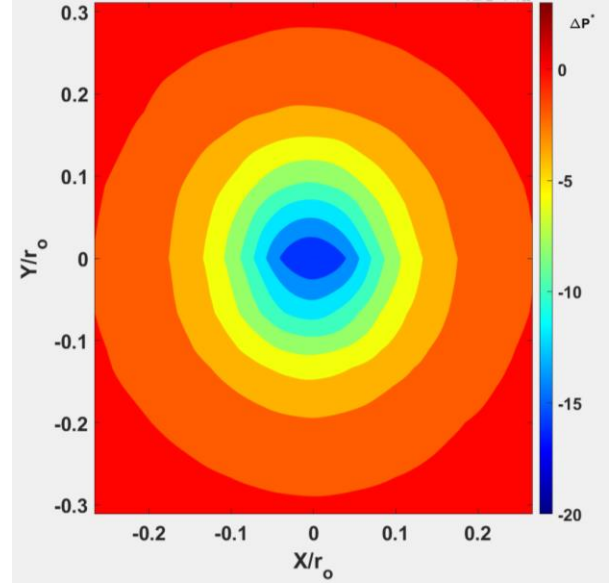
Table 2.1 Effect of removing wandering on minimum mean surface pressure values of stationary tornado

<b>Swirl Ratio (S)</b>	<b><math>\Delta P_{min}^*</math> (Original data)</b>	<b><math>\Delta P_{min}^*</math> (removed wandering)</b>	<b>Error (%)</b>
<b>0.21</b>	-10.51	-16.11	-34.74
<b>0.48</b>	-13.06	-14.84	-11.95
<b>0.59</b>	-13.40	-15.19	-11.8
<b>0.76</b>	-13.64	-16.56	-17.62
<b>1.03</b>	-15.56	-19.85	-21.60

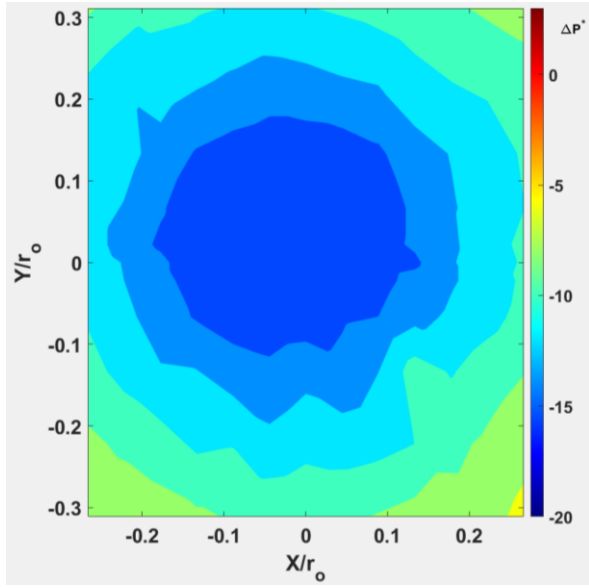
Fig. 2.5 shows the contour plot of the mean ground pressure for  $S=0.21$  and  $S=1.03$  before and after removing wandering. Table (2.1) and Figure 2.5 show that wandering affects both the minimum pressure deficit value as well as its position. Note that the wandering effects are most important for low swirl where vortex instabilities are strong and at higher swirl where two and three sub-vortices are observed.



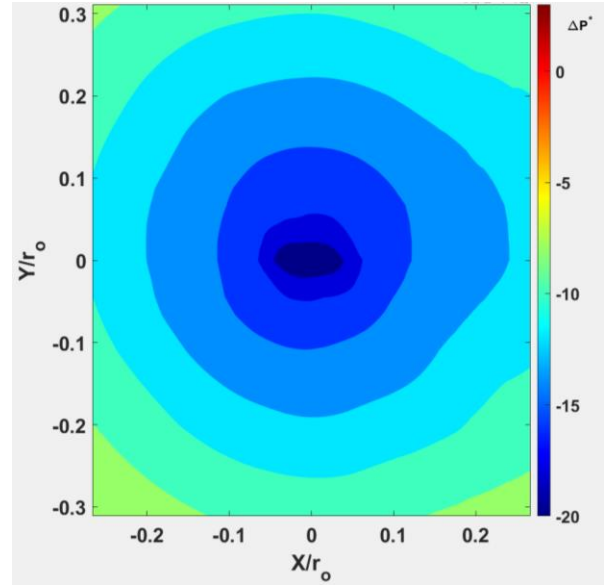
(a)



(b)



(c)



(d)

**Figure 2.5 Non-dimensional mean pressure deficit contour plot for  $S=0.21$  and  $S=1.03$  (a) with wandering( $S=0.21$ ), (b) after removing wandering ( $S=0.21$ ), (c) with wandering( $S=1.03$ ), and (d) after removing wandering ( $S=1.03$ ).**

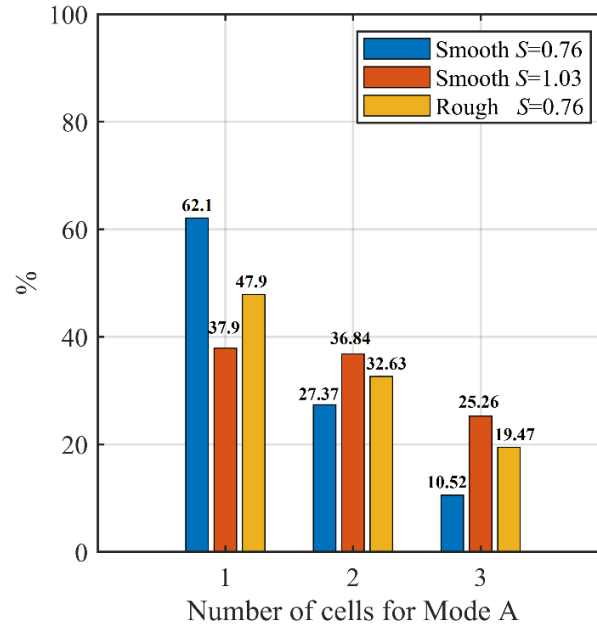
### 2.3.1.2 Swirl ratio effects:

Fig. 2.4 shows that for the lowest swirl ratio,  $S=0.21$ , the pressure deficit has a narrow profile, which indicates a small core radius, with a single minimum value characteristic for single-vortex TLV structure. Further increasing the swirl ratio,  $S=0.48$ , results in a decrease in the minimum pressure magnitude and a larger core radius which led to a wider profile of the pressure deficit with a more flattened profile possibly corresponding to a dual sub-vortex structure. The intermittent switch from one to two vortex structure is associated with the vortex break down (VBD) and specifically to the touch-down stage for swirl ratios here between  $S=0.48$  and  $S=0.59$  (Refan and Hangan 2018). Similar behavior was observed in previous studies (Snow et al. 1980; Refan and Hangan 2016; Tang et al. 2017). As swirl ratio increases, the magnitude of the minimum pressure also increases ( $S=0.76$ ) and a more pronounced two-vortex profile is observed. Moreover, the core radius keeps growing with increasing swirl. The pressure deficit was assumed to be symmetric and Fig. 2.4 was plotted using half of the data. A comparison between the stationary and translating TLV is provided in the next section.

In order to better understand the tornado vortex dynamics near the ground, the vortex structure of the TLV was analyzed for two swirl ratios,  $S=0.76$  and  $S=1.03$  for a smooth surface and for  $S=0.76$  for a rough surface. Those two swirl ratios were chosen as they represent higher swirl ratios where the tornado vortex structure is more complex and tends to deviate from the classical single structure of the lower swirl ratio profiles. The detection of the vortices was based on the ground pressure contour plots utilizing image processing toolbox through MATLAB R2019b. Fig. 2.6 shows that the one-vortex structure is dominant with two-thirds of the probability of occurrence for  $S=0.76$ . The two-vortex follows with one third and the three-vortex which is less common with as low as 10% probability. Increasing the swirl ratio to 1.03 resulted in an increase in the two-vortex structure percentage to reach the same level as the one-vortex structure by almost 37%. Also, the three-vortex structure increases by 15% compared to  $S=0.76$ . This combination between two and three vortex structure is a mark for high swirl ratios (Refan and Hangan 2018). On the other hand, adding roughness for  $S=0.76$  resulted in an increase in the two



and three vortex structure which may relate to the destabilizing of the main vortex by increased wall turbulence.



**Figure 2.6 Stationary TLV vortex structure**

### 2.3.2 Translating tornado

In this section, pressure measurements on the ground are analyzed for translating tornado-like vortices to examine the effects of swirl ratio, translation speed, tilting, veering, and roughness. Comparison between stationary and translating tornado-like vortices is carried out to explore the important aspects that distinguish between the two cases.

#### 2.3.2.1 Swirl ratio effects:

Fig. 2.7 shows the pressure deficit for simulated translating tornadoes in the WindEEE dome for two swirl ratios,  $S=0.48$  and  $S=0.76$ . Those two swirl ratios are representative of EF-1 and EF-2 tornadoes (Refan and Hangan 2017), which are more frequent than the higher-rated tornadoes according to NOAA. They are also representative of before touch-down and after vortex touch down patterns in TLVs. A translating speed of 1.5 m/s was used for this analysis. Each pressure deficit profile represents the time series of the minimum pressure tap along the centerline of the tornado simulator. Ensemble averaging

of five runs was performed. Fig. 2.7 shows that the pressure deficit for both swirl ratios is distinctly asymmetric between the leading and the rear sides of the tornado vortex, unlike the stationary tornado which has a symmetric pressure profile. This observation is similar to field tornado observations (Lee and Samaras, 2004). Also, a wider profile of the pressure deficit due to the larger core radius is observed when the swirl ratio increases from 0.48 to 0.76. The pressure distribution for  $S=0.76$  seems to present one minimum or at least one main minimum and a distorted one. This is different from stationary tornado studies (e.g. Tang et al., 2017) and can be attributed to the higher translation speed in WinDEE ( $V_{translating}=1.5$  m/s) that would result in an inclined tornado vortex central axis.

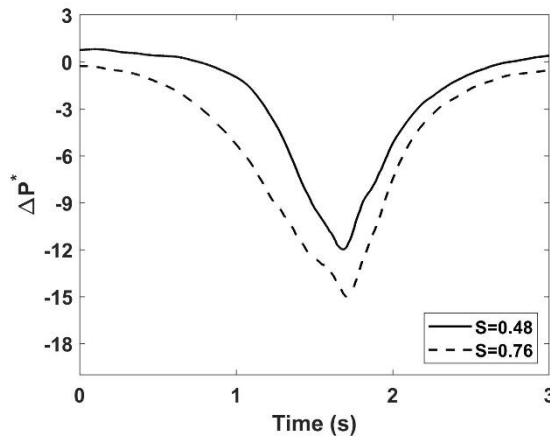


**Figure 2.7 Effect of increasing swirl ratio on the surface pressure deficit for translating tornado-like vortices.**

Fig. 2.8 represents the five runs for the two swirl ratios and the ensemble-averaged profile of the pressure deficit. It is clearly seen that ensemble averaging resulted in smoothing up the pressure deficit profiles and therefore making the two-vortex type profile (two minima) less pronounced for the two swirl ratios. This could be attributed to multiple factors. First, the veering motion of the tornado, described in detail later in the text, may explain the variability in individual profiles for the five runs considered. Second, the surface friction increases with increasing swirl and produces a more pronounced asymmetry in the profiles for  $S=0.76$  compared to  $S=0.48$ . This results in a forward inclination of the tornado central axis by less than  $20^\circ$  which was qualitatively observed in some full-scale data (Wurman and Gill 2000) as well as numerical simulations (e.g. Natarajan and Hangan 2012 and Liu

and Ishihara 2016) and WindEEE flow visualizations. Lastly, the ensemble averaging process of the five runs was based on aligning the peak pressures which considers only the higher peak of the high swirl ratio cases.

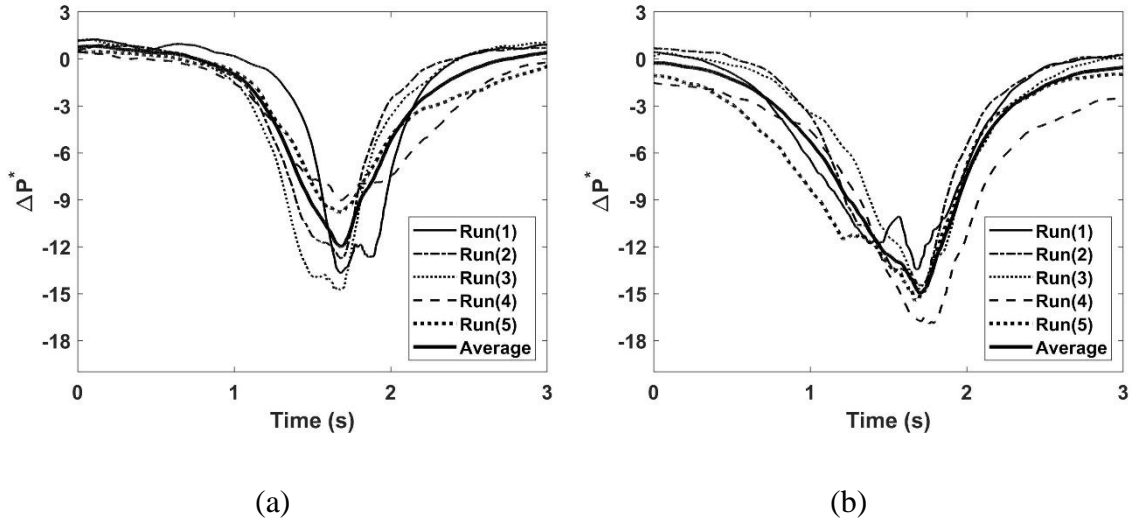


**Figure 2.8 Effect of multiple runs on pressure deficit profile for (a)  $S=0.48$  and (b)  $S=0.76$**

### 2.3.2.2 Translating vs. stationary tornado:

For  $S=0.48$  and  $S=0.76$  (see Fig. 2.9), the translation resulted in a wider pressure deficit shape and a slight decrease in the magnitude of the minimum pressure deficit compared to stationary ones. Both these effects are attributed to increased surface shear due to translation. The widening of the pressure deficit profile is more pronounced for  $S=0.76$  as the resultant velocity and therefore shear is larger for this case.

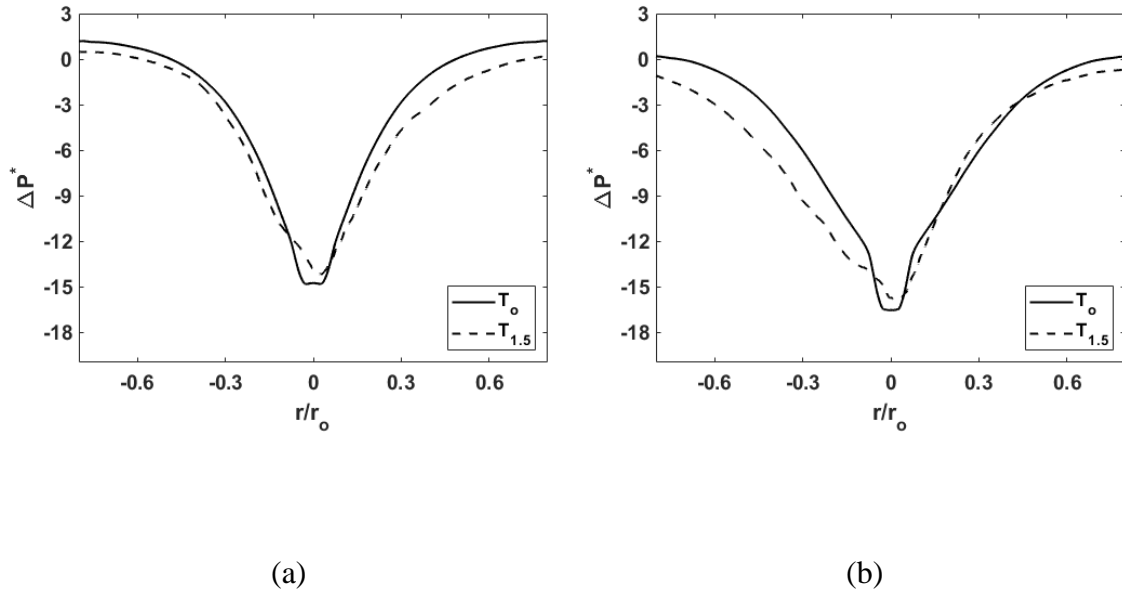


**Figure 2.9 Surface pressure deficit for Stationary ( $T_o$ ) and Translating ( $T_{1.5}$ ) tornado-like vortices for (a)  $S=0.48$ , and (b)  $S=0.76$**

Fig. 2.10 compares the minimum pressure values for stationary and translating tornado-like vortices ( $v_T = 1.5$  m/s). For stationary tornado, the maximum pressure deficit increases before vortex touch down ( $S < 0.48$ ) and decreases after. This trend is comparable to previous studies for stationary tornadoes (Natarajan and Hangan 2012; Tang et al. 2018). The trend seems to be the same for the translating cases ( $T_{1.5}$ ) with a slight decrease in the negative peak magnitude due to additional surface shear. Note that the magnitude of the minimum pressure is dependent on the translation speed (i.e. the lower the translation speed, the lower the pressure loads) (Haan et al. 2011). This emphasizes the importance of proper representation of tornado translation speed and scaling to match field tornadoes.

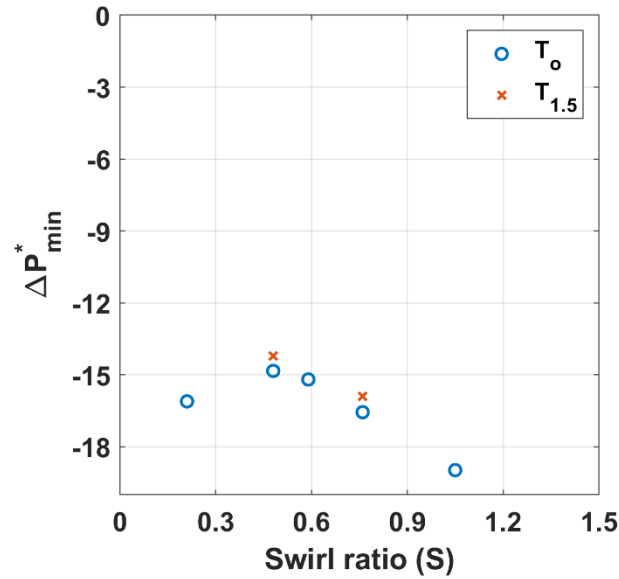


**Figure 2.10 Maximum central pressure deficit vs swirl ratio for stationary ( $T_0$ ) and translating tornado ( $T_{1.5}$ )**

### 2.3.2.3 Effect of translation speed:

The variation of tornado translating speed has a substantial effect on tornado loading patterns (e.g., Haan et al 2010). In this study, three different translating speeds,  $V_T = 1.5$  m/s “Speed (1)”, 1 m/s “Speed (2)”, and 0.11 “Speed (3)” were tested to analyze their effect on the tornado pressures on the ground surface. The higher speeds are closer to the lower end of field tornadoes which will allow attaining more realistic results without overestimation of the loads.

Fig. 2.11a and Fig. 2.11b presents pressure deficit radial profiles for the two swirl ratios considered and for several translational speeds. At lower translational speeds (2 and 3) the maximum pressure deficit is larger compared to the highest speed (1). Also, the pressure deficit profiles are more asymmetric for the lower speeds compared to the highest speed. This asymmetric behavior with multiple local minimums has been further investigated for  $S=0.48$  and it was found that wandering is more pronounced when the translation velocity is low, particularly for low swirl ratios as this is considered a supercritical stage near the

touchdown (Refan and Hangan 2018). Low translation speeds result in a higher drop in the pressure deficit which means overestimating the resultant loads. Hence, it is possible that using higher translation speeds closer to the scaled translation velocities in real tornadoes would produce more realistic and less conservative results.

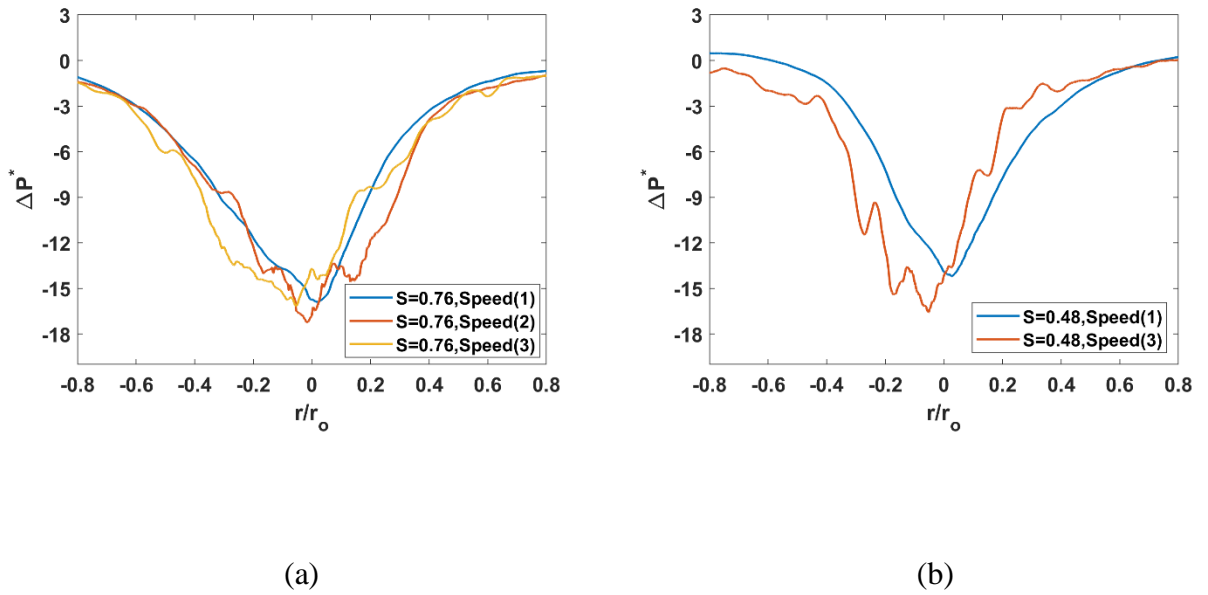


**Figure 2.11 Effect of tornado translation speed on ground pressure (a)  $S=0.76$ , and (b)  $S=0.48$**

#### 2.3.2.4 Effect of translation on tornado tilting

A prominent sighting from flow visualization was the vertical tilt of the tornado vortex axis, specifically for the highest translating speed. Fig. 2.12 shows a sketch of the tilting behavior of the simulated tornado showing the inclination angle ( $\theta$ ). This behavior was further explored, and the inclination angle was calculated to get a better understanding of tornado translation effects. The inclination angle ( $\theta$ ) was deduced by employing the guillotine velocity, the tornado vortex base velocity, and the total travel distance of the tornado ( $\cong 5$  meters).

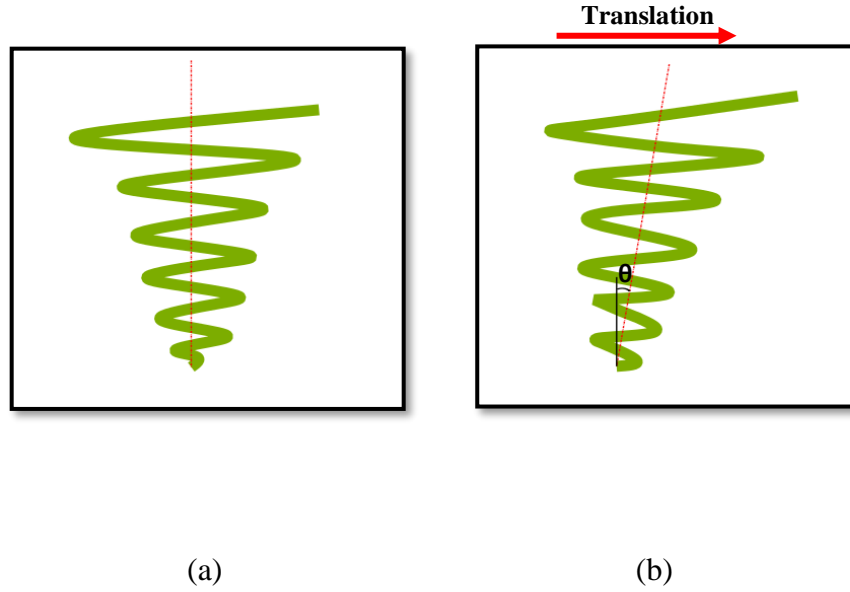


**Figure 2.12 Tornado axis inclination angle (a) Stationary tornado, (b) Translating tornado**

The tornado vortex signature on the floor was traced utilizing the tap that detects the instantaneous minimum pressure. In order to calculate the velocity of the tornado vortex base, the slope of the time series of the instantaneous minimum pressure tap's y-coordinate was obtained which represents the vortex base velocity. The guillotine velocity was precisely calculated by converting the voltage sensed by the guillotine system to velocity using the voltage/meter conversion ratio. It was established that the tilt angle was ranging between 8 to 18 degrees for the whole range of swirl ratios. This inclination of the tornado axis is attributed to higher shear stress with increasing velocity. Similar behavior was recorded in previous experimental studies (Haan et al. 2010), however, no further investigation was performed. Also, the tilt in the tornado axis was calculated in a field study (Wurman and Gill 2000) as  $20^\circ$  and in some field and numerical studies (Brooks 1951; Brown et al 1978; Alexander and Wurman 2005; Liu and Ishihara 2016; Yuan et al. 2019).

On the other hand, the tilting behavior of the TLV was examined for the lowest and highest translation speeds to understand its effect on the tornado vortex shape. For  $S=0.48$  and  $S=0.76$ , the tilting angle for  $V_T = 0.11$  m/s “Speed (3)” was found to be almost zero degrees,

unlike the highest speed  $V_T = 1.5$  m/s “Speed (1)” which resulted in a tilting angle in the range of  $10^\circ$  to  $16^\circ$ . This shows that, as expected, increasing the translation speed will result in a lagging behavior between the lower and upper parts of the tornado vortex.

### 2.3.2.5 Effects of translation speed on veering motion

Another important observation from the instantaneous contour plots of the translating tornado and the flow visualization is the veering motion of the vortex to the left of the translation direction. This veering behavior was observed mainly for the higher translation speeds for all swirl ratios. The real position of the tornado vortex near the surface was evaluated by tracking the minimum pressure tap at each instance (see Fig. 2.13b). It can be seen from the trajectories that at lower translating velocity,  $V_T = 0.11$  m/s “Speed (3)”, the tornado approximately followed a straight path. Further increasing the translating speed resulted in a redirection of the tornado path on a curvature rather than a straight line to the left which is more pronounced in the highest translating velocity,  $V_T = 1.5$  m/s “Speed (1)”. This effect is due to the asymmetry of the velocity field under translation and consequently the pressures between the right and left sides of the vortex. This phenomenon had not been reported in the literature before in tornado simulators, which may be related to the relatively low translation velocity in other simulators as the maximum achievable translating speed is 0.6 m/s (Haan et al. 2008). On the other hand, this deflection of the tornado path has been documented in field tornados by drawing the damage tracks of tornadoes (Lemon and Umscheid 2008) (see Fig. 2.13a). Wurman and Gill (2000) documented such behavior by comparing the tornado vortex signature on the lowest levels and on 1 km height which proved to be different as the highest levels showed almost a straight northward direction rather than a curved northwest direction of the lower portion of the tornado vortex on the ground.

### 2.3.2.6 Effect of roughness

A preliminary investigation of roughness effects on TLVs was carried out by investigating the pressure deficit radial profiles for two surface roughness and two swirl ratios,  $S=0.48$ ,



and  $S=0.76$ . The heights of the 1,600 roughness blocks in the WindEEE Dome were set at 0 cm (smooth) and 3 cm (rough) average heights.

Fig. 2.14a compares the pressure deficit radial profiles for the two roughness levels and the two swirl ratios. For  $S=0.48$ , which is the stage just before VBD (Refan and Hangan 2018), introducing roughness resulted in a narrower pressure deficit profile, reduction in the core radius, and increase in the magnitude of the minimum pressure. This means that for low swirl ratios, roughness creates a similar effect as decreasing swirl ratio. This supports the previous studies' findings (Natarajan and Hangan 2012; Wang et al., 2017). For  $S=0.76$  (Fig. 2.14b), the same behavior was observed,

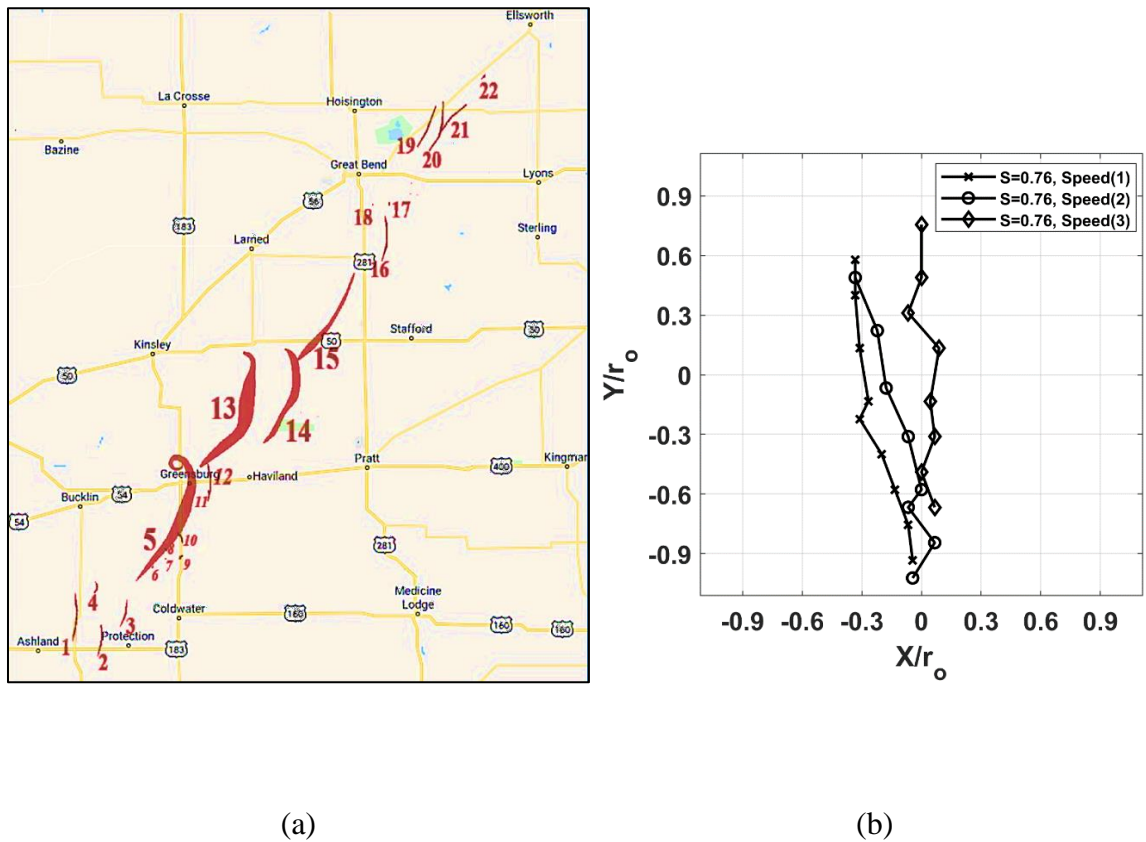
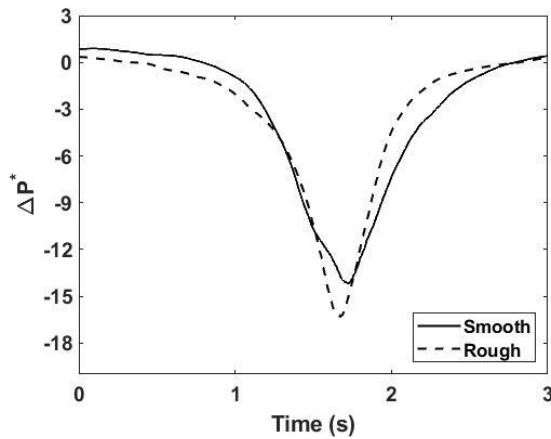


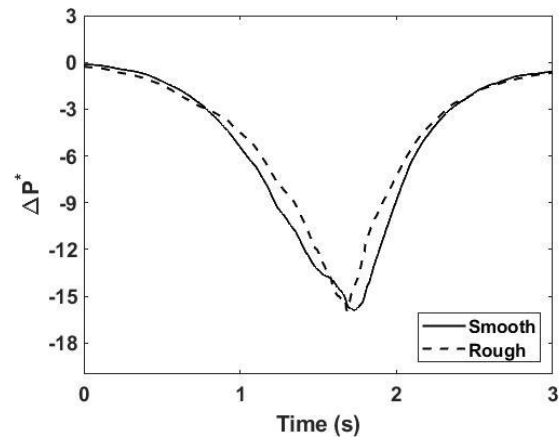
**Figure 2.13 Tornado paths (a) Damage path of the Greensburg, KS tornado. Adapted from “The Greensburg, KS tornadic storm: a storm of extremes.” by L. R. Lemon, & M. Umscheid, 2008, 24th Conf. on Severe Local Storms, 2.4. and (b) at WindEEE Dome**

and the roughness causes an analogous effect as the reduction of swirl ratio which is in agreement with previous studies' conclusions (e.g. Natarajan and Hangan, 2012, Razavi et al. 2018). More tests need to be performed to cover a wider range of swirl ratios and a larger set of roughness levels to obtain a full characterization of the overall effect of roughness with swirl ratio. The quantification of the surface layer relation to the roughness height through a roughness parameter analogous to the  $z_0$  in ABL flows needs further consideration. On the other hand, the inclination angle of the tornado vortex axis was calculated similarly to the smooth case and it was found that the tilt angle ranges between  $9^\circ$  to  $17^\circ$  for both swirl ratios compared to  $10^\circ$  to  $16^\circ$  for smooth surface results. No obvious trend was noted for the relation between the inclination and the roughness level; however, the inclination was larger for the highest translation speed.

The effect of roughness on the TLV trajectory is captured in Fig. 2.15. There is a slight tendency that increased roughness decreases the veering of the TLV to the left for both Swirl ratios. This seems to be normal as increasing roughness translates in increased surface friction and lower surface translational speeds which overall diminishes the surface veering while, as shown above, slightly increases the tilting.



(a)



(b)

**Figure 2.14 Effect of adding roughness to the ground on translating tornado surface loading (a)  $S=0.48$ , and (b)  $S=0.76$**

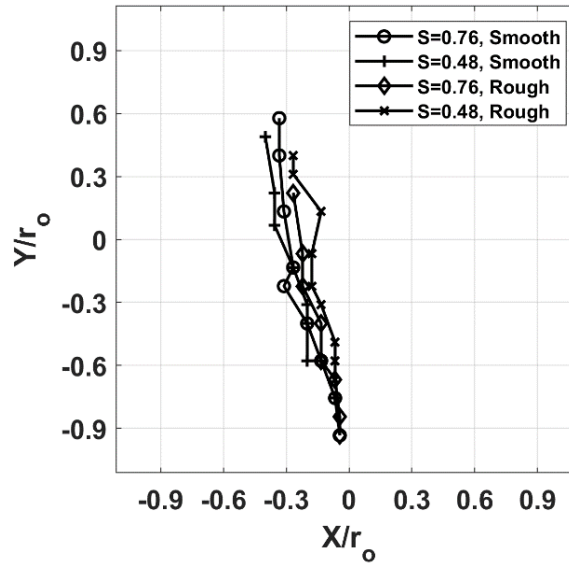


**Figure 2.15 Tornado trajectory for  $S=0.48$  and  $S=0.76$  for smooth and rough surfaces**

## 2.4 Conclusions

Characteristics of stationary and translating tornado-like vortices are investigated in the state-of-the-art tornado simulator, the WindEEE Dome at Western University. High spatial and temporal resolution ground pressure measurements are performed to reveal the dynamics of stationary and translating TLVs as a function of swirl ratio, translation speeds, and roughness. The effects of these parameters on wandering, tilting, and veering of tornado vortices are for the first time examined.

Results indicate that the wandering behavior of the vortex has a substantial impact on stationary tornado mean flow-field, particularly for low swirl ratios. Wandering can lead to erroneous magnitudes of the minimum pressure deficit as high as 35%. A new method to eliminate wandering is proposed by using moving average to detect the center of the

tornado deficit profile. This method proved to be more reliable specifically for higher swirl ratios compared to previous methods using re-centering the pressure deficit using the global minimum (e.g. Ashton et al. 2019).

For stationary tornadoes, the swirl ratio causes a reduction in the minimum pressure deficit magnitude followed by a subsequent increase. This highlights the different behavior of TLVs before and after the touchdown stage and the transition from one-vortex to multi-vortex structure.

Translation speed effects on the TLVs are for the first time investigated over a range of speeds for 0.1 m/s; 1m/s and 1.5 m/s. It was observed that the maximum pressure deficit lowers with increasing translation speed. This implies that using stationary or low-speed tornado translation speeds for loading purposes may lead to overestimations.

One of the significant observations from the present study is the tilting of the translating tornado vortex due to increasing surface shear under translation. This tilt is significantly more pronounced for the highest translation speeds (i.e.  $V_T = 1$  m/s and 1.5 m/s) compared to the lowest speed (i.e.  $V_T = 0.1$  m/s). This tilting behavior has been reported in field tornadoes as well.

Veering motion of the tornado vortex to the left of the translation direction is also observed for higher translation speeds. This behavior is attributed to the asymmetry in the velocity field resulting from translation and is observed in full-scale tornadoes as well.

The effect of increased roughness has a similar effect to decreasing swirl ratio for the two studied cases ( $S=0.48$  and  $S=0.76$ ). Increased roughness also results in an increase in tilting and a decrease in veering of the TLV.

The surface pressure data base created in this study is used to explore wandering, translation tilting, veering, and roughness effects in TLVs. The same data can provide a basis for interpretation and possible codification of tornado induced pressures and loads on buildings as a superposition of pressure deficit and aerodynamic effects.

In the future, this study can be extended to a larger range of swirl ratios, and mostly to better understand the effects of surface roughness in tornado-like vortex flows.

## Acknowledgement

This research has been made possible through funding from Natural Sciences and Engineering Research Council of Canada (NSERC) Discovery Grant (Grant number: R2811A03) and Canada Foundation for Innovation (CFI) WindEEE Dome Grant (Grant number: X2281838).

## References

Alexander, C. R., & Wurman, J. (2005). The 30 May 1998 Spencer, South Dakota, storm. Part I: The structural evolution and environment of the tornadoes. *Monthly Weather Review*, 133(1), 72–96. <https://doi.org/10.1175/MWR-2855.1>

ASCE/SEI (ASCE/Structural Engineering Institute), 2016. Minimum design loads for buildings and other structures. ASCE/SEI 7-16, Reston, VA

Ashton, R., Refan, M., Iungo, G. V., & Hangan, H. (2019). Wandering corrections from PIV measurements of tornado-like vortices. *Journal of Wind Engineering and Industrial Aerodynamics*, 189(February), 163–172. <https://doi.org/10.1016/j.jweia.2019.02.010>

Baker, C., & Sterling, M. (2019). Are Tornado Vortex Generators fit for purpose?. *Journal of Wind Engineering and Industrial Aerodynamics*, 190, 287-292. <https://doi.org/10.1016/j.jweia.2019.05.011>

Baker, G. L., & Church, C. R. (1979). Measurements of the core radii and peak velocities in modeled atmospheric vortices. In *J. Atmos. Sci.* (Vol. 36, Issues 12, Dec. 1979, pp. 2413–2424). [https://doi.org/10.1175/1520-0469\(1979\)036<2413:mocrap>2.0.co;2](https://doi.org/10.1175/1520-0469(1979)036<2413:mocrap>2.0.co;2)

Bluestein, H. B., Weiss, C. C., & Pazmany, A. L. (2004). The vertical structure of a tornado near Happy, Texas, on 5 May 2002: High-resolution, mobile, W-band, doppler

radar observations. *Monthly Weather Review*, 132(10), 2325–2337.

[https://doi.org/10.1175/1520-0493\(2004\)132<2325:TVSOAT>2.0.CO;2](https://doi.org/10.1175/1520-0493(2004)132<2325:TVSOAT>2.0.CO;2)

Brooks, E. M. (1951). Tornadoes and related phenomena. In *Compendium of Meteorology* (pp. 673-680). American Meteorological Society, Boston, MA.

[https://doi.org/10.1007/978-1-940033-70-9\\_55](https://doi.org/10.1007/978-1-940033-70-9_55)

Brown, R. A., Lemon, L. R., & Burgess, D. W. (1978). Tornado detection by pulsed Doppler radar. *Monthly Weather Review*, 106(1), 29-38. [https://doi.org/10.1175/1520-0493\(1978\)106<0029:TDBPDR>2.0.CO;2](https://doi.org/10.1175/1520-0493(1978)106<0029:TDBPDR>2.0.CO;2)

Case, J., Sarkar, P., & Sritharan, S. (2014). Effect of low-rise building geometry on tornado-induced loads. *Journal of Wind Engineering and Industrial Aerodynamics*, 133, 124–134. <https://doi.org/10.1016/j.jweia.2014.02.001>

Church, C. & Snow, John & Baker, G. & Agee, Ernest. (1979). Characteristics of Tornado-Like Vortices as a Function of Swirl Ratio: A Laboratory Investigation. *Journal of Atmospheric Sciences*. 36. 1755-1776. [https://doi.org/10.1175/1520-0469\(1979\)036<1755:COTLVA>2.0.CO;2](https://doi.org/10.1175/1520-0469(1979)036<1755:COTLVA>2.0.CO;2)

Dessens J. Jr. (1972) Influence of ground roughness on tornadoes: a laboratory simulation. (1972). *Journal of Applied Meteorology* 11(1):72–75. [https://doi.org/10.1175/1520-0450\(1972\)0112.0.CO;2](https://doi.org/10.1175/1520-0450(1972)0112.0.CO;2)

Diamond, C. J., & Wilkins, E. M. (1984). Translation effects on simulated tornadoes. *Journal of the atmospheric sciences*, 41(17), 2574-2580. [https://doi.org/10.1175/1520-0469\(1984\)041<2574:TEOST>2.0.CO;2](https://doi.org/10.1175/1520-0469(1984)041<2574:TEOST>2.0.CO;2)

Fiedler, B. H., & Rotunno, R. (1986). A theory for the maximum windspeeds in tornado-like vortices. In *Journal of the Atmospheric Sciences* 43, 2328–2340. [https://doi.org/10.1175/1520-0469\(1986\)043<2328:ATOTMW>2.0.CO;2](https://doi.org/10.1175/1520-0469(1986)043<2328:ATOTMW>2.0.CO;2)

Fleming, M. R., Haan, F. L., & Sarkar, P. P. (2013). Turbulent structure of tornado boundary layers with translation and surface roughness. In *12 th Americas Conference on Wind Engineering*.

Fujita, T. T. (1958). Tornado cyclone: Bearing system of tornadoes. In Proc. Seventh Conf. on Radar Meteorology.

Gairola, A., & Bitsuamlak, G. (2019). Numerical tornado modeling for common interpretation of experimental simulators. *Journal of Wind Engineering and Industrial Aerodynamics*, 186, 32-48. <https://doi.org/10.1016/j.jweia.2018.12.013>

Geetha Rajasekharan, S., Matsui, M., & Tamura, Y. (2013). Characteristics of internal pressures and net local roof wind forces on a building exposed to a tornado-like vortex. *Journal of Wind Engineering and Industrial Aerodynamics*, 112, 52–57. <https://doi.org/10.1016/j.jweia.2012.11.005>

Haan Jr, F. L., Balaramudu, V. K., & Sarkar, P. P. (2010). Tornado-induced wind loads on a low-rise building. *Journal of structural engineering*, 136(1), 106-116. [https://doi.org/10.1061/\(ASCE\)ST.1943-541X.00000093](https://doi.org/10.1061/(ASCE)ST.1943-541X.00000093)

Haan Jr, F. L., Sarkar, P. P., & Gallus, W. A. (2008). Design, construction and performance of a large tornado simulator for wind engineering applications. *Engineering Structures*, 30(4), 1146-1159. <https://doi.org/10.1016/j.engstruct.2007.07.010>

Hangan, H. (2014). The wind engineering energy and environment (WinEeee) dome at western university, Canada. *Wind Engineers, JAWe*, 39(4), 350-351. <https://doi.org/10.5359/jawe.39.350>

Hangan, H., Refan, M., Jubayer, C., Parvu, D., & Kilpatrick, R. (2017). Big data from big experiments. The WinEeee dome. In *Whither Turbulence and Big Data in the 21st Century?* (pp. 215-230). Springer, Cham. [https://doi.org/10.1007/978-3-319-41217-7\\_12](https://doi.org/10.1007/978-3-319-41217-7_12)

Hangan, H., Refan, M., Jubayer, C., Romanic, D., Parvu, D., LoTufo, J., & Costache, A. (2017). Novel techniques in wind engineering. *Journal of Wind Engineering and Industrial Aerodynamics*, 171, 12-33. <https://doi.org/10.1016/j.jweia.2017.09.010>

Hu, H., Yang, Z., Sarkar, P., & Haan, F. (2011). Characterization of the wind loads and flow fields around a gable-roof building model in tornado-like winds. *Experiments in Fluids*, 51(3), 835–851. <https://doi.org/10.1007/s00348-011-1102-6>

Ishihara, T., Oh, S., & Tokuyama, Y. (2011). Numerical study on flow fields of tornado-like vortices using the LES turbulence model. *Journal of wind engineering and industrial aerodynamics*, 99(4), 239-248. <https://doi.org/10.1016/j.jweia.2011.01.014>

Karami, M., Hangan, H., Carassale, L., & Peerhossaini, H. (2019). Coherent structures in tornado-like vortices. *Physics of Fluids*, 31(8), 085118. <https://doi.org/10.1063/1.5111530>

Karstens, C. D., Samaras, T. M., Lee, B. D., Gallus Jr, W. A., & Finley, C. A. (2010). Near-ground pressure and wind measurements in tornadoes. *Monthly Weather Review*, 138(7), 2570-2588. <https://doi.org/10.1175/2010MWR3201.1>

Lee, J. J., Samaras, T., & Young, C. R. (2004, October). Pressure measurements at the ground in an F-4 tornado. In *Preprints, 22d Conf. on Severe Local Storms*, Hyannis, MA, Amer. Meteor. Soc., 15.3.

Lee, W. C., & Wurman, J. (2005). Diagnosed three-dimensional axisymmetric structure of the Mulhall tornado on 3 May 1999. *Journal of the atmospheric sciences*, 62(7), 2373-2393. <https://doi.org/10.1175/JAS3489.1>

Lemon, L. R., & Umscheid, M. (2008). The Greensburg, KS tornadic storm: a storm of extremes. *24th Conf. on Severe Local Storms*, 2.4. [http://ams.confex.com/ams/24SLS/techprogram/paper\\_141811.htm](http://ams.confex.com/ams/24SLS/techprogram/paper_141811.htm)

Leslie, F. W. (1977). Surface roughness effects on suction vortex formation: A laboratory simulation. *Journal of the Atmospheric Sciences*, 34(7), 1022-1027. [https://doi.org/10.1175/1520-0469\(1977\)034<1022:SREOSV>2.0.CO;2](https://doi.org/10.1175/1520-0469(1977)034<1022:SREOSV>2.0.CO;2)

Lewellen, W. S., Lewellen, D. C., & Sykes, R. I. (1997). Large-eddy simulation of a tornado's interaction with the surface. *Journal of the atmospheric sciences*, 54(5), 581-605. [https://doi.org/10.1175/1520-0469\(1997\)054<0581:LESOAT>2.0.CO;2](https://doi.org/10.1175/1520-0469(1997)054<0581:LESOAT>2.0.CO;2)

Liu, Z., & Ishihara, T. (2015). Numerical study of turbulent flow fields and the similarity of tornado vortices using large-eddy simulations. *Journal of Wind Engineering and Industrial Aerodynamics*, 145, 42-60. <https://doi.org/10.1016/j.jweia.2015.05.008>



- Liu, Z., & Ishihara, T. (2016). Study of the effects of translation and roughness on tornado-like vortices by large-eddy simulations. *Journal of Wind Engineering and Industrial Aerodynamics*, 151, 1-24. <https://doi.org/10.1016/j.jweia.2016.01.006>
- Lombardo, F. T., Roueche, D. B., & Prevatt, D. O. (2015). Comparison of two methods of near-surface wind speed estimation in the 22 May, 2011 Joplin, Missouri Tornado. *Journal of Wind Engineering and Industrial Aerodynamics*, 138, 87-97. <https://doi.org/10.1016/j.jweia.2014.12.007>
- Matsui, M., & Tamura, Y. (2009). Influence of incident flow conditions on generation of tornado-like flow. In *Proceedings of the 11th American Conference on Wind Engineering*, Puerto Rico, USA.
- Mishra, A. R., James, D. L., & Letchford, C. W. (2008). Physical simulation of a single-celled tornado-like vortex, Part B: Wind loading on a cubical model. *Journal of Wind Engineering and Industrial Aerodynamics*, 96(8-9), 1258-1273. <https://doi.org/10.1016/j.jweia.2008.02.027>
- Nasir, Z., & Bitsuamlak, G. T. (2018). Topographic effects on tornado-like vortex. *Wind and Structures*, 27(2), 123-136. <https://doi.org/10.12989/was.2018.27.2.123>
- Natarajan, D., & Hangan, H. (2012). Large eddy simulations of translation and surface roughness effects on tornado-like vortices. *Journal of Wind Engineering and Industrial Aerodynamics*, 104, 577-584. <https://doi.org/10.1016/j.jweia.2012.05.004>
- National Research Council of Canada. (2015). *National Building Code of Canada, 2015*. National Research Council Canada.
- National Weather Service. (2011). *NWS Central Region Service Assessment Joplin, Missouri, Tornado – May 22, 2011*. July.
- NOAA National Centers for Environmental Information, *State of the Climate: Tornadoes for Annual 2011*, published online January 2012, retrieved on January 20, 2020 from <https://www.ncdc.noaa.gov/sotc/tornadoes/201113>.

- Nolan, D. S. (2005). A new scaling for tornado-like vortices. *Journal of the atmospheric sciences*, 62(7), 2639-2645. <https://doi.org/10.1175/JAS3461.1>
- Nolan, D. S., & Farrell, B. F. (1999). The structure and dynamics of tornado-like vortices. *Journal of the Atmospheric Sciences*, 56(16), 2908-2936. [https://doi.org/10.1175/1520-0469\(1999\)056<2908:TSADOT>2.0.CO;2](https://doi.org/10.1175/1520-0469(1999)056<2908:TSADOT>2.0.CO;2)
- Nolan, D. S., Dahl, N. A., Bryan, G. H., & Rotunno, R. (2017). Tornado vortex structure, intensity, and surface wind gusts in large-eddy simulations with fully developed turbulence. *Journal of the Atmospheric Sciences*, 74(5), 1573-1597. <https://doi.org/10.1175/JAS-D-16-0258.1>
- Refan, M., & Hangan, H. (2018). Near surface experimental exploration of tornado vortices. *Journal of Wind Engineering and Industrial Aerodynamics*, 175, 120-135. <https://doi.org/10.1016/j.jweia.2018.01.042>
- Refan, M., Hangan, H., & Wurman, J. (2014). Reproducing tornadoes in laboratory using proper scaling. *Journal of Wind Engineering and Industrial Aerodynamics*, 135, 136-148. <https://doi.org/10.1016/j.jweia.2014.10.008>
- Rhee, D. M., & Lombardo, F. T. (2018). Improved near-surface wind speed characterization using damage patterns. *Journal of Wind Engineering and Industrial Aerodynamics*, 180, 288-297. <https://doi.org/10.1016/j.jweia.2018.07.017>
- Sengupta, A., Haan, F. L., Sarkar, P. P., & Balaramudu, V. (2006). Transient loads on buildings in microburst and tornado winds. In *Proc. The fourth International Symposium on Comp. Wind Engr.(CWE2006)*.
- Sengupta, A., Haan, F. L., Sarkar, P. P., & Balaramudu, V. (2008). Transient loads on buildings in microburst and tornado winds. *Journal of Wind Engineering and Industrial Aerodynamics*, 96(10-11), 2173-2187. <https://doi.org/10.1016/j.jweia.2008.02.050>
- Snow, J. T. (1982). A review of recent advances in tornado vortex dynamics. *Reviews of Geophysics*, 20(4), 953-964. <https://doi.org/10.1029/RG020i004p00953>

Snow, J. T., & Lund, D. E. (1997). Considerations in exploring laboratory tornadolike vortices with a laser Doppler velocimeter. *Journal of Atmospheric and Oceanic Technology*, 14(3), 412-426. [https://doi.org/10.1175/1520-0426\(1997\)014<0412:CIELTV>2.0.CO;2](https://doi.org/10.1175/1520-0426(1997)014<0412:CIELTV>2.0.CO;2)

Snow, J. T., Church, C. R., & Barnhart, B. J. (1980). An investigation of the surface pressure fields beneath simulated tornado cyclones. *Journal of the Atmospheric Sciences*, 37(5), 1013-1026. [https://doi.org/10.1175/1520-0469\(1980\)037<1013:AIOTSP>2.0.CO;2](https://doi.org/10.1175/1520-0469(1980)037<1013:AIOTSP>2.0.CO;2)

Tang, Z., Feng, C., Wu, L., Zuo, D., & James, D. L. (2018). Characteristics of tornado-like vortices simulated in a large-scale ward-type simulator. *Boundary-layer meteorology*, 166(2), 327-350. <https://doi.org/10.1007/s10546-017-0305-7>

Tari, P. H., Gurka, R., & Hangan, H. (2010). Experimental investigation of tornado-like vortex dynamics with swirl ratio: The mean and turbulent flow fields. *Journal of Wind Engineering and Industrial Aerodynamics*, 98(12), 936-944. <https://doi.org/10.1016/j.jweia.2010.10.001>

Tepper, M., & Eggert, W. E. (1956). Tornado proximity traces. *Bulletin of the American Meteorological Society*, 37(4), 152-159. <https://doi.org/10.1175/1520-0477-37.4.152>

Thampi, H., Dayal, V., & Sarkar, P. P. (2011). Finite element analysis of interaction of tornados with a low-rise timber building. *Journal of Wind Engineering and Industrial Aerodynamics*, 99(4), 369–377. <https://doi.org/10.1016/j.jweia.2011.01.004>

Wakimoto, R. M., Atkins, N. T., & Wurman, J. (2011). The LaGrange tornado during VORTEX2. Part I: Photogrammetric analysis of the tornado combined with single-Doppler radar data. *Monthly weather review*, 139(7), 2233-2258. <https://doi.org/10.1175/2010MWR3568.1>

Wakimoto, R. M., Murphey, H. V., Dowell, D. C., & Bluestein, H. B. (2003). The Kellerville tornado during VORTEX: Damage survey and Doppler radar analyses.

Monthly weather review, 131(10), 2197-2221. [https://doi.org/10.1175/1520-0493\(2003\)131<2197:TKTDVD>2.0.CO;2](https://doi.org/10.1175/1520-0493(2003)131<2197:TKTDVD>2.0.CO;2)

Wakimoto, R. M., Stauffer, P., Lee, W. C., Atkins, N. T., & Wurman, J. (2012). Finescale structure of the LaGrange, Wyoming, tornado during VORTEX2: GBVTD and photogrammetric analyses. Monthly weather review, 140(11), 3397-3418. <https://doi.org/10.1175/MWR-D-12-00036.1>

Wang, J., Cao, S., Pang, W., & Cao, J. (2017). Experimental study on effects of ground roughness on flow characteristics of tornado-like vortices. Boundary-Layer Meteorology, 162(2), 319-339. <https://doi.org/10.1007/s10546-016-0201-6>

Wang, J., Cao, S., Pang, W., Cao, J., & Zhao, L. (2016). Wind-load characteristics of a cooling tower exposed to a translating tornado-like vortex. Journal of Wind Engineering and Industrial Aerodynamics, 158, 26-36. <https://doi.org/10.1016/j.jweia.2016.09.008>

Ward, N. B. (1972). The exploration of certain features of tornado dynamics using a laboratory model. Journal of the Atmospheric Sciences, 29(6), 1194-1204. [https://doi.org/10.1175/1520-0469\(1972\)029<1194:TEOCFO>2.0.CO;2](https://doi.org/10.1175/1520-0469(1972)029<1194:TEOCFO>2.0.CO;2)

Wurman, J. (2002). The multiple-vortex structure of a tornado. Weather and forecasting, 17(3), 473-505. [https://doi.org/10.1175/1520-0434\(2002\)017<0473:TMVSOA>2.0.CO;2](https://doi.org/10.1175/1520-0434(2002)017<0473:TMVSOA>2.0.CO;2)

Wurman, J., & Alexander, C. R. (2005). The 30 May 1998 Spencer, South Dakota, storm. Part II: Comparison of observed damage and radar-derived winds in the tornadoes. Monthly weather review, 133(1), 97-119. <https://doi.org/10.1175/MWR-2856.1>

Wurman, J., & Gill, S. (2000). Finescale radar observations of the Dimmitt, Texas (2 June 1995), tornado. Monthly weather review, 128(7), 2135-2164. [https://doi.org/10.1175/1520-0493\(2000\)128<2135:FROOTD>2.0.CO;2](https://doi.org/10.1175/1520-0493(2000)128<2135:FROOTD>2.0.CO;2)

Wurman, J., & Samaras, T. (2004). Comparison of in-situ pressure and DOW Doppler winds in a tornado and RHI vertical slices through 4 tornadoes during 1996–2004. Preprints, 22nd Conf. on Severe Local Storms, Hyannis, MA, Amer. Meteor. Soc., 15.4. [Available online at <http://ams.confex.com/ams/pdfpapers/82352.pdf>.]

Wurman, J., Straka, J. M., & Rasmussen, E. N. (1996). Fine-scale Doppler radar observations of tornadoes. *Science*, 272(5269), 1774-1777.

<https://doi.org/10.1126/science.272.5269.1774>

Wurman, J., Straka, J., Rasmussen, E., Randall, M., & Zahrai, A. (1997). Design and deployment of a portable, pencil-beam, pulsed, 3-cm Doppler radar. *Journal of Atmospheric and Oceanic Technology*, 14(6), 1502-1512. [https://doi.org/10.1175/1520-0426\(1997\)014<1502:DADOAP>2.0.CO;2](https://doi.org/10.1175/1520-0426(1997)014<1502:DADOAP>2.0.CO;2)

Yuan, F., Yan, G., Honerkamp, R., Isaac, K. M., Zhao, M., & Mao, X. (2019). Numerical simulation of laboratory tornado simulator that can produce translating tornado-like wind flow. *Journal of Wind Engineering and Industrial Aerodynamics*, 190, 200-217.

<https://doi.org/10.1016/j.jweia.2019.05.001>

Zhang, W., & Sarkar, P. P. (2008). Effects of ground roughness on tornado like vortex using PIV. In *Proceedings of the AAWE workshop*, Vail, CO.

Zhang, W., & Sarkar, P. P. (2012). Near-ground tornado-like vortex structure resolved by particle image velocimetry (PIV). *Experiments in fluids*, 52(2), 479-493.

<https://doi.org/10.1007/s00348-011-1229-5>

## Chapter 3

### 3 Tornado-Induced Internal Pressures on Low-Rise Buildings with Multiple Openings

#### 3.1 Introduction and background

Tornadoes pose a huge threat to life and properties. Every year, tornadoes claim the lives of about 60 people in the United States, on average, and leave more than 1000 injured according to NOAA (NOAA 2019). Moreover, the damaging behavior of tornadoes to properties, either partially or totally, leads to economic losses reaching billions of dollars. The destruction of properties is attributed to the net induced wind loads on buildings where the effects of atmospheric pressure deficit (APD) due to the high negative pressure in the tornado vortex as well as the tornado flow-structure interaction add together to form the resultant tornado-induced wind loading. The tornado interaction with the structures is divided into two main components, (a) the external pressure loading, and (b) the internal pressure where the building is affected by the resultant load. The external pressure loading due to tornadic hits had been studied extensively in the literature ranging from experimental studies (e.g. Ho et al. 2005; Mishra et al. 2008b; Sengupta et al. 2008; Sarkar and Kikitsu 2009; Haan et al. 2010; Hu et al. 2011; Thampi et al. 2011; Rajasekharan et al. 2013; Case et al. 2014; Razavi and Sarkar 2018) as well as numerical simulations (e.g. Selvam and Millett 2003; Nasir 2017). While these studies provided some information, most of them have either too small buildings or they cannot satisfy proper parametric scaling against real tornadoes (Refan and Hangan 2018, Baker and Sterling 2019). Studies of internal pressures inside buildings located in tornadic flow-field have started only recently (e.g. Sarkar and Kikitsu 2009), unlike internal pressure studies in Atmospheric Boundary Layer (ABL) flows which have been studied extensively since the seventies (e.g. Stathopoulos et al. 1979; Holmes 1980; Davenport and Surry 1984; Vickery and Karakatsanis 1987; Vickery 1994; Ginger et al. 1997; Oh et al. 2007; Ginger and Kim 2009; Ginger et al. 2010, Holmes and Ginger 2012). One of the main reasons for the lack of internal pressure results in physically simulated tornado-like vortices is the size of most of the simulators which do not allow a model size that is large enough to be properly instrumented.

Wind-induced internal pressure in a building depends on many factors, for instance, the external pressure distribution near the openings, the geometry of the opening, and the porosity of the building (Holmes, 1980; Vickery, 1986; Womble et al., 1995). The internal pressure plays a significant role in determining the overall wind loading on buildings, therefore their precise measurement is crucial. Most of the studies on tornadic flow concentrated on external pressures and few studies examined the role of internal pressure in rising or suppressing the net wind loads in buildings.

Sarkar and Kikitsu (2009) started one of the earliest investigations of internal pressures in tornadic flow and carried out experiments on the tornado induced wind loading on a low-rise building with a dominant opening using the tornado simulator at Iowa State University (ISU). They found that the internal pressure loading played a prominent role in determining the net wind loading and that its value depends on the porosity ratio and the dominant opening location in the building. Thampi et al. (2011) implemented a finite element method to simulate the stages of failure of the structural components of a partially damaged low-rise timber building that was affected by an EF-5 tornado in Parkersburg, Iowa, USA on May 25<sup>th</sup>, 2008. They studied the role of internal pressures inside the building in each stage of this failure. They deduced that the building porosity and the opening configuration had a major effect on internal pressures which was reflected on the net wind loads. They also found that the net winds on the building reduced considerably after partial roof and sidewall failures. Rajasekharan et al. (2013) performed experiments in the Tokyo Polytechnic University tornado simulator on a building with uniform leakage and a dominant wall opening to study the effects of internal pressure on the overall roof loading. They revealed that a dominant opening (3.9%) resulted in a higher magnitude of the mean internal pressure compared to the uniform leakage case when the tornado vortex and the building are concentric, unlike when the building is located beyond the core region where this trend was reversed. Letchford et al. (2015) studied the effect of porosity and dominant openings on the internal pressure of a low-rise building model under a simulated stationary tornado in the VorTECH simulator at Texas Tech University. They also proposed a numerical model to estimate the internal pressure using external pressure data. They deduced that resonance in the fluctuating internal pressure only occurs in the case of a dominant opening with no porosity. They also concluded that the mean roof net wind

loading was maximum for the case of a dominant opening irrespective of porosity and that their proposed numerical model needs more improvements. Wang et al. (2018) carried out experiments using the tornado simulator at Tongji University to examine the external and internal pressure loadings on a cubic building with openings under stationary tornado-like vortices. They also compared the tornadic loading with the atmospheric boundary layer flows using the ASCE code and the Chinese design code. They found that the maximum wind loading occurred when the building model was located in the core region and that the internal pressure was affected by the size and location of the dominant opening. Moreover, they found that the tornadic wind loading exceeded the two standard building codes by a large factor. Rajasekharan et al. (2019) studied the vulnerability of a low-rise building roof under tornadic hits. Using a translating simulator at Tokyo Polytechnic University, external and internal pressures were examined, and the dominant opening location was changed to investigate its effect on internal pressures. They found that the roof is more prone to damage than sidewalls. Besides, the windward dominant opening resulted in the highest internal pressure magnitude. More recently, Roueche et al. (2020) compared tornado and ABL-induced wind loads and developed a numerical model that can predict the evolution of the internal pressures based on external pressure distribution. They found that for the building corners areas tornadic loadings are about 13% higher, on average, in tornadic flows compared to ABL winds.

Although there are a number of studies in the literature investigating the internal pressures under tornado-like vortices, most of the studies have some limitations. All the previous studies utilized stationary tornado-like vortices rather than translating ones which resulted in an overestimation of the loads except Sarkar and Kikitsu (2009) and Rajasekharan et al. (2019) who used translating tornadoes. Albeit Sarkar and Kikitsu (2009) used translation in their study to examine more realistic scenarios, the translation speed was very low ( $\leq 0.24$  m/s,  $v_{full\ scale}=1.5$  m/s) which is low compared with real tornadoes and may lead to overestimated aerodynamic loads (Haan et al. 2010). Although Rajasekharan et al. (2019) utilized translation in their experiments, the translation speed was in the lower range ( $v_T=0.02$  to  $0.24$  m/s) and the velocity scale of 1:26 was debatable as no clear comparison with field tornadoes was performed. Moreover, some studies used very small models ( $\leq 5$



cm in length) that cannot provide an adequate resolution for measuring the internal and external loads on buildings particularly near the openings (Rajasekharan et al. 2013; Wang et al. 2018; Rajasekharan et al., 2019). Hence, a need for a more comprehensive study about internal pressure loadings inside low-rise buildings taking into consideration the effect of building size, building offset from tornado translation path, building orientation, opening configurations, higher translation speed as well as higher resolution using appropriate-sized models is needed for a better understanding of the tornado-structure interaction for low-rise buildings.

In this study, a detailed internal pressure measurement was carried out in the large-scale tornado simulator, the WindEEE dome, to investigate the internal pressure inside two generic low-rise buildings under several realistic scenarios by utilizing the simulator's high spatial resolution which is essential for properly explore tornadic loading on buildings. The effect of internal pressures was examined including several parameters such as the effect building offset (+RMW, +2RMW, and >+2RMW; where RMW is the Radius of Maximum Wind), building orientation ( $0^\circ$  and  $45^\circ$ ), building size (small and large building models), tornado intensity ( $S=0.48$  and  $S=0.76$ ), and opening configuration (uniform leakage, windward dominant opening, and roof opening).

### 3.2 Tornado simulator description

The state-of-the-art tornado simulator, the WindEEE dome, is a hexagonal test chamber of a 25 m diameter confined with a larger 40 m diameter circle "return circuit". The test chamber is comprised of 106 fans (Fig. 3.1) which are divided into two groups, 100 fans located along the perimeter of the test chamber and 6 fans in a plenum above the test chamber. The upper plenum is connected to the test chamber by a bell-mouth with mechanical louvers. The height of the chamber is 3.8 m. The WindEEE dome has the capability of producing both synoptic and non-synoptic winds (e.g. Atmospheric boundary layer flows (ABL), downbursts, and tornadoes) which can be reproduced at high Reynolds numbers (up to  $2 \times 10^6$ ) and Large scales (4 m height and 4.5 m max. updraft diameter) (Hangan 2014; Hangan et al. 2017a, 2017b).

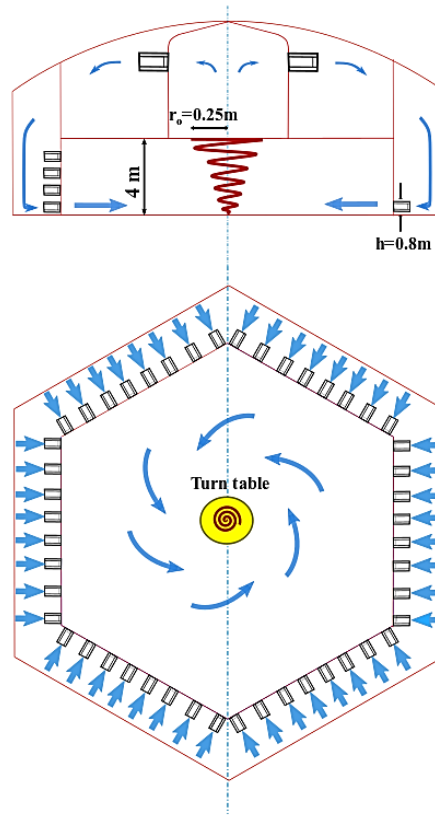


**Figure 3.1 Schematic sketch of tornado at WindEEE dome**

The simulation of tornadoes at the WindEEE dome can be achieved in two Modes. In Mode A (employed herein), tornado-like vortices (TLVs) ( Refan and Hangan 2018) are simulated using the six fans in the upper plenum to create the required updraft in conjunction with the vanes on the bottom of the periphery walls that can be controlled in different angles to produce various tornado intensities (Fig. 3.1). More recently (Ashrafi et al. 2020), Mode B larger tornadoes have been simulated by also using the periphery fans in addition to the top fans. One of the unique characteristics of the WindEEE Dome is that it supports tornado translation for up to 1.5 m/s over a 5 m distance by using a sophisticated control system, the guillotine system, and the bell-mouth. This is, to the authors knowledge, the highest achievable translational speed in all tornado simulators. In addition, the large size of the tornado simulator provides the required resolution to study loading on buildings adequately.

### 3.3 Experimental setup

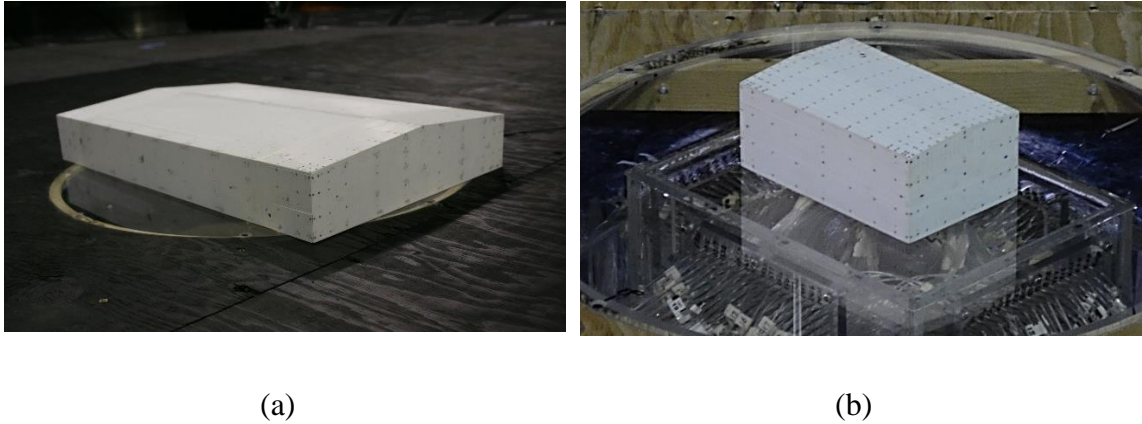


**Figure 3.2 Building models (a) Large building, and (b) Small building**

Laboratory experiments were carried out at WinDEEE Dome, Western University. A comprehensive study on the internal pressures in tornadic flow-field was conducted on two generic low-rise buildings. The present study was dedicated to translating tornado-like vortices as they are a more realistic representation of the field tornadoes' behavior.

The two low-rise buildings (Fig. 3.2) utilized in this study were similar to two buildings from the NIST aerodynamic database representing a large building (Fig. 3.2a) and a smaller building (Fig. 3.2b) to emphasize the effect of building size on the internal tornadic loading. This study was limited to two swirl ratios,  $S=0.48$  and  $S=0.76$ , which represent simulated EF-1 and EF-2 tornadoes at WinDEEE Dome respectively (Refan and Hangan 2018). The selection of EF-1 and EF-2 representative TLVs was based on their higher probability of occurrence unlike higher intensity tornadoes according to NOAA (NOAA n.d.).

#### Building models and Pressure system:

Two generic low-rise building models with a geometric scale of 1:100 and a gable roof slope of 1:12 ( $4.76^\circ$ ) were employed in this study. The two-building models, which will be referred to as large building and small building models according to their plan dimensions, have dimensions of (572 mm  $\times$  365.8 mm) and (191 mm  $\times$  122 mm), respectively. The eave height of both buildings is 73.2 mm. The models were located along the path of translating tornadoes equivalent to EF-1 and EF-2 tornadoes (Fig. 3.2) with a translating

speed of ( $\cong 1.5$  m/s), which is the highest translating velocity achieved in tornado simulators.

Fig. 3.3 shows exploded views of the large (Fig. 3.3a) and small building model (Fig. 3.3b) with internal and external pressure taps. The number of pressure taps instrumented in the large and small models is 446 and 344 external taps and 17 and 12 internal taps, respectively. In this study, we only present the internal pressure results while a parallel study analyses the external pressures and the comparison between tornadic and ABL loading on various building zones. The high density of internal pressure taps, unlike most of the previous studies (e.g. Thampi et al. 2011, Letchford et al. 2015), as well as external pressure taps is used to assess the variability of the internal pressure inside the building model as well as the relation between internal and external pressures near the openings. This will provide a full insight into the differences between internal pressure in Atmospheric Boundary Layer (ABL) flows and tornadic flow-field. The internal pressure taps are distributed evenly through the mid-height of the building walls except for the roof (Fig. 3.3).

Pressure measurements were performed utilizing sixteen electronically scanned pressure (ESP) scanners (pressure range  $\pm 1$  kPa) for the larger building model and twelve scanners for the smaller building. ESP scanners were connected to two digital temperature compensation (DTC) Initiiums (Pressure Systems, Inc.). Each scanner can be connected to up to 32 pressure ports. Each pressure tap was linked to a pressure scanner port using PVC tubing. The accuracy of the pressure scanners is  $\pm 0.03\%$ , while the uncertainty of the initiiums is  $\pm 0.05\%$  over the 0 - 70 °C temperature range. For further details about the pressure system, see Refan and Hangan (2018).

Pressure measurements were performed for two swirl ratios,  $S=0.48$  and  $S=0.76$ , at  $Re_r=10^6$  using a sampling frequency of 500 Hz and a sampling time of 15 s.

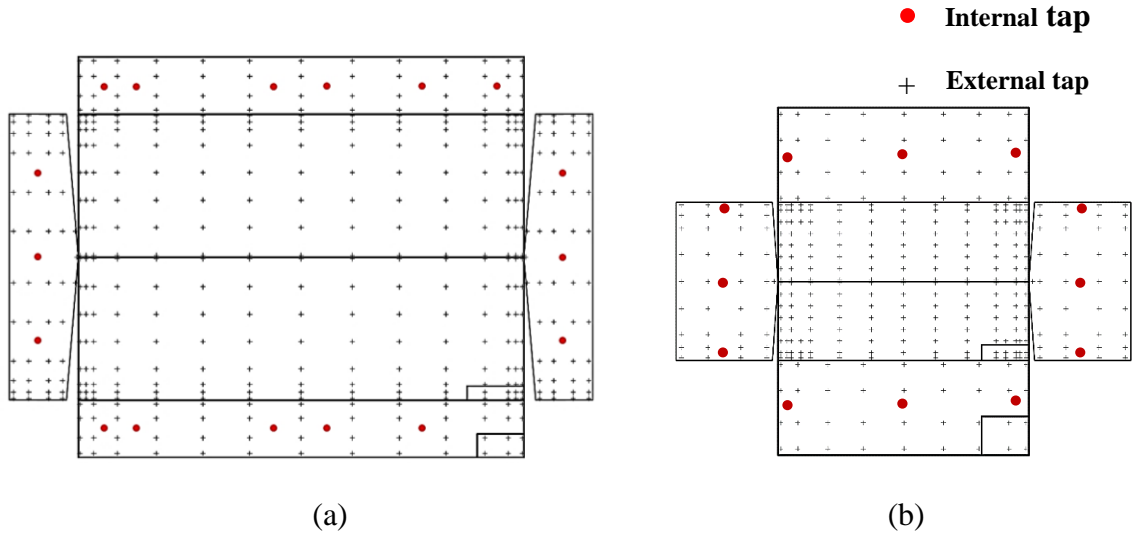


**Figure 3.3 an exploded view of the internal and external pressure taps layout and dominant openings for (a) the large building model, (b) the small building model.**

#### Reference velocity measurements:

The internal pressure inside the building is usually expressed in a non-dimensional form as an internal pressure coefficient ( $C_{p_i}$ ), which is defined as:

$$C_{p_i} = \frac{P_i - P_{ref}}{\frac{1}{2} \rho V_{ref}^2} \quad (1)$$

where  $P_i$  is the pressure recorded by the internal pressure tap,  $P_{ref}$  is the ambient pressure outside the test chamber, and  $V_{ref}$  is the reference velocity.

The reference velocity ( $V_{ref}$ ) for this study was taken as the overall maximum mean tangential velocity without the presence of the building. These reference velocities for  $S=0.48$  and  $S=0.76$  were 11.55 m/s and 13.76 respectively based on previous Particle Image Velocimetry (PIV) measurements (Refan and Hangan 2018). These PIV

measurements used six cameras to capture a large enough field of views (FOV) and covered the two swirl ratios at various heights ( $Z = 6.4, 20.3, 33, 44, 55, 66, 77, 150$  cm). For more details about the PIV setup, refer to Refan and Hangan (2018).

### Opening arrangements:

Multiple opening arrangements (uniform leakage, windward wall opening, roof opening) were tested (Fig. 3.4). In this study, for the first time, a roof opening was added which

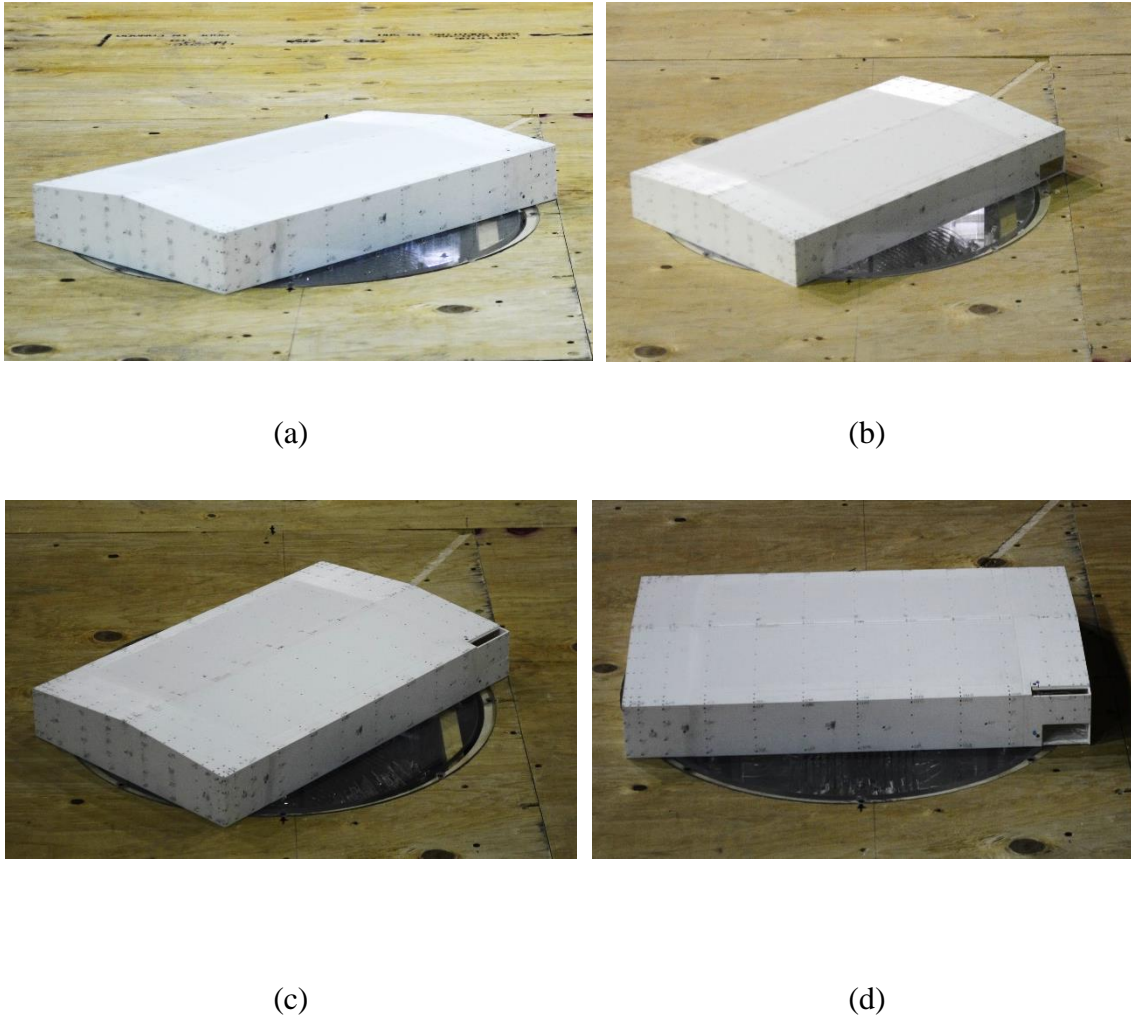


**Figure 3.4 Large building model with openings: (a) uniform leakage, uniform leakage with dominant opening on (b) the large wall, (c) the roof and (d) both the wall and roof**

represents a probable scenario of damage to the building when a roof panel fails during a tornado event. The uniform leakage in the current study is modeled by distributing circular holes throughout the whole building model surface with a total of 176 circular holes ( $d=1.6$  mm) for the large building and 36 holes for the small building model, respectively. This distributed leakage is organized in a way that ensures a total leakage area of 0.1% of the total wall areas as well as the same percentage if referred to a single wall or the roof. The porosity ratio was chosen to be in the same range as the typical leakage found in nominally sealed engineered buildings,  $10^{-4}$  to  $10^{-3}$  (Ginger et al. 1997).

Table (3.1) presents the dimensions of the openings and the associated porosities for the two models. In the present study, the porosity ratio is defined as the ratio between the dominant opening area and its corresponding wall area. The porosity ratio is commonly used in the literature to describe the extent of the openings.

**Table 3.1 Geometry and porosity ratios of leakage and dominant openings**

	Large building model		Small building model	
Opening description	Opening Dimensions (mm)	Porosity ratio	Opening Dimensions (mm)	Porosity ratio
Uniform Leakage	( $\emptyset 1.6$ ) (176 holes)	0.1 %	( $\emptyset 1.6$ ) (36 holes)	0.1 %
Dominant Opening (Front Wall)	$(60 \times 30)(L \times W)$	4.3 %	$(36 \times 30)(L \times W)$	7.72 %
Dominant Opening (Roof)	$(73 \times 18)(L \times W)$	0.63 %	$(36 \times 12)(L \times W)$	1.85 %

### Internal volume scaling:

In order to maintain the similarity of the dynamic response between building model scale and full scale, a sealed volume chamber was added underneath the turntable (Fig. 3.5). This

added volume accommodates the distortion of the internal volume due to the presence of a dominant opening by considering the air volume's dynamic response as a Helmholtz resonator (Holmes 1980). The internal volume of the building model can be calculated using the following expression (Holmes 1980):

$$V_{o,m} = V_{o,f} \frac{(L_m/L_f)^3}{(U_{H,m}/U_{H,f})^2} \quad (2)$$

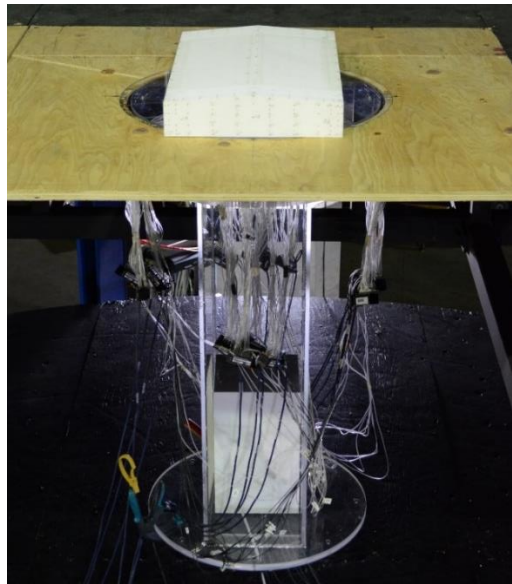


**Figure 3.5 Internal volume attached to the building model underneath the turntable**

where the subscripts  $m$  and  $f$  stand for the model and the full scale respectively,  $L$  is a characteristic length,  $U_H$  is the mean wind speed at roof height and  $V_o$  is the internal volume. This expression can be re-written as



$$\lambda_V = \frac{\lambda_L^3}{\lambda_U^2} \quad (3)$$

where  $\lambda_V$  is the volumetric scale,  $\lambda_L$  is the length scale and  $\lambda_U$  is the velocity scale. The values of these parameters for both buildings are summarized in Table (3.2). The velocity scale was obtained by comparing the overall maximum tangential velocities of the full-scale data with laboratory simulations of tornado-like vortex at WindEEE dome (Refan and Hangan 2018).

**Table 3.2 Internal volume scaling parameters**

	<b>Large Building</b>	<b>Small Building</b>
$\lambda_L$	0.01	0.01
$\lambda_U$	0.42	0.42
$V_{o,m} (m^3)$	0.097	0.01

### Test cases:

Twenty-three test cases were carried out to study the tornado-structure interaction in terms of internal pressures to better understand how these pressures behave in such severe storms. The experiments covered multifold scenarios that are expected to produce different internal loadings on the building. The test cases are categorized, Table (3.3), into four groups to study the effect of multiple variables: (a) building offset, (b) building size, (c) opening size and position, and (d) building orientation. For each case, five repeats were performed. All test cases included the uniform leakage to mimic the real porosity of the buildings.

**Table 3.3 Test cases**

Case #	Building	S	Opening	Orientation	Offset	Roughness
1	S <sup>a</sup>	0.76	uniform	0°	+RMW <sup>b</sup>	-
2	S	0.76	uniform	0°	+2RMW	-
3	S	0.76	uniform	0°	>+2RMW	-

4	S	0.48	uniform	0°	+RMW	-
5	S	0.48	uniform	0°	+2RMW	-
6	S	0.48	uniform	0°	>+2RMW	-
7	L <sup>c</sup>	0.76	uniform	0°	+RMW	-
8	L	0.76	uniform	0°	+2RMW	-
9	L	0.76	uniform	45°	+2RMW	-
10	L	0.76	uniform+roof	45°	+2RMW	-
11	L	0.76	uniform+wall	45°	+2RMW	-
12	L	0.48	uniform	45°	+2RMW	-
13	L	0.48	uniform+roof	45°	+2RMW	-
14	L	0.48	uniform+wall	45°	+2RMW	-
15	L	0.76	uniform	0°	+RMW	3 cm
16	L	0.76	uniform+roof	0°	+RMW	3 cm
17	L	0.76	uniform+roof+wall	0°	+RMW	3 cm
18	S	0.76	uniform	0°	+RMW	3 cm
19	S	0.76	uniform+wall	0°	+RMW	3 cm
20	S	0.76	uniform+roof+wall	0°	+RMW	3 cm
21	S	0.48	uniform	45°	+RMW	-
22	L	0.48	uniform	0°	+RMW	-
23	L	0.48	uniform	45°	+RMW	-

<sup>a</sup> S refers to small building model

<sup>b</sup> +RMW is the radius of the maximum wind

<sup>c</sup> L refers to large building model

### 3.4 Results and discussion

Internal pressure characteristics were examined under a translating tornadic flow-field at the WindEEE Dome. Fig. 3.6 shows a schematic drawing of the tornado translation inside

WindEEE. The results are categorized into multiple sections; Firstly the uniformity of the internal pressure inside the building model as well as the correlation between internal and external pressure near dominant openings are investigated; Secondly, the variation of the internal pressures with respect to the following four variables: offset, building size, orientation, opening size, and position are determined. The investigation, therefore, covers the variation of internal pressures for various vulnerable scenarios.

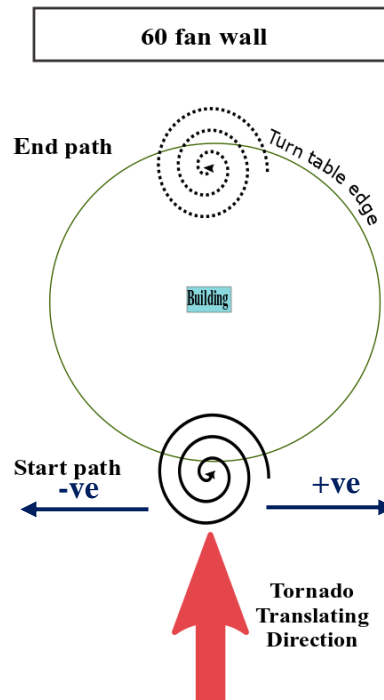


**Figure 3.6 Schematic of the tornado translation in the WindEEE Dome**

### Internal pressure correlation

One of the important features of internal pressures in ABL flows is that they are uniform throughout the interior of the building (Stathopoulos et al. 1979). Tornadoes have more complex flow-field characteristics than ABL straight-flows accompanied by a radial variation of atmospheric pressure deficit (APD) which may have an effect on the internal pressure distribution inside buildings.

In order to investigate the behavior of the internal pressure inside the building model, the correlations between the internal pressures at various taps positions were examined. These

correlations were based on the cross-correlation coefficient “ $R_{xy}$ ”:  $R_{xy}(t) = \int_{-\infty}^{\infty} x(\tau - t)y(\tau)d\tau$ , where  $x$  and  $y$  are the two signals (i.e.  $Cp_{i,tap\ n}$  and  $Cp_{i,tap\ m}$ ) and  $\tau$  is the lag. It is found that for all the cases of the current study, the internal pressure taps’ measurements are highly correlated with correlation coefficients  $R_{xy} > 0.9$ . Table (3.4) summarizes the minimum internal pressure correlation coefficient for all the cases categorized based on the four effects under investigation. This shows that the induced internal pressure field due to tornadic flow is uniform inside the building exhibiting similar behavior to the internal pressures in ABL flows. This conclusion is important as it shows that, irrespective of the building size, building orientation, tornado intensity, opening size and position of the building, the internal pressure field is uniform. This conclusion expands previous findings found in the literature (e.g. Nasir 2017; Wang et al. 2018), where Nasir (2017) used a computational model in his study and Wang et al. (2018) utilized a stationary tornado simulator at Tongji University.

On the other hand, the correlation between internal and external pressures near the dominant openings (i.e. windward and roof openings) was examined to understand the extent of resemblance between tornadic flow-field and ABL flow. In ABL flow, the internal and external pressures near the dominant opening are highly correlated (Stathopoulos et al., 1979). Utilizing seven external pressure taps surrounding the roof opening, it was found that, for the dominant opening in the roof, the external pressures near the opening are highly correlated with the internal pressure except for the roughness cases. This behavior is in agreement with previous studies’ findings (Rajasekharan et al. 2013; Letchford et al. 2015). It should be noted that the effect of roughness is peripheral to the scope of this study and needs further investigation.

Furthermore, the correlation between internal and external pressure near the dominant opening was studied for the case of a dominant windward wall. For case 19 where the building is positioned at +RMW, the internal and external pressures are highly correlated, while for case 11 and 14 (at +2RMW) they are not highly correlated ( $R_{xy} < 0.9$ ). This is attributed to the fact that the external pressure taps on the windward wall are not adjacent to the opening like the ones near the roof opening. This affected the correlation specifically when the tornado vortex is beyond the core region. A first estimation of the internal

pressure coefficient  $C_{p_i}$  under uniform leakage is the expected value of  $C_{p_e}$  or in other words, the spatial average of external pressure:  $(C_{p_i} \approx \int_{-\infty}^{\infty} C_p f_{C_p}(C_p) d C_p \approx E(C_p))$  (Davenport 2007). The applicability of this internal pressure approximation for tornadic flow-field may provide an initial estimation of internal pressure in tornadoes. Hence, a comparison between the internal pressure deficit and the spatial average of external pressures was performed (Fig. 3.7). It can be seen from Fig. 3.7a,b,c that overall the internal pressure follows closely the same trend as the expected value of the external pressure (i.e. the spatial average of external pressure) with some difference in their magnitudes which decreases with increasing building offset. This slight difference could be attributed to the translation, particularly high translation speed  $\cong 1.5$  m/s, of the tornado flow-field in the present study.

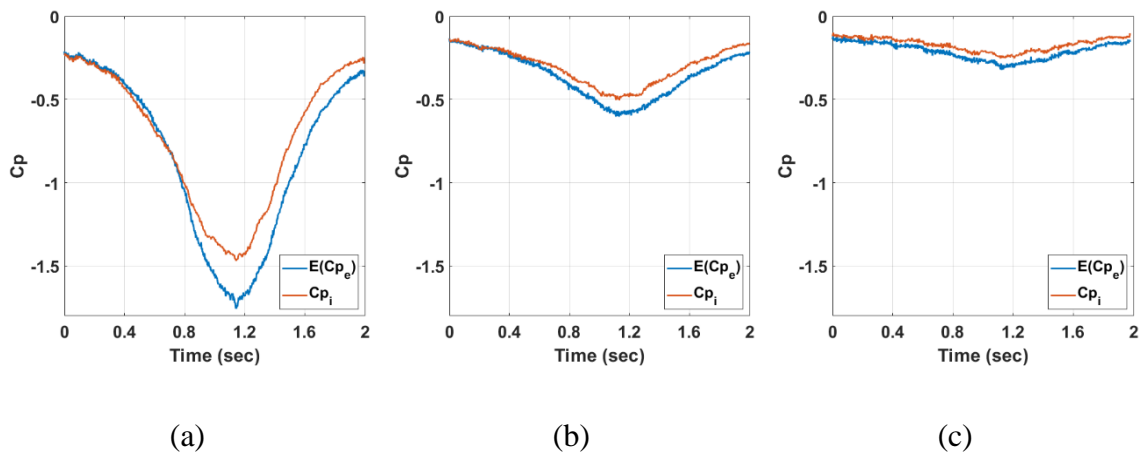


**Figure 3.7 Comparison between internal pressure and the spatial average of external pressure for uniform leakage (Small building) at (a) +RMW (as per case 4), (b) +2RMW (as per case 5), and (c) >+2RMW (as per case 6),**

**Table 3.4 Internal pressure correlation**

	$R_{xy_{min}}$
Effect of offset	0.996
Effect of building size	0.999

<b>Effect of openings</b>	0.924
<b>Effect of orientation</b>	0.999

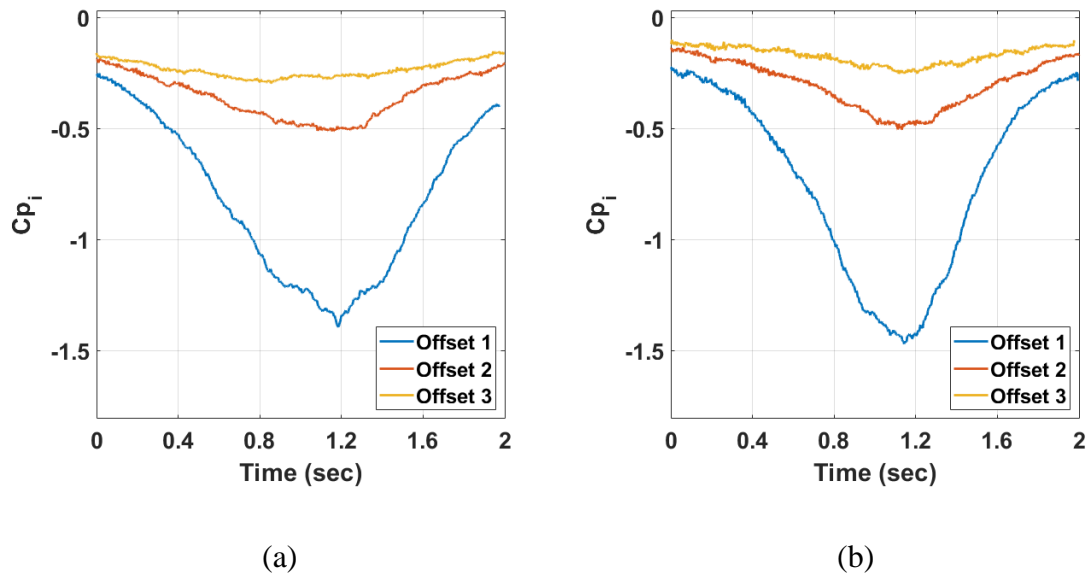


**Figure 3.8 Effect of offset on internal pressure (Small building) for (a)  $S=0.76$  (EF-2) (as per cases 1,2, and 3), (b)  $S=0.48$  (EF-1) (as per cases 4,5, and 6).**

### The effect of offset

Three building offsets, offset 1 (+RMW), offset 2 (+2RMW), and offset 3 (>+2RMW), were examined to investigate the internal pressure as a function of building location either inside or outside the core region (case 1 to case 6) of the TLV as summarized in Table (3.1). Fig. (3.8 a,b) shows that the internal pressure is negative (suction) for all the cases. The variation of internal pressures with offset is attributed to the combined effects of the atmospheric pressure deficit (APD) producing an overall suction as well as the tornado-aerodynamic effects. Comparing the first three cases of EF-2 rated tornado ( $S=0.76$ ), the largest peak internal pressure coefficient is for the case of offset 1 (+RMW) which is consistent with previous studies (e.g. Wang et al. 2018). This is logical as shifting the building model further outside the core region will decrease the APD pressure

substantially. Moving the building from (+RMW) to (+2RMW) caused a reduction of two-thirds of the peak internal pressure.

This shows the drastic effect that the building location can have on the internal pressures in tornadic flows. Further increasing the offset ( $>+2\text{RMW}$ ), the magnitude of the peak internal pressure is decreased only by 15%. This shows that going beyond the core region, the internal pressure loading will be less impacted by the tornadic hit as the effect of tornadic suction diminishes gradually, approaching the behavior of straight-flow wind. Moreover, the examination of the second scenario, cases (4,5, and 6), of simulated EF-1 tornado ( $S=0.48$ ) shows the same trend as the first three cases but with a slightly higher magnitude of the minimum  $C_{p_i}$  of -1.47. This is coherent as lower intensity tornadoes (one-celled) should produce higher  $C_p$  negative peaks (Haan et al. 2010). The negative peak pressures are decreasing with increasing the offset which was observed in Nasir (2017) and Wang et al. (2018) and that this relation is not linear.

### The effect of building size

Another important parameter is the ratio between the tornado core diameter and the maximum plan dimension of the building. This ratio correlates to the balance between aerodynamic and APD effects in tornado-structure interactions. This aspect was explored by Case et al. (2014) but their study was confined to external pressures only. Cases 1, 2, 7, and 8 of our study represent different scenarios to tackle the buildings' plan dimension effect.

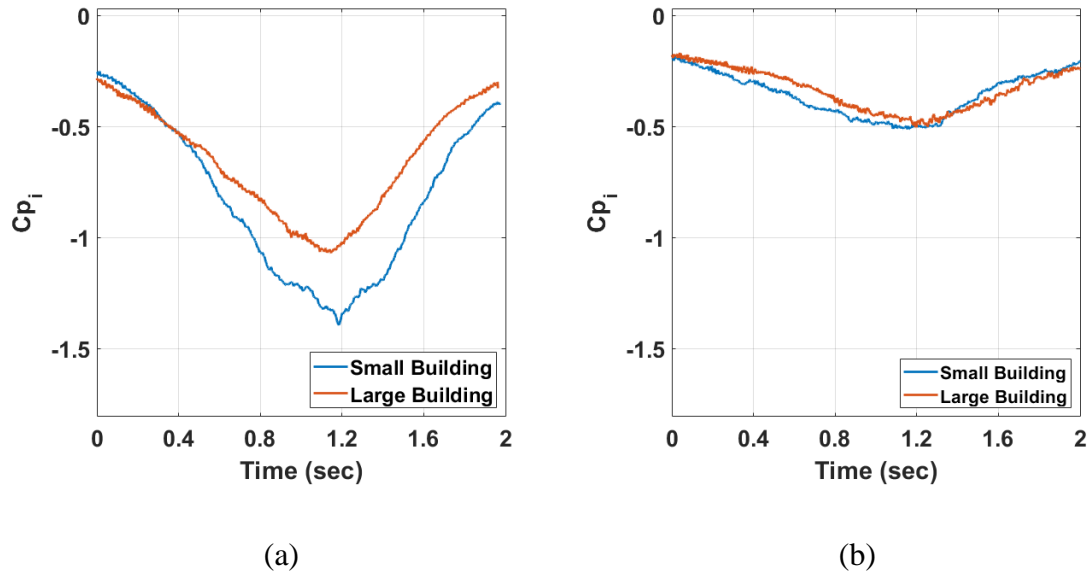


**Figure 3.9 Effect of building size on internal pressure (uniform leakage) for (a)  $S=0.76$  (EF-2) at +RMW (as per cases 1 and 7), (b)  $S=0.76$  (EF-2) at +2RMW (as per cases 2 and 8).**

Fig. (3.9a) illustrates that the small building experienced a higher internal pressure peak compared to the large building by 25% at +RMW. This is attributed to the dominant APD effect when the building is engulfed in the tornado core due to its smaller length, 191 mm, compared to the large building that has three times the length of the small building. By increasing the offset distance to +2RMW (Fig. 3.9b), the difference in internal pressure between the two buildings becomes negligible as the effect of the APD diminishes.

### The effect of orientation

Four cases were examined to study the effect of building orientation (cases 4, 21, 22, and 23). The test cases include both large and small buildings to explore the difference of their interaction with the simulated tornadoes. Fig. 3.10 illustrates that changing the building orientation from  $0^\circ$  to  $45^\circ$  led to a time lag in the occurrence of the minimum pressure. This may be associated with additional tilting of the tornado vortex due to the longer time (distance) that it interacts with the building at  $45^\circ$  orientation. This observation is not similar to ABL flow in which changing the orientation from  $0^\circ$  to  $45^\circ$  does not affect the



peak internal pressures (Tecle et al. 2015). Moreover, not just the shift of the whole signal was observed but also the difference in magnitude of the peak pressures. Fig. 3.10 a,b shows that there is a slight difference in the peak pressure magnitudes between the two orientations for the two studied cases, whether large or small building.

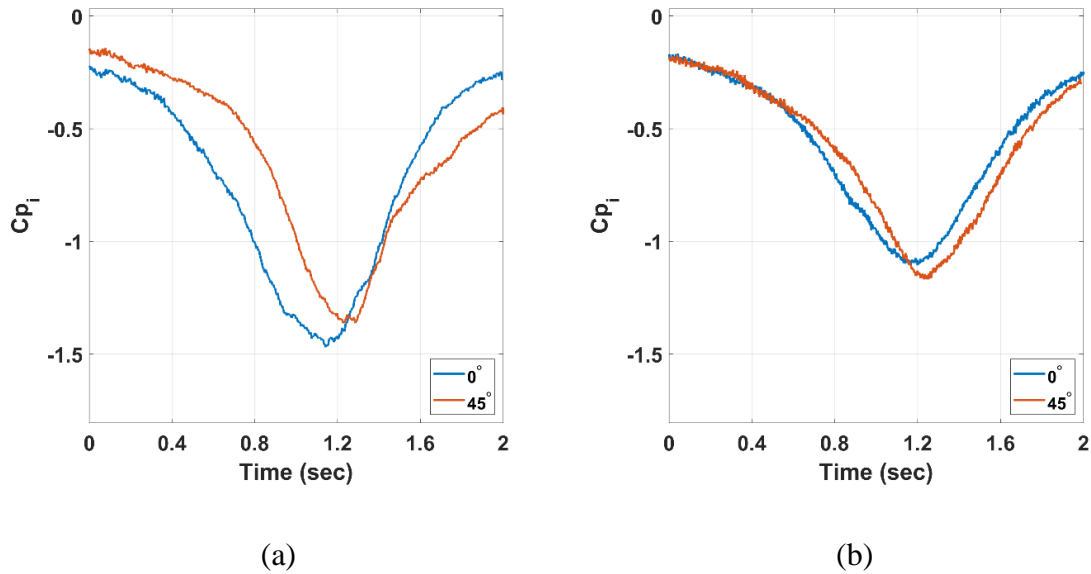


**Figure 3.10 Effect of building orientation on internal pressure for (a)  $S=0.48$  (EF-1) for the small building (as per cases 4 and 21), (b)  $S=0.48$  (EF-1) for the large building (as per cases 22 and 23).**

### The effect of openings

In ABL flow, a dominant opening in the windward wall causes the peak internal pressure (Stathopoulos et al. 1979), while in tornadic flow-field, the nature of the rotating flow-field may cause differences in the peak pressure occurrence. Cases (9-20) were examined to investigate the effect of the opening configuration in altering the internal pressure pattern. First, cases 9,10, and 11 were used to compare the uniform leakage, roof, and wall opening configurations for  $S=0.76$  for the large building model at +2RMW (Fig. 3.11a). It is well observed from Fig. 3.11a that the internal pressure is negative for all the cases because of the dominant APD effects. For the first three cases (9,10, and 11) ( $S=0.76$ , large building at +2RMW), the roof opening produced a higher suction compared to uniform leakage and

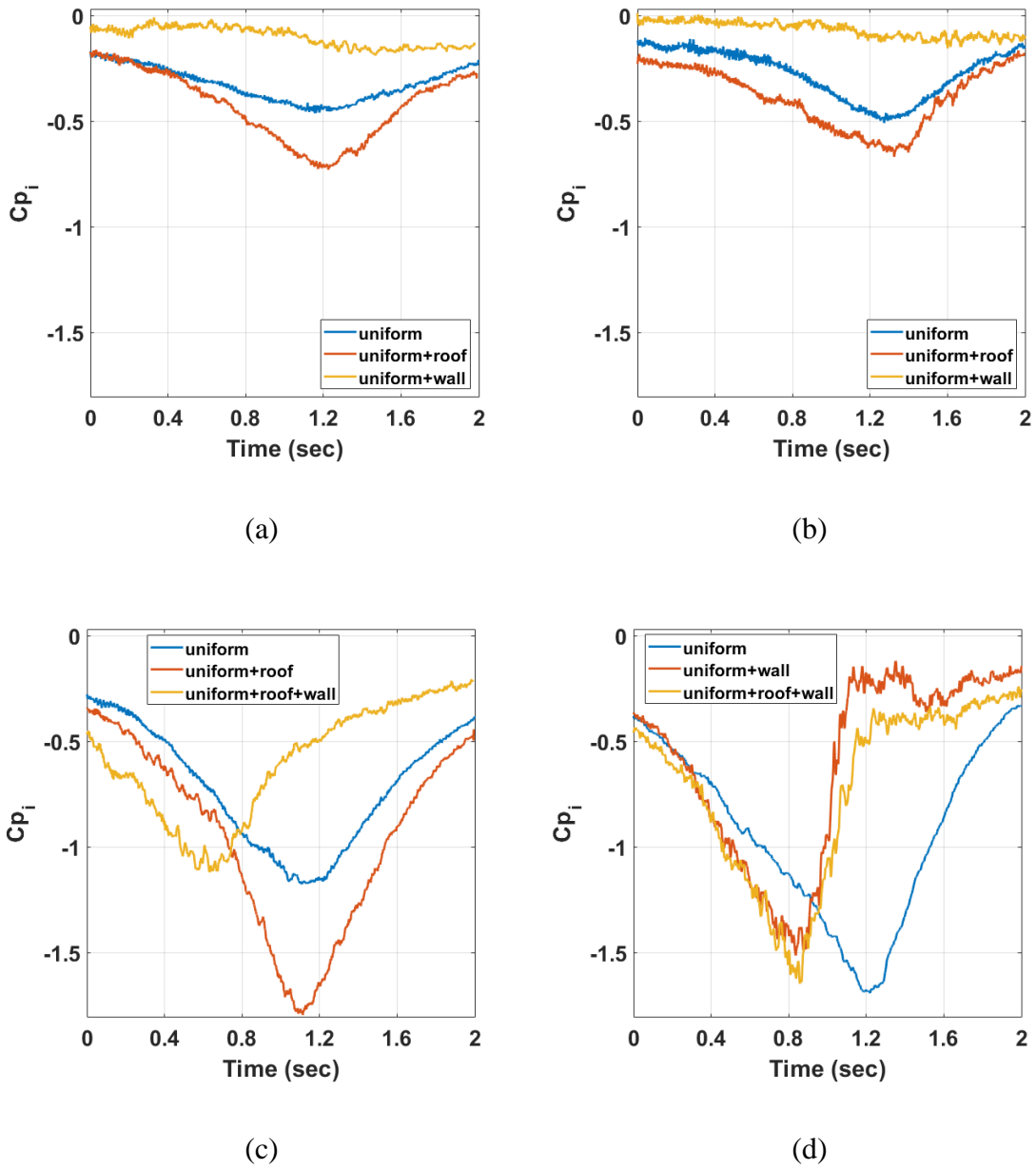


**Figure 3.11 Effect of opening configuration on internal pressure for (a)  $S=0.76$  (EF-2) for the large building (as per cases 9, 10 and 11), (b)  $S=0.48$  (EF-1) for the large building (as per cases 12, 13 and 14), (c)  $S=0.76$  (EF-2) for the large building (as per cases 15, 16 and 17), (d)  $S=0.76$  (EF-2) for the small building (as per cases 18, 19 and 20).**

the wall opening (Fig. 3.11a). Similar observations apply for the second three cases (12,13, and 14) for  $S=0.48$  for the large building at +2RMW, where the only difference was the tornado strength (EF-1 rated tornado) (Fig. 3.11b).

This behavior could be due to the dominant effect of the APD over the roof area. The fact that the negative internal pressures are minimized by a wall opening highlights the fact that opening windows or doors during a tornadic event can in reality increase the differential pressure over the building increasing its vulnerability. At the same time, the increase in the magnitude of negative internal pressures under roof opening can provide future solutions for reducing building vulnerability. The overall behavior of the internal pressure with the opening configuration can be further explored by investigating the induced internal pressures at the radius of the maximum wind location (+RMW). Hence, another 6 cases (15- 20) were explored to study the effect of combining the wall and roof openings, Figs 3.11c and 11d.

It can be seen from Fig. 3.11d that the combination of wall and roof openings resulted in a similar behavior to the case of the wall opening solely. This could be due to the early admittance of the tornado flow-field through the large windward wall opening prior to the roof opening. Another important observation is that the wall opening resulted in an earlier peak of the pressure deficit because of the building located at the core radius which caused early access of the tornadic flow into the interior of the building (Fig. 3.11d). The same scenario applied for the combined roof and wall opening as the presence of the windward dominant opening overweighted the tornadic suction through the roof (Fig. 3.11c and 11d). Also, a dominant opening in the windward wall produced a slightly lower peak pressure magnitude than the uniform leakage case. This finding contradicts findings in previous studies (Kikitsu and Sarkar 2011, Wang et al. 2018). Both these studied exhibited a similar porosity ratio as the present study for the large building model case. The differences may be attributed to the ratio between the TLV core diameter and the building dimension which is 2 for the large building model in this study and  $> 7$  in Kikitsu and Sarkar (2011) and 4.4 for Wang et al. (2018). Also, both studies were confined to the tornado translating directly over the building (i.e. building offset=0).

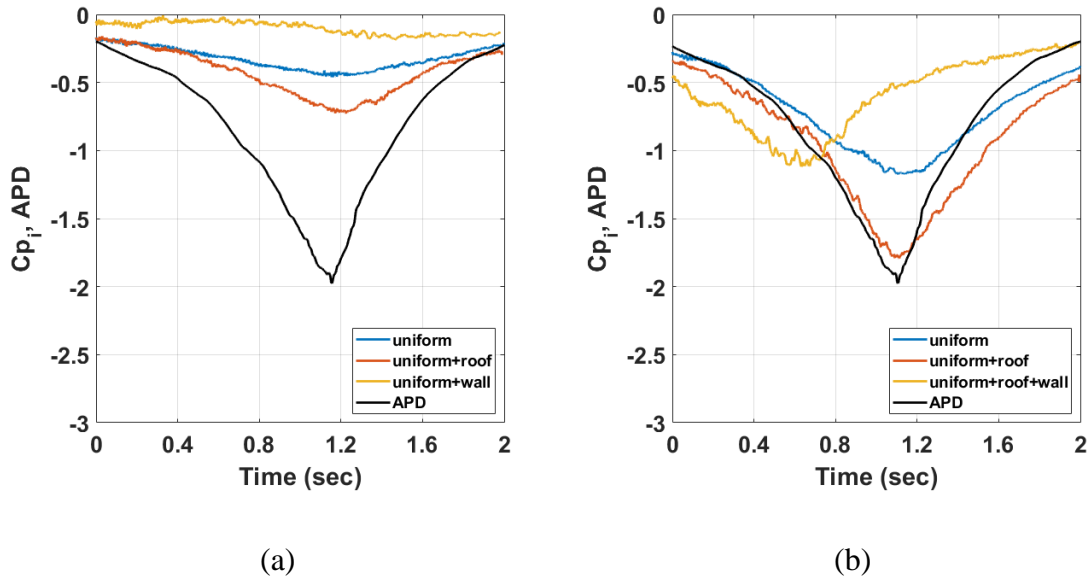


**Figure 3.12 Comparison between internal pressure coefficients and APD for (a)  $S=0.76$  (EF-2) for the large building at +2RMW (as per cases 9, 10 and 11), and (b)  $S=0.76$  (EF-2) for the large building at +RMW (as per cases 15, 16 and 17).**

It is shown from Fig. 3.11a,b,c that an opening in the roof may cause the peak negative pressure. This behavior can be favorable if compared with the APD. Hence, a need for further exploring the relation between the internal pressure and the APD is crucial.

The APD of the tornado flow-field without the presence of the building was plotted and compared with the internal pressure coefficients in Fig. 3.11a and 11c (Fig. 3.12). It should be noted that the internal pressure measurements and the APD measurements were not synchronized. Therefore, the APD profile was compared with the internal pressure profiles by aligning the peaks of the pressure deficits. It is shown from Fig. 3.12a, for cases 9,10 and 11 (i.e. uniform, uniform+roof, and uniform +wall) for  $S=0.76$  at +2RMW, that the APD has higher peak pressure compared to the internal pressure coefficients for all the cases, however, the roof opening would produce the lowest differential pressure compared to a dominant windward opening and uniform leakage. The difference in peak pressures between the APD and the internal pressure is attributed to the building being positioned beyond the core region where the APD effects are minimized. In order to understand the

building position effect on this comparison, the APD and internal pressures were compared for +RMW (cases 15, 16, and 17) for  $S=0.76$  (Fig. 3.12b). It can be seen that the APD profile is close to the (uniform+roof) case. This shows that a building positioned at +RMW would experience an equalized differential pressure, to some extent, in the presence of an opening in the roof, however, a windward opening (i.e. open door or broken window) or a uniform leakage would result in an unfavorable differential pressure. This reflects the importance of induced internal pressures inside buildings and the possible effects of different opening configurations on building vulnerability.

## Conclusions

The internal pressures for two generic low-rise buildings under translating tornado-like vortices (TLVs) were examined experimentally for volume size, resolution, and translation velocity never achieved before. The effects of building offset with respect to the tornado path, building size, building orientation, and openings on the internal pressure loadings were investigated. The main findings from the study are summarized as follows:

- The internal pressure is uniform inside the building model irrespective of the opening configuration, building size, building offset, or orientation. This shows the similarity between ABL flows and tornadoes in terms of internal pressure distribution.
- The external pressure adjacent to the dominant opening correlates well with the internal pressure inside the building. This shows the resemblance between the behavior of the internal pressure for straight-line winds and tornadic flow-field.
- Building offsets were found to have an important effect on the peak internal pressure. Peak internal pressure was shown to decrease by  $2/3$  in the outer core compared to the core region of the translating TLVs. In addition, the relation between the offset distance and the peak internal pressure is not linear.
- In terms of the size of the building, it has been shown that the smaller the building size compared to the tornado vortex core, the higher the peak internal pressure the building experiences. This highlights the severe damage a small building may experience during tornadic hits.

- Changing the orientation angle of the building model from  $0^\circ$  to  $45^\circ$  slightly affects the internal pressure peak magnitude and causes a lag of the whole pressure deficit due to the longer interaction between the tornado and the building in the  $45^\circ$  case.
- It was found that the negative pressure flow-field in tornadic flow dominates the internal pressure behavior irrespective of the type of opening. Moreover, a roof opening will produce the highest peak of the internal pressure compared to a windward dominant opening or uniform leakage.
- A roof opening would equalize the APD when the building is at +RMW, which in turn would mitigate the differential pressure and the building's vulnerability.

At last, it was found that the induced internal pressure due to tornadic flow-field is a complex problem that plays a vital role in determining the overall wind load on buildings which cannot be neglected or underestimated in calculating the net loading on buildings. Further research should be done to understand the effect of roughness on internal pressures in tornadic flow-field and to develop models that can predict the internal pressure behavior utilizing the broad and easy-to-access datasets of pressure loading in ABL flow-field.

## Acknowledgment

This research has been made possible through funding from Natural Sciences and Engineering Research Council of Canada (NSERC) Discovery Grant (Grant number: R2811A03) and Canada Foundation for Innovation (CFI) WinDEEE Dome Grant (Grant number: X2281838).

## References

Ashrafi, A., Romanic, D., Kassab, A., Hangan, H., & Ezami, N. (2020). Experimental investigation of large-scale tornado-like vortices. *Journal of Wind Engineering and Industrial Aerodynamics*, 104449. <https://doi.org/10.1016/j.jweia.2020.104449>

Baker, C., & Sterling, M. (2019). Are Tornado Vortex Generators fit for purpose?. *Journal of Wind Engineering and Industrial Aerodynamics*, 190, 287-292.  
<https://doi.org/10.1016/j.jweia.2019.05.011>

Case, J., Sarkar, P., Sritharan, S., 2014. Effect of low-rise building geometry on tornado induced loads. *J. Wind Eng. Ind. Aerod.* 133, 124–134.  
<https://doi.org/10.1016/j.jweia.2014.02.001>.

Davenport, A. G. (2007). *Wind tunnel testing: a general outline*. AG Davenport Wind Engineering Group, University of Western Ontario, Ontario.

Davenport, A. G., & Surry, D. (1984, March). The estimation of internal pressures due to wind with application to cladding pressures and infiltration. In *Proc., Wind pressure workshop* (pp. 1-19). Brussels, Belgium: International Energy Agency.

Ginger, J. D., Holmes, J. D., & Kim, P. Y. (2010). Variation of internal pressure with varying sizes of dominant openings and volumes. *Journal of Structural Engineering*, 136(10), 1319-1326. [https://doi.org/10.1061/\(ASCE\)ST.1943-541X.0000225](https://doi.org/10.1061/(ASCE)ST.1943-541X.0000225)

Ginger, J. D., Mehta, K. C., & Yeatts, B. B. (1997). Internal pressures in a low-rise full-scale building. *Journal of wind engineering and industrial aerodynamics*, 72, 163-174. [https://doi.org/10.1016/S0167-6105\(97\)00241-9](https://doi.org/10.1016/S0167-6105(97)00241-9)

Ginger, J., & Kim, P. (2009, November). Variation of internal pressure with size of dominant opening and volume. In *Proceedings of Seventh Asia-Pacific Symposium on Wind Engineering* (pp. 8-12).

Haan Jr, F. L., Balaramudu, V. K., & Sarkar, P. P. (2010). Tornado-induced wind loads on a low-rise building. *Journal of structural engineering*, 136(1), 106-116.  
[https://doi.org/10.1061/\(ASCE\)ST.1943-541X.0000093](https://doi.org/10.1061/(ASCE)ST.1943-541X.0000093)

Hangan, H. (2014). The wind engineering energy and environment (WindEEE) dome at western university, Canada. *Wind Engineers, JAWE*, 39(4), 350-351.  
<https://doi.org/10.5359/jawe.39.350>

Hangan, H., Refan, M., Jubayer, C., Parvu, D., & Kilpatrick, R. (2017). Big data from big experiments. The WindEEE dome. In *Whither Turbulence and Big Data in the 21st Century?* (pp. 215-230). Springer, Cham. [https://doi.org/10.1007/978-3-319-41217-7\\_12](https://doi.org/10.1007/978-3-319-41217-7_12)

Hangan, H., Refan, M., Jubayer, C., Romanic, D., Parvu, D., LoTufo, J., & Costache, A. (2017). Novel techniques in wind engineering. *Journal of Wind Engineering and Industrial Aerodynamics*, 171, 12-33. <https://doi.org/10.1016/j.jweia.2017.09.010>

Ho, T. C. E., Surry, D., Morrish, D., & Kopp, G. A. (2005). The UWO contribution to the NIST aerodynamic database for wind loads on low buildings: Part 1. Archiving format and basic aerodynamic data. *Journal of Wind Engineering and Industrial Aerodynamics*, 93(1), 1-30. <https://doi.org/10.1016/j.jweia.2004.07.006>

Holmes, J. D. (1980). Mean and fluctuating internal pressures induced by wind. In *Wind Engineering* (pp. 435-450). Pergamon. <https://doi.org/10.1016/B978-1-4832-8367-8.50046-2>

Holmes, J. D., & Ginger, J. D. (2012). Internal pressures—The dominant windward opening case—A review. *Journal of wind engineering and industrial aerodynamics*, 100(1), 70-76. <https://doi.org/10.1016/j.jweia.2011.11.005>

Hu, H., Yang, Z., Sarkar, P., & Haan, F. (2011). Characterization of the wind loads and flow-fields around a gable-roof building model in tornado-like winds. *Experiments in fluids*, 51(3), 835. <https://doi.org/10.1007/s00348-011-1102-6>

Mishra, A. R., James, D. L., & Letchford, C. W. (2008). Physical simulation of a single-celled tornado-like vortex, Part B: Wind loading on a cubical model. *Journal of Wind Engineering and Industrial Aerodynamics*, 96(8-9), 1258-1273. <https://doi.org/10.1016/j.jweia.2008.02.027>

Nasir, Z. (2017). Numerical modeling of tornado-like vortex and its interaction with bluff-bodies. *Electronic Thesis and Dissertation Repository*. 4451. <https://ir.lib.uwo.ca/etd/4451>



- Oh, J. H., Kopp, G. A., & Inculet, D. R. (2007). The UWO contribution to the NIST aerodynamic database for wind loads on low buildings: Part 3. Internal pressures. *Journal of Wind Engineering and Industrial Aerodynamics*, 95(8), 755-779.  
<https://doi.org/10.1016/j.jweia.2007.01.007>
- Rajasekharan, S. G., Masahiro, M., & Tamura, Y. (2019). Vulnerability of roof and building walls under a translating tornado like vortex. *Frontiers in built environment*, 5, 53. <https://doi.org/10.3389/fbuil.2019.00053>
- Rajasekharan, S. G., Matsui, M., & Tamura, Y. (2013). Characteristics of internal pressures and net local roof wind forces on a building exposed to a tornado-like vortex. *Journal of Wind Engineering and Industrial Aerodynamics*, 112, 52-57.  
<https://doi.org/10.1016/j.jweia.2012.11.005>
- Razavi, A., & Sarkar, P. P. (2018). Tornado-induced wind loads on a low-rise building: Influence of swirl ratio, translation speed and building parameters. *Engineering Structures*, 167, 1-12. <https://doi.org/10.1016/j.engstruct.2018.03.020>
- Refan, M., & Hangan, H. (2018). Near surface experimental exploration of tornado vortices. *Journal of Wind Engineering and Industrial Aerodynamics*, 175, 120-135.  
<https://doi.org/10.1016/j.jweia.2018.01.042>
- Roueche, D. B., Prevatt, D. O., & Haan, F. L. (2020). Tornado-induced and straight-line wind loads on a low-rise building with consideration of internal pressure. *Frontiers in built environment*, 6, 18. <https://doi.org/10.3389/fbuil.2020.00018>
- Sarkar, P. P., & Kikitsu, H. (2009). Experimental studies on internal pressure and debris strike for improved tornado induced loads of low-rise buildings. *Proceedings of the 41st US-Japan Panel on Wind and Seismic Effects*, Tsukuba, Japan.
- Selvam, R. P., & Millett, P. C. (2003). Computer modeling of tornado forces on a cubic building using large eddy simulation. *Journal of the Arkansas Academy of Science*, 57(1), 140-146.

Sengupta, A., Haan, F. L., Sarkar, P. P., & Balaramudu, V. (2008). Transient loads on buildings in microburst and tornado winds. *Journal of Wind Engineering and Industrial Aerodynamics*, 96(10-11), 2173-2187. <https://doi.org/10.1016/j.jweia.2008.02.050>

Stathopoulos, T., Surry, D., Davenport, A.G. (1979). Internal pressure characteristics of low-rise buildings due to wind action. In: *Proceedings of the Fifth International Conference on Wind Engineering*, Colorado State University, pp. 451–463.

Tecle, A. S., Bitsuamlak, G. T., & Chowdhury, A. G. (2015). Opening and compartmentalization effects of internal pressure in low-rise buildings with gable and hip roofs. *Journal of Architectural Engineering*, 21(1), 04014002. [https://doi.org/10.1061/\(asce\)ae.1943-5568.0000101](https://doi.org/10.1061/(asce)ae.1943-5568.0000101)

Thampi, H., Dayal, V., & Sarkar, P. P. (2011). Finite element analysis of interaction of tornados with a low-rise timber building. *Journal of Wind Engineering and Industrial Aerodynamics*, 99(4), 369-377. <https://doi.org/10.1016/j.jweia.2011.01.004>

Vickery, B. J. (1994). Internal pressures and interactions with the building envelope. *Journal of Wind Engineering and Industrial Aerodynamics*, 53(1-2), 125-144. [https://doi.org/10.1016/0167-6105\(94\)90022-1](https://doi.org/10.1016/0167-6105(94)90022-1)

Vickery, B. J., & Karakatsanis, C. (1987). External wind pressure distributions and induced internal ventilation flow in low-rise industrial and domestic structures. *ASHRAE transactions*, 93, 2198-2213.

Vickery, B. J., & Karakatsanis, C. (1987). External wind pressure distributions and induced internal ventilation flow in low-rise industrial and domestic structures. *ASHRAE transactions*, 93, 2198-2213.

Vickery, B. J., (1986). Gust factors for internal pressures in low-rise buildings. *Journal of Wind Engineering and Industrial Aerodynamics*, 23, 259–271. [https://doi.org/10.1016/0167-6105\(86\)90047-4](https://doi.org/10.1016/0167-6105(86)90047-4)

Wang, J., Cao, S., Pang, W., & Cao, J. (2018). Experimental study on tornado-induced wind pressures on a cubic building with openings. *Journal of Structural Engineering*, 144(2), 04017206. [https://doi.org/10.1061/\(ASCE\)ST.1943-541X.0001952](https://doi.org/10.1061/(ASCE)ST.1943-541X.0001952)

Wang, J., Pang, W., Cao, S., Zhou, Q., & Liao, H. (2019). Fragility analysis of the roof structure of low-rise buildings subjected to tornado vortices. *Journal of Wind Engineering and Industrial Aerodynamics*, 189, 45-55.  
<https://doi.org/10.1016/j.jweia.2019.03.006>

Womble, J. A., Yeatts, B. B., Cermak, J. E., & Mehta, K. C. (1995, January). Internal wind pressures in a full and small-scale building. In *Proc., 9th Int. Conf. on Wind Engineering* (pp. 1079-1090). New Delhi, India: Wiley Eastern Science.

## Chapter 4

### 4 Estimation of tornadic wind loads on building components and cladding as outlined in ASCE7 for straight line winds

#### 4.1 Introduction

Extensive research has been performed to understand the responses of civil engineering structures in straight-line wind or the atmospheric boundary layer (ABL) wind. Building codes, such as ASCE 7-16 (ASCE/SEI 7-16, 2017), provide specific guidelines to calculate minimum design loads (e.g., flood, rain, wind, snow, ice) for buildings and other structures. Wind load provision in ASCE 7-16 has design criteria for structures for the main wind force resisting system and components and claddings. Types of structures include but are not limited to low to mid-rise buildings (4.6 to 48.8 m tall), freestanding walls, free roofs, circular bins, silos, tanks, and solar panels. Wind tunnel procedure for determining wind pressures on the buildings and other structures is also outlined in the code, and wind tunnel tests are permitted in lieu of the design criteria presented in the code for different structures.

Although hurricane winds dictate the design wind speed in the coastal areas, local wind systems such as tornadoes and thunderstorm downbursts, can be more detrimental inland (Solari et al., 2015). These localized wind systems have very different flow characteristics than hurricane winds causing structures to behave differently (Sarkar et al., 2006; Sengupta et al., 2008; Elawady et al., 2017; Jubayer et al., 2019). The research with regards to understanding the flow characteristics of tornadoes and thunderstorm downburst and their effects on structures is still in the early stage (Lombardo et al., 2014; Solari et al., 2015; Romanic et al., 2016; Refan and Hangan, 2018; Razavi and Sarkar, 2018; Bezabeh et al., 2018; Junayed et al., 2019; Jubayer and Wu, 2020). Researchers all around the world have been conducting studies on understanding tornadoes, more now than ever, to provide design guidelines for building tornado resistant structures, especially for weaker, more frequent tornadoes.

In 1971, Theodore Fujita came up with a scale for estimating tornado intensity and their impacts (Fujita, 1971). The scale ranged from F0-F5 and is based on the severity of damages produced by the tornado. There is a range of wind speeds associated with the scale, not from direct measurements in tornadoes, rather from what wind speed could have caused the particular damage. Later in early 2000, meteorologists and engineers revised the Fujita scale to better associate the damage with wind speeds. The revised scale, known as Enhanced Fujita (EF) scale, has been in use around the world since 2007 (McDonald et al., 2006). During 1991-2010, 97% of the tornadoes were rated EF2 or weaker in the USA (National Oceanic and Atmospheric Administration, NOAA). This means designing buildings to withstand up-to EF2 strength tornadoes could significantly reduce the probability of damages and inflicted losses. However, since the EF rating is solely based on the damage, an EF5 equivalent tornado going over a barren land would be rated as EF0. Thus, some of the tornadoes could have been rated lower than their actual strength.

Investigation of wind loads on building due to tornadic flows has been reported in published literature. Several buildings with different sizes and shapes have been tested in the tornado simulator at the Iowa State University. Sarkar et al. (2006) evaluated tornadic wind loads on a 1:500 geometrically scaled tall building and found that tornadoes with strength F2 or higher would exceed the minimum design load set by ASCE 7-02 by a factor of 1.8 or higher. A 1:100 scaled gable roof building with a roof slope of  $35^\circ$  was tested by Haan et al. (2010) and it was found that the peak external uplift force coefficients exceed the minimum design wind loads in ASCE 7-05 by factors between 1.8 and 3.2. Roueche et al. (2015) utilized the pressure data from Haan et al. (2010) and observed that for roof-to-wall connections, peak shear forces were 1.8 times stronger in tornadoes compared to ASCE 7-10 building standard. These studies have two main drawbacks: (i) they used empirical ways of scaling tornado-like vortices (TLVs) with no proper scaling demonstrated between real and simulated tornadoes. (ii) they investigated the peak wind loads on the building as a whole and due to size and spatial resolution problems lack of information regarding wind loads on different zones on the building surfaces, which is of importance for designing components and claddings as outlined in the ASCE 7-16 (ASCE/SEI 7-16, 2017) building code.

In the present study, we address these two previous limitations: (i) the TLV simulations are performed in the Wind Engineering, Energy and Environment (WindEEE) Dome, (Hangan, 2014) which has demonstrated proper geometric scaling against real tornadoes (Refan et al. 2014) and best possible general scaling (Baker and Sterling 2019) and (ii) as having enough spatial resolution capability to perform in detail analysis for building zones loading. Wind loads on two gable-roofed (slope 1:12) low-rise (eave height 7.32 m full scale) building models with different plan dimensions are determined. The two buildings are referred to as large (plan dimension: 57.2 m by 36.58 m) and small (plan dimension: 19.1 m by 12.2 m) buildings. External pressure coefficients are measured on the buildings for two different translating tornado strengths (EF1 and EF2 rated tornadoes), two building orientations ( $0^\circ$  and  $45^\circ$ ), and multiple tornado translation paths. External pressure coefficients are calculated for different zones on the building surfaces as identified in the ASCE 7-16 provision and compared with the recommended design values for straight-line ABL winds.

## 4.2 Component and cladding (C&C) wind load in ASCE 7-16

Chapter 30 of the ASCE 7-16 provides design wind loads for components and claddings for enclosed, partially enclosed, or open buildings in ABL wind. Since the eave height of both buildings in the present study is 7.32 m in full scale, the focus will be given to the design wind loads for buildings with roof height ( $h$ )  $\leq 18$  m (60 ft). The same definition of  $h$  in ASCE 7-16, which is the mean roof height for roof slope ( $\theta$ )  $> 10^\circ$  or eave height for  $\theta \leq 10^\circ$ , is used. As the roof slope of both buildings is 1:12 ( $4.76^\circ \leq 10^\circ$ ), in the present study  $h$  is the eave height, 7.32 m.

External pressure coefficients ( $GC_p$ ) to calculate design wind pressures for components and claddings are provided in the code for different zones on the roof and walls of a low-rise building. For enclosed and partially enclosed buildings with  $h \leq 18$  m (60 ft), the depiction of the wall and roof (for gable roofs with  $\theta \leq 7^\circ$ ) zones is given in Fig. 4.1, where  $a$  is the smaller of 10% of the least horizontal dimension or  $0.4h$ , but not less than 4% of the least horizontal dimension or 0.9 m (3 ft). The plan dimensions of the large and small buildings are 57.2 m (length)  $\times$  36.6 m (width) and 19.1 m (length)  $\times$  12.2 m (width) in full scale,

respectively. Therefore,  $a$  is 2.93 m and 1.22 m for the large and small buildings in the current study, respectively.

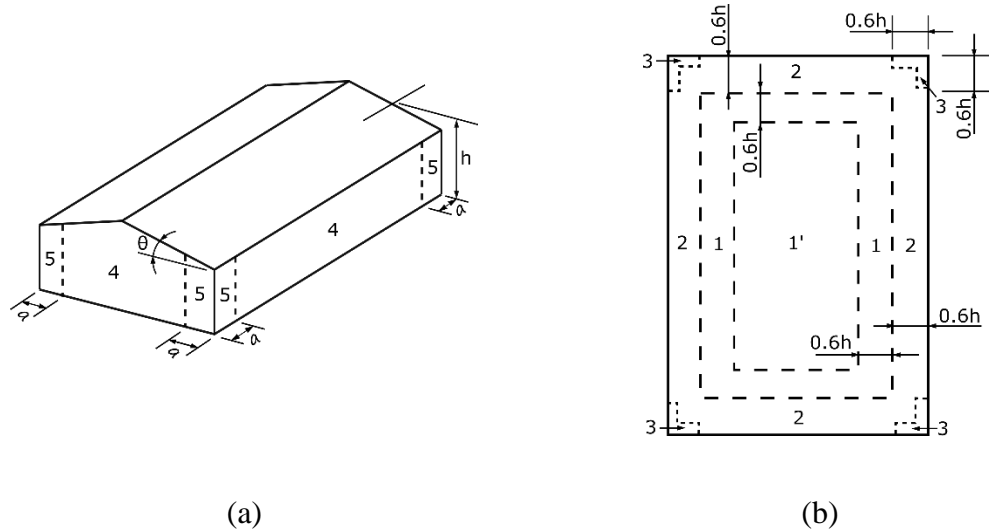


**Figure 4.1 Different zones as defined by ASCE7-16 on (a) walls and (b) roof**

$GC_p$  values for the zones depicted in Figure 4.1 for  $h \leq 18$  m (60 ft) are shown in Figure 4.2. Note that the  $GC_p$  values for the wall zones have been reduced by 10% as outlined in the ASCE7-16 provision for  $\theta \leq 10^\circ$ . Both design maximum (positive) and minimum (negative) pressure coefficients are shown in Figure 4.2. Effective wind area is the area used to determine the  $GC_p$  values. Gust-effect factor ( $G$ ) from  $GC_p$  should not be separated for the values presented in Figure 4.2. The pressure coefficient values from the wind tunnel data were based on mean hourly wind speed. The values presented in Figure 4.2 were divided by 3-s gust wind pressure at  $h$  to adjust the pressure coefficient values associated with a 3-s gust wind speed. Envelope approach (rotating the building model for full  $360^\circ$  in wind tunnels) was used in determining the coefficients reported in Figure 4.2.

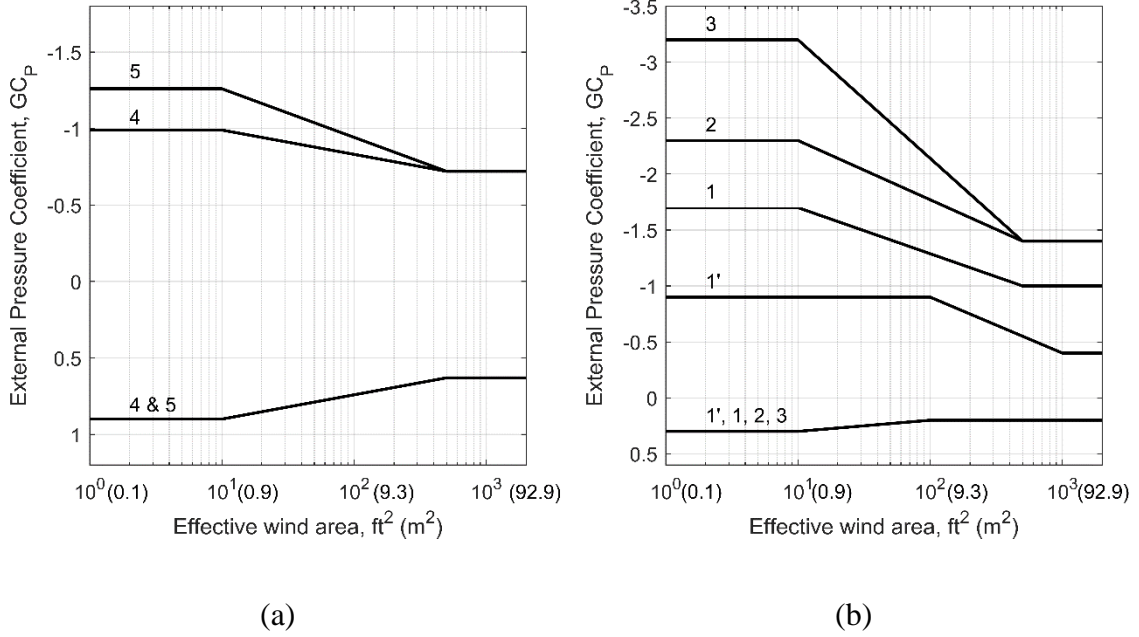


**Figure 4.2 Components and cladding external pressure coefficients for (a) wall and (b) roof (ASCE/SEI 7-16, 2017, Figure 30.3-1 and 30.3-2A).  $GC_p$  values for walls have been reduced by 10% for  $\theta \leq 10^\circ$**

### 4.3 Reference static and dynamic pressures in calculating pressure coefficients

Pressure coefficient ( $C_p$ ), a dimensionless parameter for pressure, is calculated based on Equation 1.

$$C_p = \frac{P - P_{ref}}{q_{ref}} = \frac{P - P_{ref}}{\frac{1}{2} \rho V_{ref}^2} \quad (1)$$

Where,  $P$  is the surface pressure,  $P_{ref}$  is the reference static pressure,  $q_{ref}$  is the reference dynamic pressure,  $\rho$  is the density of air and  $V_{ref}$  is the reference dynamic pressure. In typical wind tunnel test with ABL flow, especially for low-rise buildings  $P_{ref}$  and  $q_{ref}$  are measured at an upper level, much higher than the building height, where the flow is uniform with low level of turbulence.  $C_p$ 's are then re-referenced to building height by multiplying with a conversion factor corresponding to the ratio of reference height to roof height



dynamic pressures. This approach is adopted to reduce the measurement uncertainty due to the higher level of turbulence at the building height (Ho et al., 2005).

For tornadoes, currently, there are no standard guidelines for reference static and dynamic pressures to calculate  $C_p$  which would provide a meaningful comparison of  $C_p$ 's between ABL and tornadic flows. In the study by Haan et al. (2010) maximum mean horizontal velocity at the building height was used as  $V_{ref}$  whereas  $P_{ref}$  was the ambient pressure in the laboratory outside the tornado simulator. Both studies by Sarkar et al. (2006) and Sengupta et al. (2008) employed force balance to measure aerodynamic forces on a model building and used the overall maximum tangential velocity in the tornado to calculate force coefficients.  $P_{ref}$  was not required for this study as the results were presented in force coefficients only. Similar to Sarkar et al. (2006), Hu et al. (2011) also employed overall maximum tangential velocity as  $V_{ref}$  while they used ambient pressure far away from the tornado vortex center as  $P_{ref}$ . Horizontal velocity at the eaves height of the building without the presence of the building was taken as  $V_{ref}$  by Mishra et al. (2008) with mean static pressure on the ground surface in the vicinity of the pressure taps on the building surface as  $P_{ref}$  while calculating  $C_p$  at the pressure taps.

Literature review on the previous studies reveals that when it comes to choosing the  $V_{ref}$  for calculating  $C_p$ 's in tornadoes, researchers have employed either horizontal or tangential velocity recorded either at the height of the building or at the height of the overall maximum velocity. Now as for  $P_{ref}$ , ambient pressure outside the simulator away from the vortex (Haan et al., 2010) and the mean static pressure on the ground surface (Mishra et al. 2008) seem to be the two choices reported in the previous studies. In a recent study by Jubayer et al. (2019), it was shown that using the same approach for reference pressures between synoptic (ABL) and non-synoptic (non-Gaussian impinging jet) flows to calculate  $C_p$ 's do not provide meaningful comparisons of wind loads. In the present study, ambient pressure outside the test chamber isolated from the flow is used as  $P_{ref}$  and overall maximum mean horizontal velocity without the presence of the building is used as  $V_{ref}$ .

## 4.4 Methodology

External and internal pressure measurements were carried out on two low-rise building models with different plan dimensions at the state-of-the-art tornado simulator, the WindEEE Dome. In the current study, external pressures are studied in detail while internal pressures are investigated in a parallel study. In this section, a comprehensive description of the experimental setup and the test cases are provided.

WindEEE Dome, a novel state-of-the-art three-dimensional wind testing chamber, (Hangan 2014) and world's largest tornado simulator, has a hexagonal footprint with 25 m diameter and 3.8 m height. WindEEE Dome has a total of 106 fans among which 60 fans are attached to one wall, 8 fans each on the other five walls of the test chamber, and 6 fans in a plenum above the test chamber ceiling with a 4.5 m diameter circular opening on the ceiling for flow exchange between the test chamber and the upper plenum. Using a different combination of these fans, WindEEE Dome can operate in three major modes: ABL, Tornado, and Downburst. In this study, focus is given to the tornado mode of operation. In the tornado mode, suction is created with the six fans pulling the air out of the upper plenum and the chamber, inflow is obtained through the 8 fans on each of the six peripheral walls, and louvers in front of the peripheral fans provide the necessary swirl. A schematic of the tornado mode of operation at the WindEEE Dome is shown in Figure 4.3. In the present study, a translating EF-1 and EF-2 rated tornadoes were simulated on the low-rise buildings with a translating velocity of 1.5 m/s. The swirl ratios for these tornadoes are  $S=0.48$  (EF-1 rated) and  $S=0.76$  (EF-2 rated) where the swirl ratio is calculated using the following expression:  $S = r_o \Gamma_{max} / 2Qh$ , where  $r_o$  is the updraft radius,  $h$  is the inflow depth,  $\Gamma_{max}$  is the maximum flow circulation and  $(Q)$  is the volumetric flow rate per unit axial length. For the current experiments, the updraft radius is 2.25 m, while the inflow depth is 0.8 m.

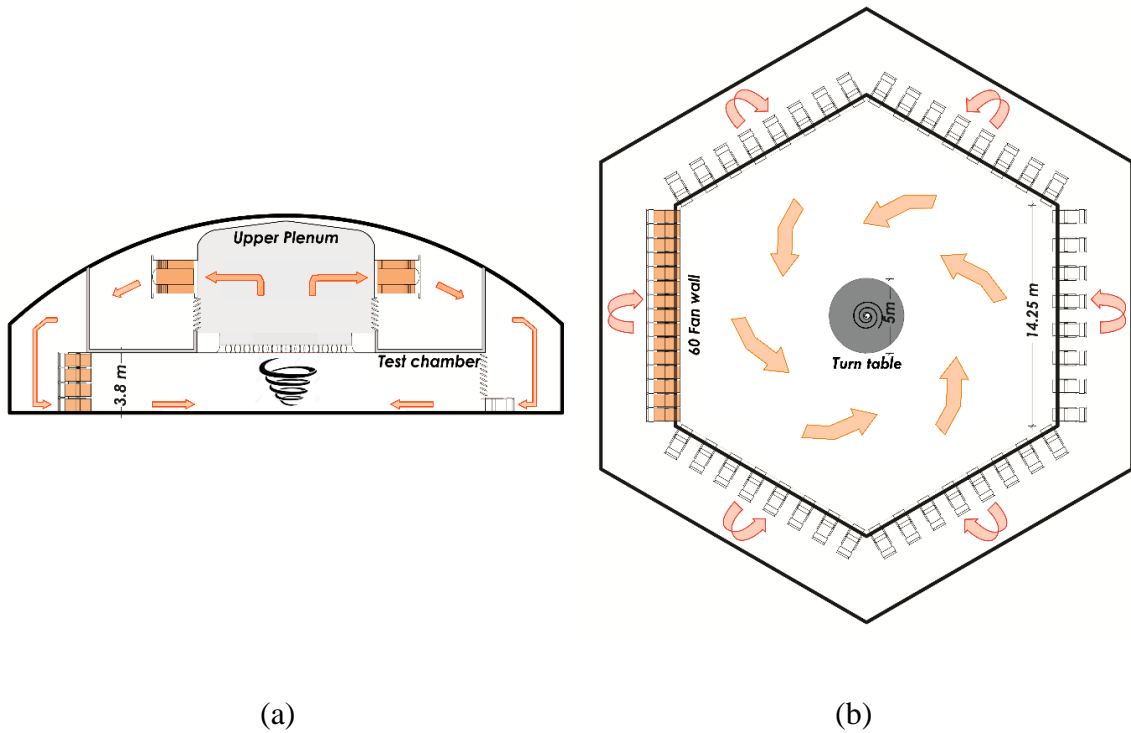
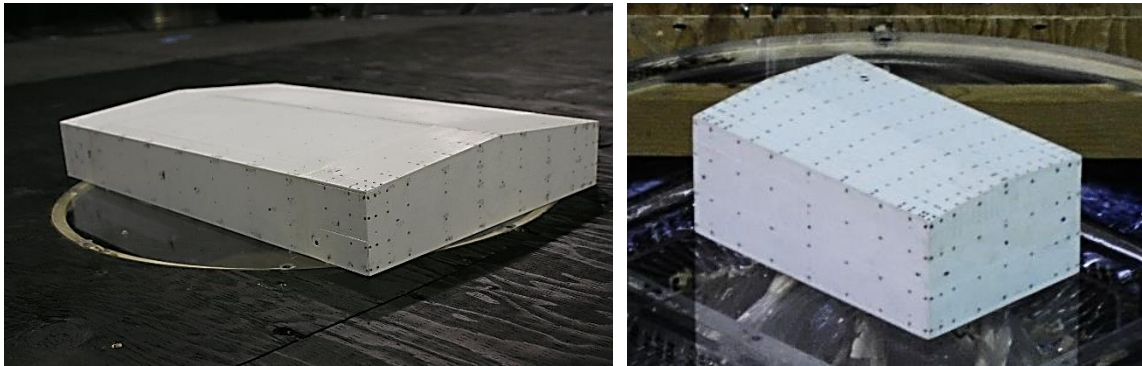


**Figure 4.3: Schematic of tornado flow at WinDEEE Dome (a) side view and (b) top view**

#### 4.4.1 Building Model

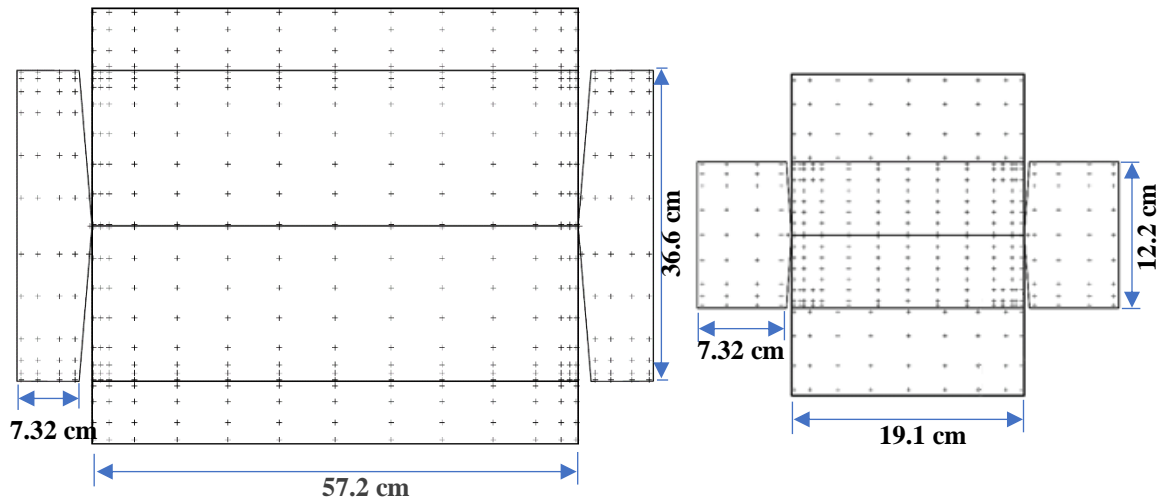
The building models chosen for this study are two gable-roofed buildings with a full-scale plan dimension of 57.2 m (L) by 36.6 m (W) (large building) and 19.1 m (L) by 12.2 m (W) (small building), eaves height of 7.32 m and roof slope of 1:12. The geometric scale of the building models is 1:100. The two buildings were similar to two buildings from the National Institute of Standards and Technology (NIST) database (Ho et al., 2005) where buildings with different sizes were tested in the ABL wind. The large and small buildings are comprised of 446 and 344 external pressure taps, respectively (Fig. 4.4). The pressure taps were distributed among the building walls and roof with a denser distribution in the most vulnerable areas like roof, roof corners, and wall corners as illustrated in the exploded view of the building models (Fig. 4.5).



(a)

(b)

**Figure 4.4 Building models (a) Large building, and (b) small building**



(a)

(b)

**Figure 4.5 Exploded views of the external pressure taps layout and for (a) the large building model, (b) the small building model.**

#### 4.4.2 Test Cases

In this paper, sixteen test cases, as summarized in Table (4.1), are studied to investigate the tornado-structure interaction for two different intensity tornadoes,  $S=0.48$  (EF-1) and  $S=0.76$  (EF-2) and two low-rise buildings with different plan dimensions. The cases were designed to emphasize the effect of building location and building orientation with respect to the tornado path as well as building size on the overall pressure distributions on the buildings and comparison with the ASCE loading. Five runs were performed for each case. Since the same building models were used to investigate internal pressures as well, the models had uniform leakage distributed on all surfaces of the building. For each building, the total leakage area is 0.1% of the overall wall area. This ratio is compared to the real distributed leakage in nominally sealed buildings which is  $10^{-4}$  to  $10^{-3}$  as stated by Ginger et al. 1997.

**Table 4.1 Test cases**

Case #	Building	$S$	Orientation	Offset (from the
1	S <sup>a</sup>	0.76	0°	+RMW <sup>b</sup>
2	S	0.76	0°	+2RMW
3	S	0.76	0°	>+2RMW
4	S	0.48	0°	+RMW
5	S	0.48	0°	+2RMW
6	S	0.48	0°	>+2RMW
7	L <sup>c</sup>	0.76	0°	+RMW
8	L	0.76	0°	+2RMW
9	S	0.48	45°	+RMW
10	L	0.48	0°	+RMW
11	L	0.48	45°	+RMW
12	L	0.76	45°	+RMW
13	L	0.76	45°	+2RMW

14	L	0.48	0°	+2RMW
15	L	0.48	45°	+2RMW
16	S	0.76	45°	+2RMW

<sup>a</sup> S denotes small building model

<sup>b</sup> +RMW denotes the radius of the maximum wind

<sup>c</sup> L denotes large building model

#### 4.4.3 Measurement Details

External pressures on the building models were measured using ESP (electronically scanned pressure) scanners, pressure range  $\pm 1$  kPa, (Pressure Systems, Inc.) coupled with two digital temperature compensation (DTC) initiators. The accuracy of the pressure scanners is  $\pm 0.03\%$  and the initiators' uncertainty is  $\pm 0.05\%$  over the whole temperature range (0 - 70 °C). A sampling frequency of 500 Hz and a sampling time of 15 s were utilized in the present study at  $Re_r = 10^6$ , where  $Re_r$  denotes the radial Reynolds number ( $Re_r = Q/2\pi\nu$ , where  $Q$  is the volumetric flow rate per unit axial length and  $\nu$  is the kinematic viscosity of the fluid). This sampling time (15 s) along with a translation speed of 1.5 m/s ensured that the translating tornado passed the whole building model. Reference velocity measurements were performed by means of cobra probes without the presence of the buildings. The reason behind that is the existence of the maximum horizontal velocities in tornadic flow near the ground where the building affects the peak velocity magnitude, unlike ABL flow where the building does not alter the maximum velocities that subsist just above the structure. Cobra probe is a multi-hole pressure probe that is designed to resolve three components of velocity as well as local static pressure in real-time. It is designed to measure flow-fields within a  $\pm 45^\circ$  cone at high frequencies that makes it suitable for turbulent flow measurements such as tornadic flow. The translating tornado adds complexity to the wind speed measurements due to the swirling motion of the vortex. This resulted in expecting the wind from multiple directions for a single measurement location. The near region of the tornado translating trajectory is more prone to multi-directional winds than beyond the tornado core. Hence, in order to envelope the whole 360° with the  $\pm 45^\circ$  measurement range, cobra probes were oriented four times to cover the four quadrants. Multiple cobra probes at up to six locations across the centerline

of the turntable ( $X/r_o = -0.39, -0.2, 0, 0.2, \text{ and } 0.51$  for  $S=0.48$  (EF-1) and  $-0.39, -0.27, 0, 0.27, 0.33, 0.39, \text{ and } 0.51$  for  $S=0.76$  (EF-2)) at five different heights ( $H/H_{eave} = 0.14, 0.48, 0.82, 1.23, \text{ and } 1.67$ ) were used to measure the wind speed. The cobra probe's sampling frequency was set to 1250 Hz. Fig. 4.6 shows a set of cobra probes used in the wind speed measurements. The peak horizontal velocity at the building height was used as the reference velocity in the current study (13.21 m/s and 15.55 m/s for EF-1 and EF-2 rated tornadoes, respectively) while the 3-sec peak horizontal velocity at the building height was utilized in the comparison with the ASCE 7-16 code.

Two swirl ratios ( $S=0.48$  and  $S=0.76$ ), two orientations ( $0^\circ$  and  $45^\circ$ ) and three offsets (+RMW, +2RMW, >+2RMW) were investigated in the present study to investigate the effect of these parameters on the external pressure distribution as well as comparing the  $C_p$ 's with the ASCE loadings.

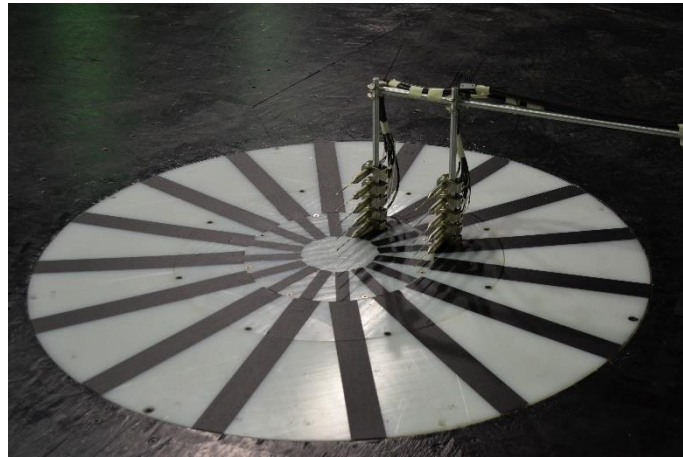


**Figure 4.6 Set of cobra probes to measure reference velocity**

## 4.5 Results and discussion

In this section, the distribution of the external pressure coefficients on the surfaces of the two low-rise buildings are analyzed for different building offsets, two building orientations, and two tornado intensities,  $S=0.48$  and  $S=0.76$ . Moreover, external pressure coefficients ( $GC_p$ ) from the present study are compared with the ASCE7-16  $GC_p$  for ABL wind.

### 4.5.1 Distribution of external pressure coefficients

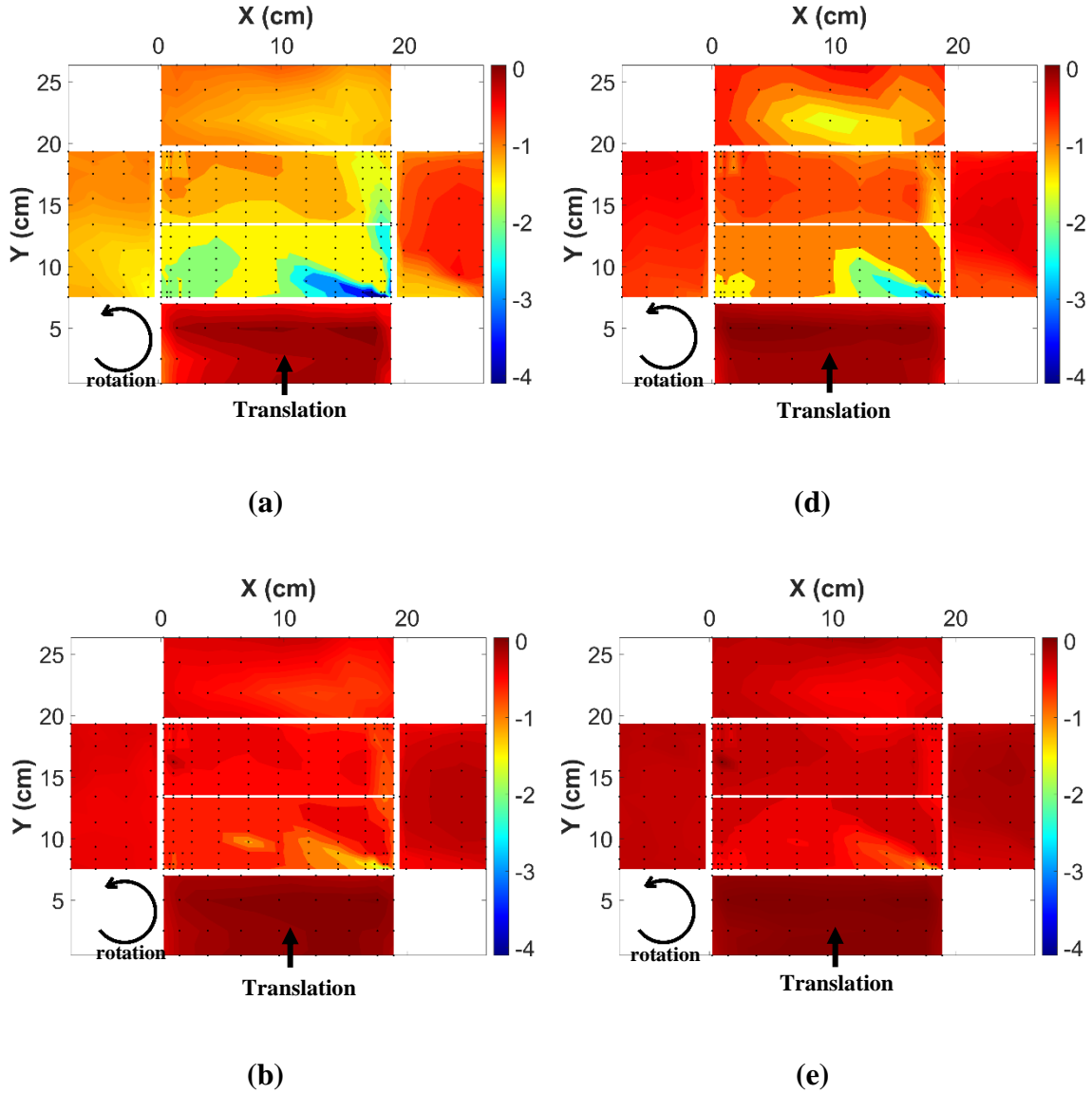
$GC_p$  distributions on the surfaces of the low-rise buildings in tornadic flow are categorized according to the studied effects. The measured exterior pressures are presented in the form of contour plots.

#### 4.5.1.1 5.1.1 The effect of offset

External pressure distribution was investigated under three building locations (i.e. offsets), +RMW, +2RMW, and  $> +2RMW$ . These offsets were analyzed to understand the vulnerability of buildings to higher suctions, particularly at +RMW which is considered a highly susceptible region to higher winds while the larger offsets are studied to assess the extent of tornado effect. Fig. 4.7 represents contour plots of  $GC_p$ 's, where Fig. 4.7a, b, c represents  $S=0.76$  (EF-2 rated) and Fig. 4.7d, e, f depicts  $S=0.48$  (EF-1 rated) at the three offsets. It is clearly observed from Fig. 4.7 that increasing the offset resulted in an overall decreased  $GC_p$ 's for both EF-1 and EF-2 rated tornadoes, with the same corner of the roof showing the maximum suction. This is attributed to the dominance of the Atmospheric Pressure Deficit (APD) in tornadic flows that resulted in high suction in the tornado core. This can be seen from Fig. 4.8 where the surface pressure deficit of both EF-1 and EF-2 rated tornadoes are plotted. The pressure deficits are normalized by the peak horizontal velocity at the building height for each tornado intensity while the distance is normalized by the radius of maximum wind 'RMW' (i.e. core radius ' $r_c$ ') for each swirl ratio. Please note that the pressure deficits are adapted to the simulator's center to get a full insight into the change of pressure with radius. Fig. 4.8 shows that the tornado flow-field is dominated by suction until +2RMW. In addition, it is seen from Fig. 4.7 that beyond the core region, the overall pressure distribution did not alter as the effect of the APC started to diminish. For EF-2 rated tornado at the core radius location (i.e. +RMW) (Fig.4.7a), the windward wall is dominated by positive pressure. This is due to the direct strike of the tornado with its high tangential velocities at this location. On the other hand, the roof, roof corners, leeward wall, and the left side wall experienced the maximum uplift. This complies with the counterclockwise rotation of the tornado vortex as well as the separation and convergence due to the tornado swirling motion. Also, conical-shaped pressure distribution is observed in the southeast corner of the roof for  $S=0.48$  and  $S=0.76$  (Fig. 4.7a, d) which



indicates the presence of corner vortices in this roof corner. Similar observations can be seen for  $S=0.48$  (Fig. 4.7d). Overall, the +RMW location is considered the most critical position in terms of  $GC_P$ 's compared to the studied cases.



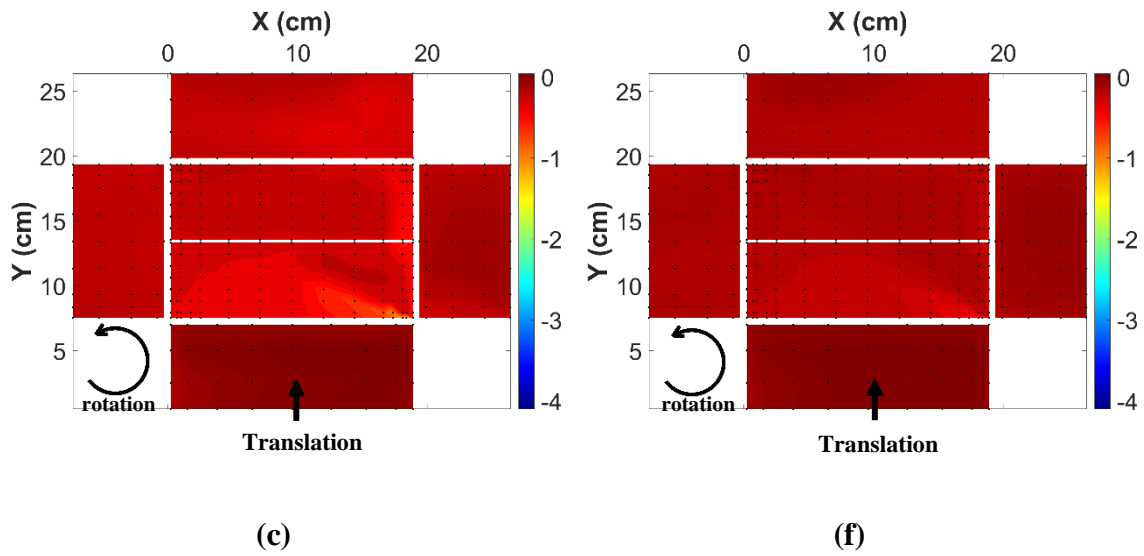


**Figure 4.7** Contour plots of ensemble-averaged peak pressure coefficients ( $GC_p$ ) for the small building for  $S=0.76$  at (a) +RMW (case 1), (b) +2RMW (case 2), (c) >+2RMW (case 3), and for  $S=0.48$  at (d) +RMW (case 4), (e) +2RMW (case 5), (f) >+2RMW (case 6)

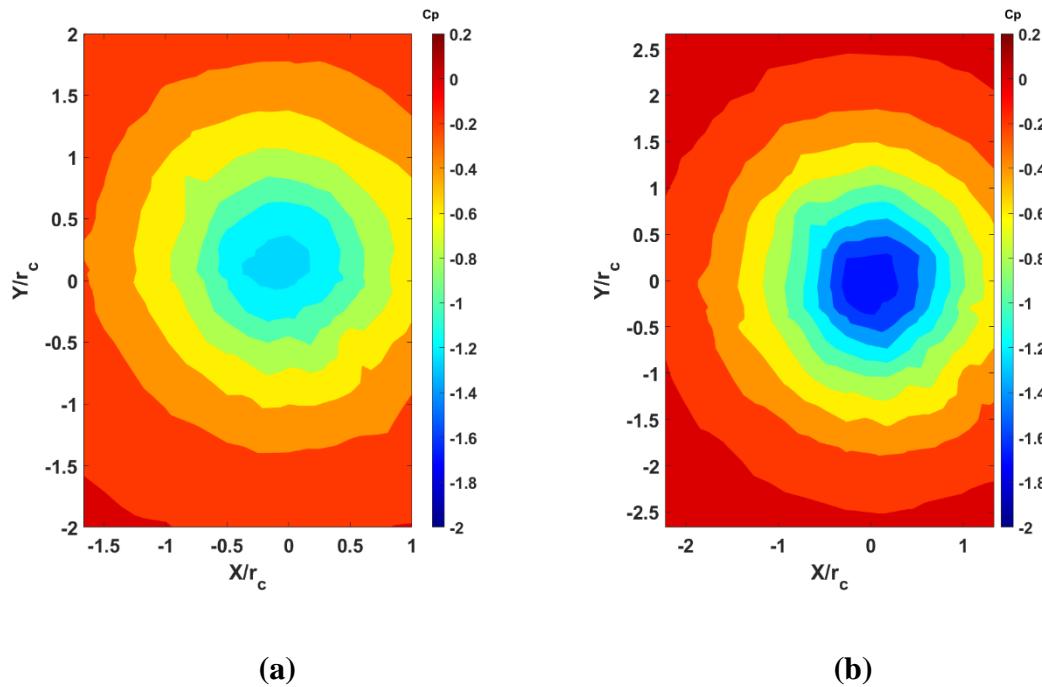


**Figure 4.8** Surface pressure deficit of stationary tornado for (a)  $S=0.76$  (EF-2 rated), and (b)  $S=0.48$  (EF-1 rated)

#### 4.5.1.2 5.1.2 The effect of building size

Distributions of  $GCp$  on both small and large buildings at +RMW for  $S=0.76$  (EF-2) are shown in Fig. 4.9a. As can be seen from Fig. 4.9a, both buildings experienced conical-shaped pressure distribution in the Southeast corner of the roof with higher suction for the small building. This could be attributed to the closeness of the roof corner of the small building to the radius of maximum wind due to its smaller length which is one-third of the larger building. This has a great implication on understanding the building size effect. The main parameter herein is not the building plan dimensions but the ratio between the building length to the tornado core diameter (i.e.  $L_{Building}/D_{core}$ ) which is 0.48 and 0.16 for the large building and small building, respectively for EF-2 rated tornado. This shows that the smaller the building length compared to the tornado core diameter, the higher the negative pressures the building can experience. Placing the building beyond the core region at +2RMW (Fig. 4.9b) did not show a difference in the pressure distribution for both buildings. This indicates that beyond +RMW, the pressure distribution is not affected by the size of the building.

#### 4.5.1.3 5.1.3 The effect of orientation

Fig. 4.9a illustrates that for the small building, the rotation of the building by  $45^\circ$  caused a redistribution of the low-pressure areas in the roof corners and leeward wall. Lower pressure zones can be observed in the rear wall of the  $45^\circ$  case due to the high extent of separation in this zone that resulted from building rotation. Conical pressure distribution was more pronounced in the southwest corner of the building that is attributed to the corner vortices developed in this corner, unlike a southeasterly conical pressure distribution in the  $0^\circ$  case. Also, lower pressure in the east corner of the windward wall can be seen for the  $45^\circ$  case (Fig. 4.10a) due to the tornado flow-field separation. Expanding the results to the large building model (Fig. 4.10b) shows the same behavior as the smaller building in Fig. 4.10a except that the large building experienced larger separation and bigger corner vortices on the roof and leeward face.

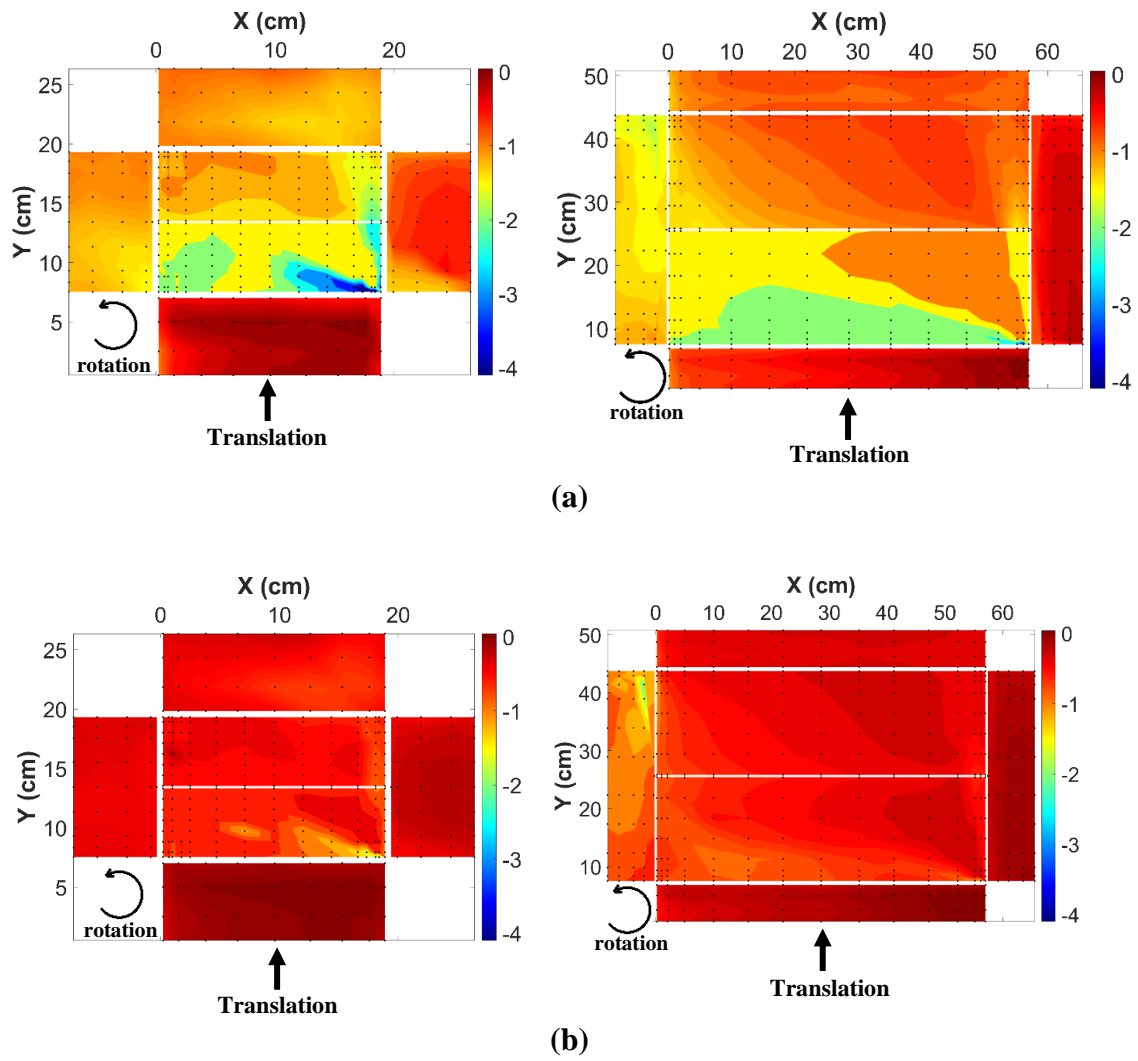


**Figure 4.9 Effect of building size on  $GC_p$  distribution for  $S=0.76$  at (a) +RMW (cases 1 and 7), (b) +2RMW (cases 2 and 8)**

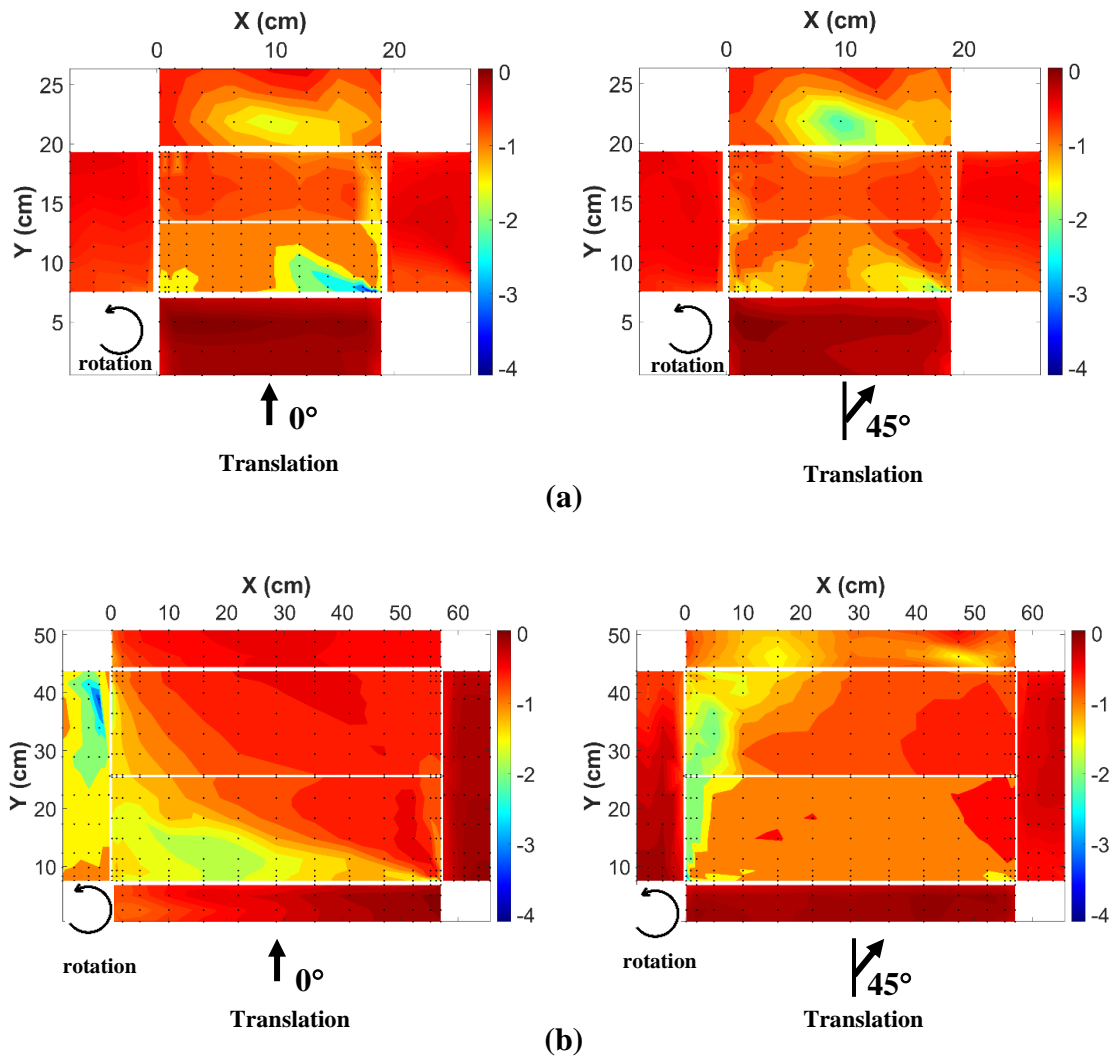


**Figure 4.10 Effect of building orientation on  $GC_P$  distribution at +RMW for (a)  $S=0.48$  (cases 4 and 9), small building, (b)  $S=0.48$ , large building (cases 10 and 11)**

#### 4.5.2 Comparison with ASCE 7-16

The results of the present study (cases 1-16) for the small and large buildings, different offsets, the two tornado intensities, and orientations were compared with the components and cladding in ASCE7-16 standard provisions to get a thorough insight of the current provisions and its applicability for tornado flow-field. The peak values of the ensemble-averaged 3-sec  $C_p$ 's are used in this comparison. Fig. 4.11 illustrates the zones' configurations according to the ASCE for the two low-rise buildings employed in this

study. Fig. 4.12-17 represents the measured external pressure coefficients ( $GC_p$ ) values for the six zones and the ASCE 7-16' values. The blue lines indicate the maximum negative pressures as indicated by the ASCE 7-16 provisions, while the green lines represent the maximum negative pressures after multiplying by the tornado factor (TF). The tornado factor (TF) is based on tornado design considerations outlined in chapter 26 in the ASCE 7-16 code. A tornado factor of 1.5 that represents Exposure C terrain condition from Table C26.14-4 was used in the current study.

Starting the analysis with the roof zones, Fig. 4.12 shows that for zone 1', the measured  $GC_p$  exceeded the ASCE coefficient values even after applying the tornado factor. This is attributed to the great difference between the tornadic flow-field and the ABL flow on which the recommended values in the ASCE code are based on. The atmospheric pressure deficit (APD) developed in the center of the tornado flow is dominating over the tornado-structure interaction, particularly near the core region that results in overall suction on the mid-roof zone. This has a great implication on the design of low-rise buildings as it shows that the middle of the roof is a highly vulnerable area. It should be noted that the small building does not have zone 1' due to its small plan dimensions, so the results in Fig. 4.12 are confined to the large building. Expanding the results to zone 1 (Fig. 4.13) that considers the small and large buildings, the  $GC_p$  values seem to have good agreement with the ASCE. This shows that the large building is more prone to high suction in the mid-roof zone than the small building which is due to its larger plan dimensions.

On the contrary to zone 1', zone 2 (Fig. 4.14) that contains the roof edges, and zone 3 (Fig. 4.15) which represents the roof corners are considered resilient zones as the peak pressure values fall below the recommended values of the ASCE with the TF. This shows the similarity between the tornadic flow-field and ABL flow in these zones. The reason behind that is that zone 2 is away from the critical areas like the mid-roof zone and roof corners so it is not prone to higher suctions. On the other hand, zone 3, which represents the roof corners, is considered as a highly prone area of separation in ABL flow. That is why the ASCE 7-16 recommendations perform well for this zone. It should be noted that the derived conclusions are confined to the studied cases.

After delving into the roof zones (zones 1', 1, 2, and 3) and perceiving the most vulnerable areas, further investigation for the wall zones needs to be performed to assess their susceptibility to high suctions. Fig. 4.16 and 4.17 depict that peak negative pressures exceeded the ASCE values for zones 4 (middle of the walls) and 5 (wall corners) which means that the code is underestimating the loads in these areas. This would be attributed to the low-pressure areas on the sidewalls, which are a direct result of the separation and re-attachment of the tornadic flow-field due to the counter clock-wise rotation direction of the tornado flow which is not the case for ABL flow where the peak pressures are experienced in the corners of the roof facing the wind direction.

The comparison with the ASCE 7-16 outlined that the code recommendations underestimated the peak pressures for three main zones, middle of the roof (zone 1'), the wall and wall corner zones (zone 4 and 5). Moreover, the plan dimensions of the buildings affect the vulnerability of the structures as the smaller building didn't exceed the standard peak pressures, unlike the large building.

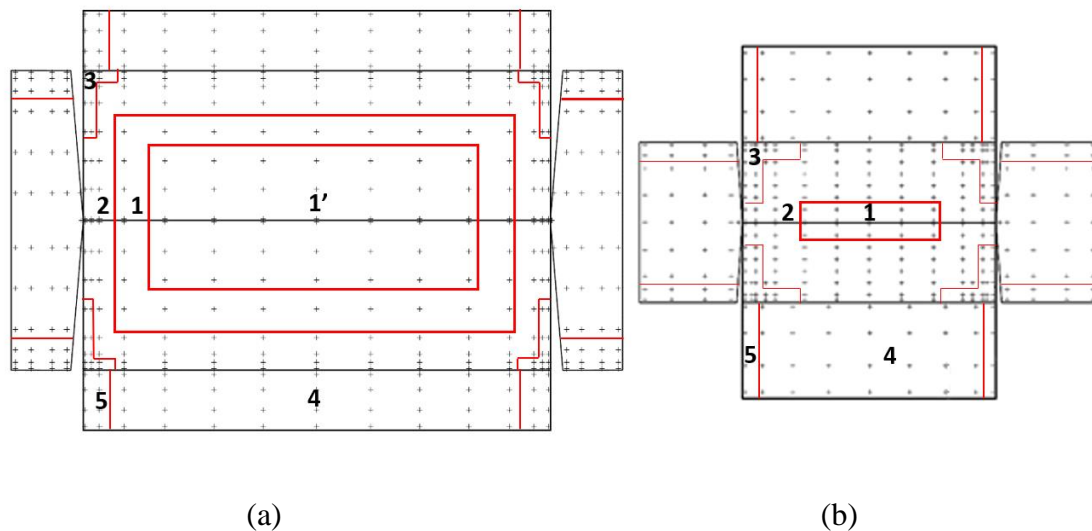


**Figure 4.11 Building zones according to ASCE 7-16 for (a) Large building, and (b) small building**

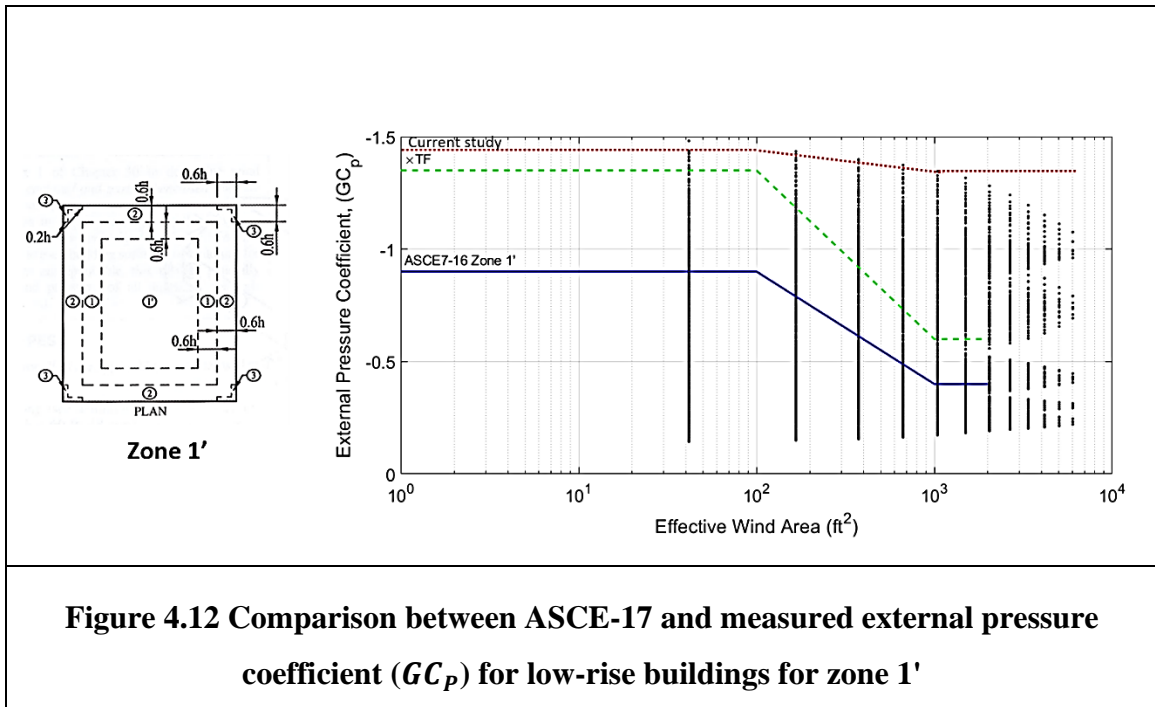


**Figure 4.12 Comparison between ASCE-17 and measured external pressure coefficient ( $GC_p$ ) for low-rise buildings for zone 1'**

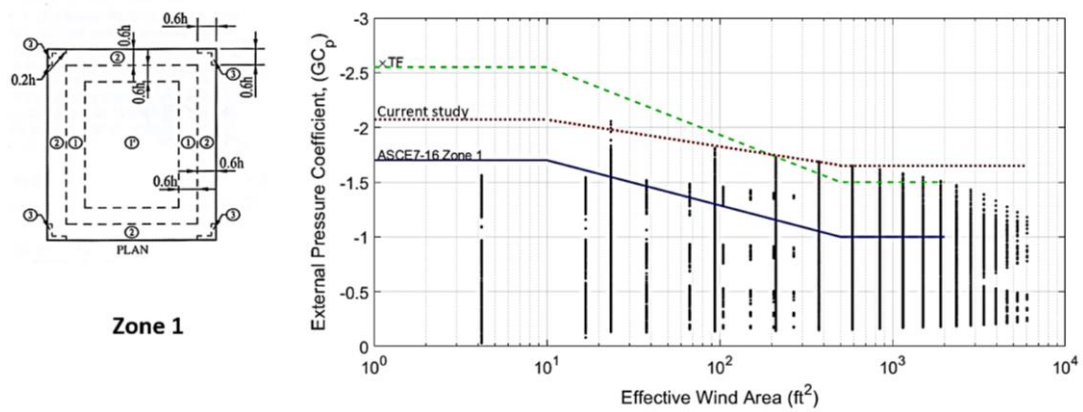


**Figure 4.13 Comparison between ASCE-17 and measured external pressure coefficient ( $GC_p$ ) for low-rise buildings for zone 1**



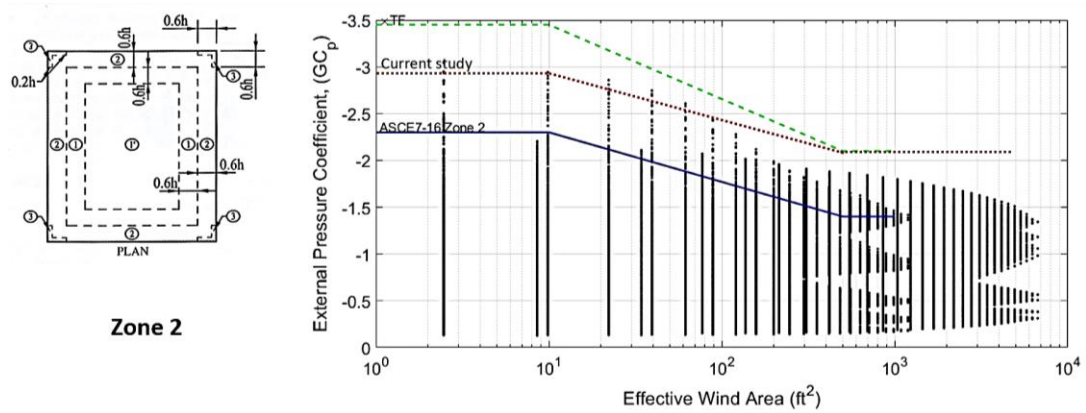


**Figure 4.14 Comparison between ASCE-17 and measured external pressure coefficient ( $GC_p$ ) for low-rise buildings for zone 2**

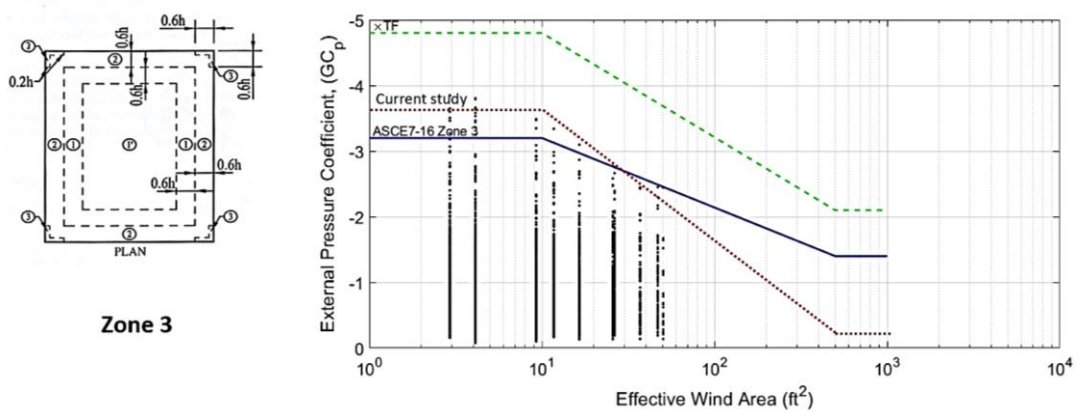


**Figure 4.15 Comparison between ASCE-17 and measured external pressure coefficient ( $GC_p$ ) for low-rise buildings for zone 3**

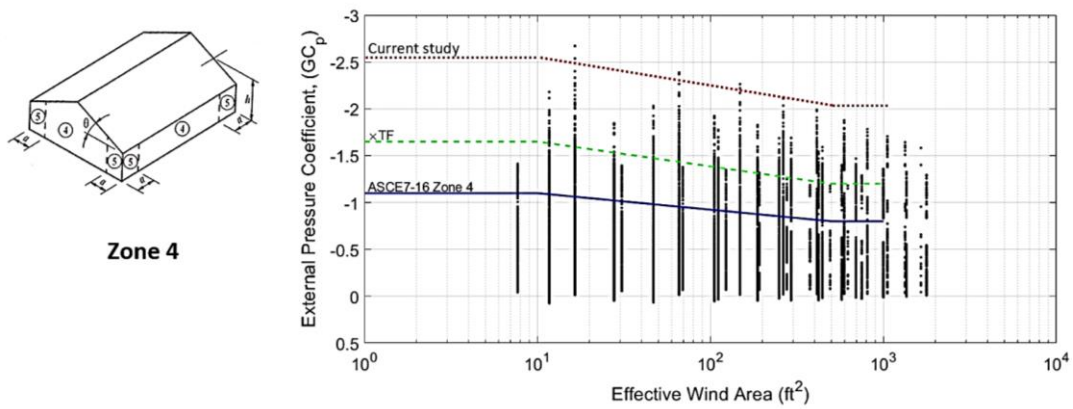


**Figure 4.16 Comparison between ASCE-17 and measured external pressure coefficient ( $GC_p$ ) for low-rise buildings for zone 4**

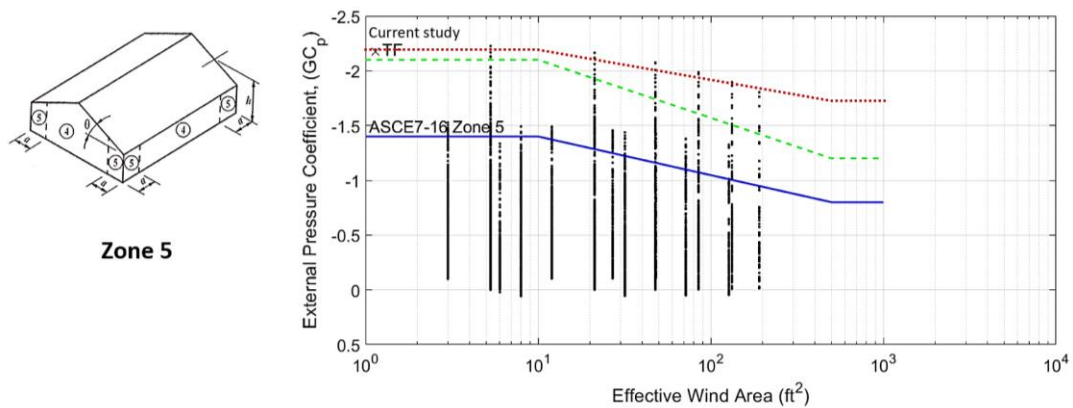


**Figure 4.17 Comparison between ASCE-17 and measured external pressure coefficient ( $GC_p$ ) for low-rise buildings for zone 5**

## 4.6 Conclusions

External pressure measurements have been performed in the WindEEE Dome at Western University for two generic low-rise buildings under translating tornado-like vortices. The building size, building offset, and building orientation were altered to study their effects on the external pressure distribution. Moreover, a comparison between the peak ensemble-averaged pressure coefficients and the ASCE 7-16 recommended values have been accomplished to assess the building code applicability for the studied cases.

From the current study, it was concluded that:

- The roof, leeward wall, and the left side wall experienced the maximum uplift at +RMW. Increasing the offset beyond the core radius resulted in a less pronounced suction on the roof and a significant drop in the loads.
- Conical pressure distribution for the case of  $0^\circ$  (windward wall is normal to the translation path) was observed for all the cases.
- The smaller of the two buildings experienced higher negative peak pressures at +RMW. This is attributed to the total submergence of the whole small building length in the core region, unlike the large building that has a larger plan dimension.
- Changing the building orientation from  $0^\circ$  to  $45^\circ$  caused a redistribution of the peak pressures and separation locations. The rear wall experienced lower pressure and the conical pressure distribution was shifted to the southwest corner of the building that faces the translating tornado.
- For roof corner zones, ASCE 7-16 wind load provision performed well for all the studied cases.
- The middle of the roof and middle of the wall experienced higher suction in tornadoes than the recommended wind loads in ASCE 7-16.

## Acknowledgment

This research has been made possible through funding from Natural Sciences and Engineering Research Council of Canada (NSERC) Discovery Grant (Grant number: R2811A03) and Canada Foundation for Innovation (CFI) WindEEE Dome Grant (Grant number: X2281838).

## References

- ASCE/SEI 7-16, 2017. Minimum design loads and associated criteria for buildings and other structures. American Society of Civil Engineers, Reston, Virginia.
- Baker, C. and Sterling, M., 2019. Are Tornado Vortex Generators fit for purpose?. J. Wind Eng. Ind. Aerodyn. 190, pp.287-292. <https://doi.org/10.1016/j.jweia.2019.05.011>
- Bezabeh, M.A., Gairola, A., Bitsuamlak, G.T., Popovski, M., Tesfamariam, S., 2018. Structural performance of multi-story mass-timber buildings under tornado-like wind field. Eng. Struct. 177, 519–539. <https://doi.org/10.1016/j.engstruct.2018.07.079>
- Elawady, A., Aboshosha, H., El Damatty, A., Bitsuamlak, G., Hangan, H., Elatar, A., 2017. Aero-elastic testing of multi-spanned transmission line subjected to downbursts. J. Wind Eng. Ind. Aerodyn. 169, 194–216. <https://doi.org/10.1016/j.jweia.2017.07.010>
- Fujita, T.T., 1971. Proposed characterization of tornadoes and hurricanes by area and intensity.
- Ginger, J. D., Mehta, K. C., & Yeatts, B. B., 1997. Internal pressures in a low-rise full-scale building. J. Wind Eng. Ind. Aerodyn. 72, 163-174. [https://doi.org/10.1016/S0167-6105\(97\)00241-9](https://doi.org/10.1016/S0167-6105(97)00241-9)
- Haan, F.L., Balaramudu, V.K., Sarkar, P.P., 2010. Tornado-Induced Wind Loads on a Low-Rise Building. J. Struct. Eng. 136, 106–116. [https://doi.org/10.1061/\(ASCE\)ST.1943-541X.0000093](https://doi.org/10.1061/(ASCE)ST.1943-541X.0000093)

Hangan, H., 2014. The wind engineering energy and environment (WindEEE) dome at western university, Canada. *Wind Engineers, JAWE*, 39(4), pp.350-351.

<https://doi.org/10.5359/jawe.39.350>

Ho, T.C.E., Surry, D., Morrish, D., Kopp, G.A., 2005. The UWO contribution to the NIST aerodynamic database for wind loads on low buildings: Part 1. Archiving format and basic aerodynamic data. *J. Wind Eng. Ind. Aerodyn.* 93, 1–30.

<https://doi.org/10.1016/j.jweia.2004.07.006>

Hu, H., Yang, Z., Sarkar, P., Haan, F., 2011. Characterization of the wind loads and flow fields around a gable-roof building model in tornado-like winds. *Exp. Fluids* 51, 835.

<https://doi.org/10.1007/s00348-011-1102-6>

Jubayer, C., Romanic, D., Hangan, H., 2019. Aerodynamic loading of a typical low-rise building for an experimental stationary and non-Gaussian impinging jet. *Wind Struct.* 28, 315–329. <https://doi.org/10.12989/was.2019.28.5.315>

Jubayer, C., Wu, T., 2020. Aerodynamic Loading Due to Non-Synoptic Wind Systems. *Oxf. Handb. Non-Synop. Wind Storms*.

<https://doi.org/10.1093/oxfordhb/9780190670252.013.17>

Junayed, C., Jubayer, C., Parvu, D., Romanic, D., Hangan, H., 2019. Flow field dynamics of large-scale experimentally produced downburst flows. *J. Wind Eng. Ind. Aerodyn.*

188, 61–79. <https://doi.org/10.1016/j.jweia.2019.02.008>

Lombardo, F.T., Smith, D.A., Schroeder, J.L., Mehta, K.C., 2014. Thunderstorm characteristics of importance to wind engineering. *J. Wind Eng. Ind. Aerodyn.* 125, 121–

132. <https://doi.org/10.1016/j.jweia.2013.12.004>

McDonald, J.R., Mehta, K.C., Texas Tech University Wind Science and Engineering Center, 2006. A recommendation for an enhanced Fujita scale (EF-scale). *Wind Science and Engineering Center*, Texas Tech University, Lubbock, Tex.

- Mishra, A.R., James, D.L., Letchford, C.W., 2008. Physical simulation of a single-celled tornado-like vortex, Part B: Wind loading on a cubical model. *J. Wind Eng. Ind. Aerodyn.* 96, 1258–1273. <https://doi.org/10.1016/j.jweia.2008.02.027>
- Razavi, A., Sarkar, P.P., 2018. Tornado-induced wind loads on a low-rise building: Influence of swirl ratio, translation speed and building parameters. *Eng. Struct.* 167, 1–12. <https://doi.org/10.1016/j.engstruct.2018.03.020>
- Refan, M., Hangan, H. and Wurman, J., 2014. Reproducing tornadoes in laboratory using proper scaling. *J. Wind Eng. Ind. Aerodyn.* 135, pp.136-148.
- Refan, M., Hangan, H., 2018. Near surface experimental exploration of tornado vortices. *J. Wind Eng. Ind. Aerodyn.* 175, 120–135. <https://doi.org/10.1016/j.jweia.2018.01.042>
- Romanic, D., Hangan, H., Ćurić, M., 2016. Wind climatology of Toronto based on the NCEP/NCAR reanalysis 1 data and its potential relation to solar activity. *Theor. Appl. Climatol.* 1–17. <https://doi.org/10.1007/s00704-016-2011-7>
- Roueche, D.B., Prevatt, D.O., Haan, F.L., Datin, P.L., 2015. An estimate of tornado loads on a wood-frame building using database-assisted design methodology. *J. Wind Eng. Ind. Aerodyn.* 138, 27–35. <https://doi.org/10.1016/j.jweia.2014.11.011>
- Sarkar, P.P., Haan, Jr.F.L., Balaramudu Vasanth, Sengupta Anindya, 2006. Laboratory Simulation of Tornado and Microburst to Assess Wind Loads on Buildings. *Struct. Congr.* 2006. [https://doi.org/10.1061/40889\(201\)11](https://doi.org/10.1061/40889(201)11)
- Sengupta, A., Haan, F.L., Sarkar, P.P., Balaramudu, V., 2008. Transient loads on buildings in microburst and tornado winds. *J. Wind Eng. Ind. Aerodyn.* 96, 2173–2187. <https://doi.org/10.1016/j.jweia.2008.02.050>
- Solari, G., Burlando, M., De Gaetano, P., Gaetano, M.P., 2015. Characteristics of thunderstorms relevant to the wind loading of structures. *WIND Struct.* 20, 763–791. <https://doi.org/10.12989/was.2015.20.6.763>

## Chapter 5

### 5 Conclusion

In the present thesis, near-surface pressure measurements were carried out on the ground as well as on two generic low-rise building models in the state-of-the-art tornado simulator, the WindEEE Dome. The analysis of the tornado-like vortices ground pressure data was utilized to serve in the interpretation of the tornado induced pressures on buildings as a superposition of pressure deficit and aerodynamic effects.

In the beginning, high resolution, in space and time, ground pressure measurements were performed to understand the dynamics of stationary and translating TLVs as a function of swirl ratio, translation speeds, and roughness. A broad range of swirl ratios was tested ( $S=0.21$  to  $1.03$ ) representing tornado vortex development from single-celled vortex to vortex breakdown to two-celled structure. The effect of multiple swirl ratios ( $S=0.21$  to  $1.03$ ), three translation speeds ( $V_T = 0.1, 1$  and  $1.5$  m/s) and two roughness levels (smooth and rough) on wandering, tilting, and veering of tornado vortices were for the first time examined.

A comprehensive study on internal pressures was carried out on two generic low-rise buildings under translating tornado-like vortices (TLVs) were examined experimentally for volume size, resolution, and translation velocity never achieved before. The effects of building offset with respect to the tornado path, building size, building orientation, and openings on the internal pressure loadings were investigated.

Afterward, induced external pressures were quantified for the two generic low-rise buildings under translating tornado-like vortices. The effect of the building's plan dimension, building location as well as building orientation on the resulted external loading on buildings were explored. In addition, a comparison was provided between the induced peak pressures and the recommended value of components and claddings stated in the ASCE 7-16 standard building code to assess the building code applicability for the studied cases.

## 5.1 Summary of findings

Results of the ground pressure measurements showed that the increase of swirl ratio for stationary tornado-like vortices (TLVs) resulted in a reduction of the peak pressure at first which was then followed by a gradual rise. This indicates the different development stages of tornado vortex structure where the vortex transitions from a single vortex to a multi-vortex structure.

Wandering behavior was found to have a significant outcome, particularly for lower swirls, on the mean flow-field of the stationary tornado. The error can exceed 35% for the peak pressure magnitudes. In the current study, a new method for removing wandering was suggested that was reliable, particularly for higher swirl ratios with more complex vortex structure.

Translating TLVs was found to have some remarking differences compared to stationary ones. Three translation speeds were utilized in this study (0.1 m/s; 1m/s and 1.5 m/s) where the higher speeds are investigated for the first time in tornado simulators. The results indicate that increasing translation speed led to a lower magnitude of the observed peak pressure deficits which assures the importance of studying translating TLVs instead of stationary ones where the last could produce overestimated loads.

An inclination of the translating TLV in the translation direction was observed where the base of the vortex postdated the upper part of the vortex attached to the guillotine system. This is attributed to the shear that the vortex experience near the ground. This tilting behavior was only detected in higher translation speeds ( $V_T = 1$  m/s and 1.5 m/s) and was increasing with increased translation velocity. In addition, a left curved deviating behavior of the tornado vortex signature on the ground was detected for high translations. This is apparently a direct result of the imbalance in the velocity field for both sides of the tornado vortex which was documented in some field studies.

Increasing the surface roughness was found to cause a similar effect to decreasing swirl ratio for the two studied cases ( $S=0.48$  and  $S=0.76$ ). An increased inclination of the tornado vortex axis and a less veering motion was noticed with increasing the roughness level.



After delving into the tornado vortex flow-field structure, the induced internal pressures were explored for multifold opening configurations, building offset, building orientation, and tornado intensities. It was deduced that the internal pressures are uniform for all the studied cases which shows a resemblance with ABL flow-field studies in the literature. A high correlation between internal and external pressures adjacent to the openings, similar to ABL flow, was also found.

Increasing the building size resulted in a lower internal pressure peak. This emphasizes the large destruction a small building can experience in tornadic hits. A 45° orientation slightly affected the peak internal pressures while it resulted in a lag of the pressure deficit profile that is attributed to the longer interaction (i.e. diagonally) between the translating TLV and the building. A reduction of the peak internal loads by two-thirds was observed when shifting the building beyond the core region.

Investigating the multifold scenarios of the opening configurations revealed that a roof opening will produce the highest peak of the internal pressure compared to a windward dominant opening or uniform leakage. Also, a roof opening would equalize the APD when the building is at +RMW, which would mitigate the differential pressure and the building vulnerability.

Lastly, external pressure study revealed that the most vulnerable areas to negative peaks were the roof, leeward wall, and the left side wall at the core radius (i.e. +RMW). Increasing the offset beyond the core radius resulted in a significant drop in the loads. The small building experienced higher negative peak pressures at +RMW. This is because the small building is totally enveloped inside the core region due to its smaller length, unlike the large building which is 3 times larger in length.

The comparison between the peak pressures and the components and claddings in the ASCE 7-16 showed that the roof corner zones are not considered a vulnerable area to high suctions unlike the middle of the roof and the middle of the wall zones that experienced higher suctions than the recommended ASCE 7-16 values. This highlights the need for

considering tornadic loadings in evaluating the recommended value of pressure loading in the building codes.

## 5.2 Recommendations for future work

The current thesis studied the near-surface structure of tornado-like vortices in terms of ground pressure loading, internal and external pressures. The following recommendations are suggested for future work:

- A larger range of swirl ratios can be investigated for translating tornado-like vortices (TLV) for a better understanding of surface roughness on TLV structure.
- Development of an analytical model that takes into account wandering, veering, and tilting motions for translating tornado-like vortices.
- The induced pressure loads, internal and external, on buildings can be extended to investigate multiple heights' effect on the overall loading pattern.
- Further research should be done to understand the effect of roughness on internal pressures in tornadic flow-field and to develop models that can predict the internal pressure behavior utilizing the broad and easy-to-access datasets of pressure loading in ABL flow-field.
- More cases need to be enveloped in the comparison between the measured peak external pressures and the ASCE 7-16 standard building code.
- Extending the internal and external pressure to examine the resultant tornado loading on buildings.

## Appendix A: Damage Indicators and Degree of Damage

The present tables (Table A.1 and A.2) summarize the Damage Indicators (DI) that is utilized to estimate the degree of severity of a tornado and the Degree of Damage (DOD) for one- and two-family residence.

**Table A.1 EF- scale damage indicators (DI)**

<b>DI No.</b>	<b>Damage Indicator (DI)</b>
1	Small Barns or Farm Outbuildings (SBO)
2	One- or Two-Family Residences (FR12)
3	Manufactured Home – Single Wide (MHSW)
4	Manufactured Home – Double Wide (MHDW)
5	Apartments, Condos, Townhouses [3 stories or less] (ACT)
6	Motel (M)
7	Masonry Apartment or Motel Building (MAM)
8	Small Retail Building [Fast Food Restaurants] (SRB)
9	Small Professional Building [Doctor's Office, Branch Banks] (SPB)
10	Strip Mall (SM)
11	Large Shopping Mall (LSM)
12	Large, Isolated Retail Building [K-Mart, Wal-Mart] (LIRB)
13	Automobile Showroom (ASR)
14	Automobile Service Building (ASB)
15	Elementary School [Single Story; Interior or Exterior Hallways] (ES)
16	Junior or Senior High School (JHSH)
17	Low-Rise Building [1-4 Stories] (LRB)
18	Mid-Rise Building [5-20 Stories] (MRB)
19	High-Rise Building [More than 20 Stories] (HRB)
20	Institutional Building [Hospital, Government or University Building] (IB)
21	Metal Building System (MBS)
22	Service Station Canopy (SSC)
23	Warehouse Building [Tilt-up Walls or Heavy-Timber Construction](WHB)
24	Electrical Transmission Lines (ETL)
25	Free-Standing Towers (FST)
26	Free-Standing Light Poles, Luminary Poles, Flag Poles (FSP)
27	Trees: Hardwood (TH)
28	Trees: Softwood (TS)

**Table A.2 One- and Two-Family Residences (FR12) (DOD)**

<b>DOD*</b>	<b>Damage description</b>	<b>Exp**</b>	<b>LB</b>	<b>UB</b>
1	Threshold of visible damage	65	53	80
2	Loss of roof covering material (<20%), gutters and/or awning; loss of vinyl or metal siding	79	63	97
3	Broken glass in doors and windows	96	79	114
4	Uplift of roof deck and loss of significant roof covering material (>20%); collapse of chimney; garage doors collapse inward or outward; failure of porch or carport	97	81	116
5	Entire house shifts off foundation	121	103	141
6	Large sections of roof structure removed; most walls remain standing	122	104	142
7	Exterior walls collapsed	132	113	153
8	Most walls collapsed in bottom floor, except small interior rooms	152	127	178
9	All walls collapsed	170	142	198
10	Destruction of engineered and/or well constructed residence: slab swept clean	200	165	220

\* DOD is degree of damage \*\*Wind Speed values are in mph

EXP refers to expected wind speed (mph)

LB refers to lower bound wind speed (mph)

ECP refers to higher bound wind speed (mph)

## References

McDonald, J. R., & Mehta, K. C. (2006). *A recommendation for an Enhanced Fujita scale (EF-Scale)*. Wind Science and Engineering Center, Texas Tech University.

## Curriculum Vitae

<b>Name:</b>	Aya Kassab
<b>Post-secondary Education and Degrees:</b>	<p>Faculty of Engineering, Alexandria University Alexandria, Egypt 2006-2011 B.Sc.</p> <p>Faculty of Engineering, Alexandria University Alexandria, Egypt 2011-2014 M.Sc.</p> <p>The University of Western Ontario London, Ontario, Canada 2017-Present Ph.D.</p>
<b>Honours and Awards:</b>	B.Sc. Alexandria University award for distinctive 2006-2007, 2007-2008, 2009-2010, 2010-2011
<b>Related Work Experience</b>	<p>Teaching and Research Assistant Faculty of Engineering, Alexandria University, Egypt 2012-2016</p> <p>Teaching and Research Assistant The University of Western Ontario 2017-Present</p>

### Publications and Conference Proceedings:

**Kassab A**, Vickery P, Jubayer C, Banik S, Hangan H. 2019. Tornado-Induced Internal and External Pressures on a Low-Rise Building with Multiple Openings. CSME-CFDSC Congress 2019, London, Canada, June 2-5, 2019.

**Kassab A**, Romanic D, Costache A, Hangan H. 2017. Simultaneous pressure and PIV measurements on low-rise building. 1000 Islands Fluid Mechanics Meeting (T.I.M. 2017), 21-23 April 2017, Gananoque, On, Canada.

Ashrafi A, Romanic D, **Kassab A**, Hangan H, Ezami N. 2020. Experimental investigation of large-scale tornado-like vortices. Journal of Wind Engineering and Industrial Aerodynamics, 104449.